POLYTYPISM AND SILICON CARBIDE.

A Solid State Nuclear Magnetic Resonance Study.

by

BEATRICE G. WINSBORROW

A thesis submitted to the Department of
Chemistry in partial fulfillment
of the requirements for the degree of
Master of Science

Brock University
St.Catharines, Ontario

ABSTRACT

A survey of predominantly industrial silicon carbide has been carried out using Magic Angle Spinning nuclear magnetic resonance (MAS nmr); a solid state technique.

Three silicon carbide polytypes were studied; 3C, 6H, and 15R. The ^{13}C and ^{29}Si MAS nmr spectra of the bulk SiC sample was identified on the basis of silicon (carbon) site type in the different polytypes. Out to 5.00 A from a central silicon (or carbon) atom four types of sites were characterized using symmetry based calculations. This method of polytype analysis was also considered, in the prelminary stages, for applications with other polytypic material; $CdBr_2$, CdI_2, and PbI_2.

In an attempt to understand the minor components of silicon carbide, such as its surface, some samples were hydrofluoric acid washed and heated to extreme temperatures. Basically, an HF removable species which absorbs at -110 ppm (SiO_2) in the ^{29}Si MAS nmr spectrum is found in silicon carbide after heating. Other unidentified peaks observed at short recycle delays in some ^{29}Si MAS nmr spectra are considered to be impurities that may be within the lattice. These components comprise less than 5% of the observable silicon.

A T_1 study was carried out for ^{29}Si nuclei in a 3C

polytype sample, using the Driven Equilibrium Single-Pulse Observation of T_1 (DESPOT) technique. It appears as though there are a number of nuclei that have the same chemical shift but different T_1 relaxation times. The T_1 values range from 30 seconds to 11 minutes. Caution has to be kept when interpreting these results because this is the first time that DESPOT has been used for solid samples and it is not likely in full working order.

MAS nmr indicates that the ^{13}C and ^{29}Si isotropic chemical shifts of silicon carbide appear to have a reciprocal type of relationship. Single crystal nmr analysis of a 6H sample is accordance with this finding when only the resultant isotropic shift is considered. However, single crystal nmr also shows that the actual response of the silicon and carbon nuclear environment to the applied magnetic field at various angles is not at all reciprocal. Such results show that much more single crystal nmr work is required to determine the actual behavior of the local magnetic environment of the SiC nuclei.

ACKNOWLEDGEMENTS

As usual the acknowledgements have been left to the end. It is so difficult deciding how to thank all of those people who have had some influence on this project without listing each person that I have known over the past two years or so.

I would like to thank Dr.J.S.Hartman, my supervisor, for his never ending help and advice. Thanks also go to Dr.Richardson for teaching me everything that I wanted to know about crystallography and more; and to Dr.D.Hiatt who had spent countless hours modifying the DESPOT analysis programme.

This project was supported by NSERC funding and an Ontario Graduate Scholarship.

The General Abrasive people were life savers by opening up their dome and allowing me to pick pounds of silicon carbide. Thank you, Gene, Chris, Tom, and Larry. Of course, I would have also been lost if it were not for the technical help and friendly advice from the electronic and machine shops, and Tim, all from Brock.

Finally, on a more personal and spiritual level, I must thank all of my family and friends; without such distractions this thesis would only have been an experience of "all knowledge and no wisdom".

No acknowledgement is complete without a list of names,

and this one is no exception. Years from now, when I reflect back on this period in my life, there are some moments that will immediately come to mind. So I won't forget these moments, permit me to list a few names associated with the memories: Vi, Bob, Kevin, Eric, Mike, Jo and brats, Ken and Maria, Richard, Dr.Moule, Gypsy, Anne-Marie, Fr.Keating, Heather, Scott and Chris, Robbie, Barb, Zheng, Jim and Bill and Rand, Meinhart, and oh ya, Doug. Thanks for rounding out my education, I love you all.

CONTENTS

LIST OF FIGURES

LIST OF TABLES

Chapter I

INTRODUCTION

A. Progress In Solid State NMR

The nuclear magnetic resonance (nmr) technique has been developed over roughly three decades, predominantly for solution nmr work. So much so, that when one speaks of high resolution nmr the usual assumption is that the sample is in solution. In general, solid state nmr was used find the chemical shift; the signal was very broad and the technique had more utility in the domain of the physicist.

Problems with sample insolubility and the fact that a sample has different chemical properties while in solution as compared to its solid state were driving forces for the development of the solid state nmr technique. Work by scientists like Lowe (1), Andrew (2), Lippmma (3), and Fyfe (4,5), especially in the past decade, has escalated solid state nmr to a high resolution nmr technique, routinely used by many researchers from varying backgrounds. The improvement in solid state nmr is

predominantly due to three techniques; high power decoupling, Magic Angle Spinning (MAS), and Cross Polarization (CP) (4,6,7).

Since its inception (1,2), the technique of Magic Angle Spinning (MAS) nmr was not fully appreciated until 1978, when MAS nmr was first used for inorganic solids (3). Presently the field of MAS nmr has grown almost exponentially and there seems to be no upper limit on how far the technique will go.

In general terms, the broad nmr line of a powdered solid is narrowed using high powered decoupling to eliminate heteronuclear coupling, and MAS to average out the chemical shift anisotropy (CSA). CP with MAS increases the sensitivity and quickens the experiment by the transference of polarization from a magnetically abundant nucleus to a magnetically dilute nucleus being observed within the sample. The application of these techniques to solid state nmr is widespread in many fields; geology, catalyst chemistry, polymer chemistry, surface science, biology. and medicine.

Minerals (4,8,9), especially zeolites, and glass (10,11) have all been widely studied by MAS nmr. The basic structure of these samples is a silicate and/or aluminosilicate network. The commonly used method of characterizing these materials is via x-ray crystallography. Unfortunately the scattering power of aluminun and silicon is very similar, which makes structure analysis difficult. Another drawback to x-ray crystallography is

that it is only useful to study long range order. Nmr can be used to obtain information on short range order (or disorder). For example, glasses, which are amorphous, can be successfully studied in detail by MAS nmr (10,11).

The study of fossil fuels by CP/MAS has also been found to be very useful. Classification of fossil fuels is done by determining the aromaticity of a particular sample, which is measured directly by nmr. Other methods of analysis can be both indirect and unrepresentative of the heterogeneous nature of the samples. Some other methods are infrared analysis, heat of combustion, and fluorination reactions (12,13,14).

Amino acids, polypeptides, proteins, simple sugars, polysaccharides, and other biological samples (15,16) are also well studied using CP/MAS. A growing field is nmr imaging. The ^{1}H and ^{13}C nmr of simple solids have been studied by imaging the solid (17,18). This technique is analogous to the x-ray technique used by physicians which indicates the potential for future solid state nmr in imaging.

Essentially, the most fascinating aspect of solid state nmr is that a major technical stumbling block was overcome by an apparently trivial modification, MAS. This modification simplifies a broad line spectrum, which has too much information, to a solution-like nmr spectrum, which gives the isotropic chemical shift.

B. NMR Background

1. Quantum Mechanical Considerations

Each proton and neutron of a nucleus has its own spin ($\pm$ 1/2). I, the spin quantum number, is the resultant of these spins in a nucleus (I = 0, 1/2, 1, 3/2..). For nuclei with I not equal to zero, the nuclear charge spins (precesses) about the nuclear axis, generating a magnetic dipole (μ) along the axis:

$$\mu = \gamma I \hbar$$

γ = gyromagnetic ratio, a nuclear property

$\hbar$ = Planck's constant/2π

I determines the number of orientations the magnetic dipole may have while in an external uniform magnetic field (H_0):

$$\#\text{of orientations} = 2I+1$$

These orientations correspond to Zeeman energy levels (Figure 1.1). The higher the energy of the energy level, the more the magnetic dipole is aligned away from the applied magnetic field. The energy of each level is E_m:

$$E_m = -\gamma \hbar m H_0$$

Figure 1.1: Zeeman energy levels produced by putting an $I = 1/2$ nucleus in a magnetic field H_o. The number of levels are $2nI + 1$.

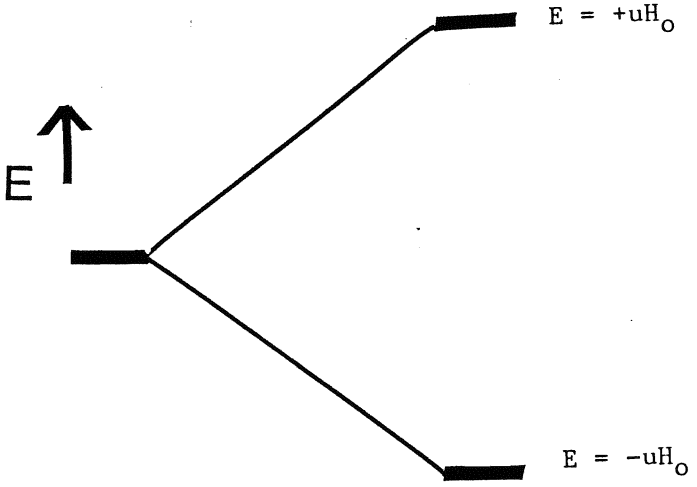

NO APPLIED MAGNETIC FIELD

APPLIED MAGNETIC FIELD, H_o

ALIGNMENT

m = the magnetic quantum number; m = -I, -I+1,..,I-1,I

In accordance with the Boltzman distribution theory, the populations of the Zeeman levels are temperature dependent. At room temperature, there is a slight excess of magnetic dipoles in the lower energy state aligned with H_0. The resultant is a net magnetization parallel to the applied magnetic field (along the H_0 z axis).

While the magnetic dipoles are aligned along the magnetic field they precess about the magnetic field z axis at the nuclear Larmor frequency (see section on chemical shifts). If a radio frequency magnetic field, H_1, is applied perpendicular to H_0 that matches the Larmor frequency, the net magnetization will be caused to resonate and tilt away from the H_0 z axis. The longer the radio frequency pulse, the greater the angle of tilting. Detection of the tilted magnetization is in the H_ox-y plane.

There are many books and reviews available which treat the theories of nmr with varying degrees of sophistication (6,7,12,19). The above has been a very general commentary on the fundamental principles of nmr.

2. Chemical Shifts

A chemical shift to higher field indicates that the nucleus of the higher field signal is more "shielded" than the lower field nucleus. Therefore a greater proportion of energy is required to cause the magnetization to resonate because the observed nucleus has a larger shielding from the external perturbations. The characteristic behavior of each nucleus in this manner is used to identify the chemical species studied.

The Larmor frequency is the frequency at which the nuclear dipoles precess about the applied magnetic field at equilibrium. It is dependant upon the gyromagnetic ratio of the nucleus and the applied magnetic field:

$$\nu = \gamma H_0 / 2\pi$$

The gyromagnetic ratio of a particular nucleus is constant, but in different electronic environments a nucleus may not see the same proportion of the applied magnetic field. The frequency ultimately required to cause the net nuclear magnetization to resonate is dependant upon the local magnetic field:

$$H_{local} = H_0 (1 - \sigma)$$

Where σ is the shielding tensor of the nucleus, it is dimensionless and dependent upon the local magnetic environment of the nucleus (see VI.A).

Then, if $H_0 = H_{local} + \sigma H_0$, the magnetization of a bare nucleus would resonate at the lowest applied frequency (energy). With progressive shielding about the nucleus, more energy and so a greater portion of the applied magnetic field is required to cause the nuclear magnetization to resonate. The frequency at which resonance occurs is known as the chemical shift. It is calibrated in terms of the portion of the magnetic field applied (part per million, ppm) with respect to a reference signal.

3. Relaxation In Solid State NMR

The two means by which the nuclear magnetizations relax after they resonate is by longitudinal and transverse interactions. The former involves a transfer of energy from the nucleus to its environment, spin-lattice relaxation. The time it takes to regain the spin population equilibrium is known as T_1. The latter interaction is spin-spin relaxation, there is no net loss of energy in the system, the effect is a loss of phase coherence of magnetization in the H_0 x-y plane. The time

required for this to occur is T_2.

The mechanism for spin-lattice relaxation in liquids is quite different from that of solids. Relaxation in liquids is most commonly due to molecular tumbling and dipole-dipole interactions (6). Any magnetic nucleus in a molecule has a magnetic dipole field, which is proportional to the magnetic moment of the nucleus. Relaxation of one nucleus by another is possible by interactions of the magnetic dipoles. These are known as dipole-dipole interactions. Solids are fairly static and molecular motions are definitely not a major cause of relaxation.

Dipole-dipole interactions in solids for magnetically abundant nuclei are possible as a means of relaxation. However, the strength of this interaction decreases with increasing distance ($\cong r^{-6}$, r = through space distance between nuclei) so this sort of interaction is not likely to occur with magnetically dilute nuclei. The relaxation process for dilute nuclei in solids is most likely due to spin diffusion through the lattice (6,20). This sort of relaxation mechanism is not efficient which is consistent with the fact that spin-lattice relaxation in solids is much slower than in liquids.

Transverse relaxation in solids tends to be much shorter than longitudinal relaxation. The natural linewidth of an nmr peak at half height is inversely proportional to T_2:

$$\omega_{1/2} = 2\pi / T_2$$

Since T_2 is significantly shorter than T_1, its importance, aside from linewidth effects, has not been investigated in solid state nmr.

4. Nuclei To Consider

The focus of this study will be on ^{29}Si and ^{13}C of silicon carbide, however, some attention will be given to ^{207}Pb, ^{111}Cd, and ^{113}Cd. Since all five nuclei have I = 1/2, there will only be two Zeeman levels and hence, only one nmr transition (m = 1/2 <-> -1/2). The respective natural abundances of ^{13}C, ^{29}Si, ^{207}Pb, ^{111}Cd, and ^{113}Cd are 1.1%, 4.7%, 12.8%, 12.3%, and 22.6%. The I value of all of the other isotopes of the nuclei is zero, so there should be no further broadening or complication of the nmr signal with satellite peaks of the other isotopes. Also, all of the nuclei are magnetically dilute so line broadening from homonuclear dipole-dipole interactions should be at a minimum (see section on MAS). However, with dilute nuclei the nmr signal is not very strong, so signal averaging with Fourier Transformation is necessary to obtain the required signal intensity (4,6).

C. Magic Angle Spinning

The broad resonance lines which are characteristic of the nmr spectra of solids are due predominantly to two factors: coupling from dipole-dipole interactions ant the different orientations of the nuclear magnetization in the applied magnetic field. The latter effect is chemical shift anisotropy (CSA).

Many solid samples studied by nmr have protons; $I = \frac{1}{2}$ and ^{1}H is $\cong$100% abundant in nature. Any other nucleus studied by nmr that is proximal to a proton will spin-couple with the proton. Such coupling broadens any solid nmr line because the coupling value, in hertz, is not larger than the natural line width of the nmr signal. One way around this problem is to decouple these interacions by irradiating the sample with a high power radio frequency pulse corresponding to the Larmor frequency of the proton. Problems arise when the nucleus studied is magnetically abundant because broad band homonuclear decoupling is not possible since the decoupling would wipe out the spectrum. Some complicated pulse sequences have been designed to give the appearance of such decoupled spectra which have met with some success (6,21). Magnetically dilute nuclei are the nuclei of choice for solid state nmr because there are few if any dipole-dipole interactions which broaden the nmr line.

The shielding tensor, and so the chemical shift, of a nucleus is not only dependent on the electronic environment of a particular nucleus (see I.B.2 and VI.A), but also on the orientation of that nucleus relative to H_0 (4,22). Anisotropy in the magnetic susceptibilities of the bonds is transformed into anisotropies in the magnetic susceptibilities of the crystal. This causes the chemical shift to vary as a function of the crystal orientation. CSA then arises from a nonspherical electron density around the nucleus studied.

The same CSA is present in liquid as in solid samples, however molecular motion in liquids allows averaging and an isotropic chemical shift is observed. It has been found experimentally, and can be shown mathematically (1,2,12), that the same isotropic averaging is possible in solids if the sample is spun at 54.7^0 to H_0 z axis. The isotropic chemical shift is dependent upon the term $(3 \cos^2\theta - 1)$, when θ is equal to 54.7^0 this term reduces to zero and the solid nmr signal becomes like that of liquids with the chemical shift tensors averaged (see VI.A). The MAS nmr signal will look like a high resolution liquid signal and only the isotropic chemical shift is observed (Figure 1.2). The spinning rate has to be faster (in hertz) than the natural line width at half height of the nmr signal, in order for the technique to be effective (4).

Many reviews have been written which explain the theory and applications of MAS nmr (4, 6, 12).

Figure 1.2: ^{29}Si MAS nmr spectra of BGW4 silicon carbide to demonstrate the effect of Magic Angle Spinning. Recycle delay was 30 seconds, in both cases.

a) not spinning

b) spinning 3300 Hz, at an angle of 54.74° to the applied magnetic field, H_0.

ppm
-50
+50
A)
B)

D. Crystallography of SiC

1. Geometric Considerations

Silicon carbide (SiC) is a synthetic refractory material well known for its ability to withstand extreme heat (>2000°C) and its hardness (about 9.3 where diamond is 10) (23). These characteristics are due to the SiC structure which is a three dimensional network of tetrahedrally bonded Si and C atoms. Such an arrangement is easily envisioned as alternately stacked Si and C layers of hexagonally close packed spheres. Each Si layer is directly above a carbon layer and each SiC double layer is stacked over the holes in other SiC double layers. There are then three possible layers (A,B,and C); with respect to a chosen layer (A layer, say) two other layers are made depending over which set of holes in the A layer the other layers are placed (24) (Figure 1.3).

SiC can crystallize into different crystallographic modifications, known as polytypes, which are all similar along *a* and *b* axes (the plane parallel to the SiC layers) but differ from each other along the *c* axis (25). Polytypism may be regarded structurally as a one-dimensional polymorphism, but the two

Figure 1.3: Diagram of the three possible layers when spheres are close packed.

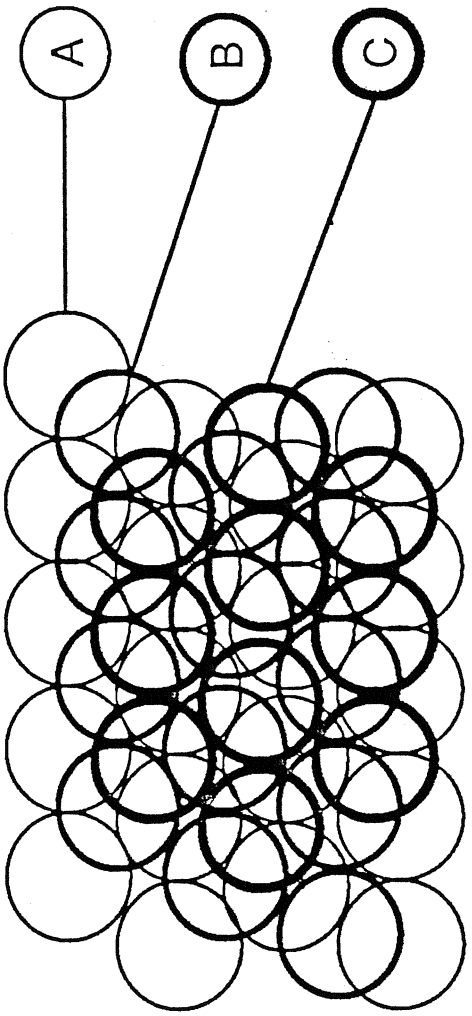
A
B
C

phenomena are physically quite distinct. Each modification of a polymorph forms under different conditions of temperature and pressure. The resulting polymorphs differ in their physical properties; a popular example of a polymorphic pair is graphite and diamond, both consist of only carbon.

Polytypes do not tend to undergo transformations from one to another at different temperatures or pressures (except the SiC polytypes 2H and 3C). In addition, the different SiC polytypes form under similar conditions and they have nearly the same physical properties (eg. density and refractive index) (26) (Figure 1.4).

Original goniometric studies (28) of various SiC crystals led to the classification of SiC structures into three symmetry groups; cubic, hexagonal, or rhombohedral. A fourth more recently defined group has trigonal symmetry (29). The following table lists the symmetries possible for the close packed sphere type of SiC structure (Table 1.1).

With the proper choice of axes, the rhombohedral unit cell can be described in hexagonal or cubic unit cell terms(25). The body diagonal [(000) -> (111)] of the rhombohedron is the c axis of a triply primitive hexagonal cell. Whereas the length of a quadruply primitive cubic cell is the rhombohedron (001) -> (110) vector. Also note that the unit cell restrictions for the trigonal and hexagonal unit cells are the same. The difference

Figure 1.4: The 6H silicon carbide structure (25).
Black spheres represent carbon atoms,
White spheres represent silicon atoms.

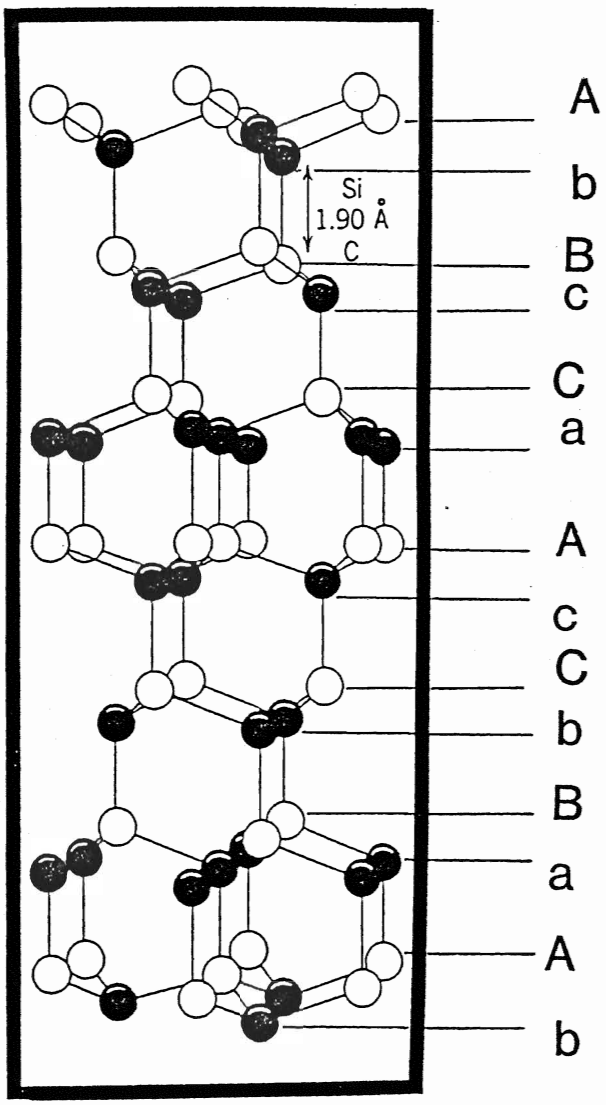
Si
1.90 Å
C
A
b
B
c
C
a
A
c
C
b
B
a
A
b

Table 1.1 : Unit Cell Restrictions for SiC Cell Types

unit cell symmetry	cell restrictions	space group
cubic	$\underline{a} = \underline{b} = \underline{c}$ $\alpha = \beta = \gamma = 90$	F43m
rhombohedral	$\underline{a} = \underline{b} = \underline{c}$ $\alpha = \beta = \gamma \neq 90$	R3m1 (hexagonal axes used)
hexagonal	$\underline{a} = \underline{b}$ $\alpha = \beta = 90, \gamma = 120$	$P6_3mc$
trigonal	$\underline{a} = \underline{b}$ $\alpha = \beta = 90, \gamma = 120$	P3m1

is that the highest axis of symmetry for the trigonal cell is three-fold and for the hexagonal cell it is six. The highest order symmetry axis of the cubic unit cell is a four-fold rotation axis along any of its faces. The cube and rhombohedron both have a three-fold rotation axis along their body diagonals.

For such an apparently simple structure it is interesting to note that over 200 polytypes of SiC have been characterized (26) and that many more are theoretically feasible. There is also a great deal of information gathered about this "simple" compound; enough to sufficiently fill two volumes of the Gmelin series of inorganic chemistry (26,27). The focus of many ongoing crystallographic studies of SiC is to characterize more polytypes and to find out what exactly causes the crystals to grow with c axes with as many as 500 repeat layers if not higher (that is, unit cells having a repeating c axis that is about 12500 A long) (30,31,32).

2. Nomenclature

With the study of polytypism, several nomenclatures and classifications have been devised to enable polytype identification. Originally, the SiC structures were labelled in chronological order of appearance, totally unrelated to symmetry

(See Table 1.2). A very popular notation for SiC (originally hexagonally oriented only) is that of Ramsdell (33), which uses two symbols. The first is a number, corresponding to the number of layers in a unit cell before they repeat for the next unit cell. The second is the letter H or R depending on whether the unit cell is hexagonal or rhombohedral, respectively. Therefore, if an SiC sample has six layers to a unit cell and is hexagonal primitive, it is 6H in Ramsdell notation. A rhombohedral primitive unit cell with 33 repeating layers is denoted as 33R. Crystals with cubic symmetry are now described using this notation as 3C (26). Also, trigonal structures can be described using the same approach. For example, a trigonal crystal with a 21 layer repeat is 21T (29).

The problem with the Ramsdell notation is that it doesn't give any insight to the actual arrangement of layers in the unit cell. The classical ABC sequence is a simple and at times lengthy means of specifying polytypic stacking sequences. This method simplified lists the layer sequence of Si (or C) in SiC; for 15R the sequence is /ABCBACABACBCACB/ABCBACABA.... The actual sequence would also include Greek letters after each letter to denote the carbon (or Si) layers. This is redundant for SiC since Si and C have the same layering. Three simpler notations are the Hagg notation (34), Zhdanov symbol (35), and the Ramsdell zigzag sequence (33) which all relate the

Table 1.2 The structure of some polytypes of SiC as described using various notations. (25)

Classical Notation	Ramsdell Notation	ABC Sequence	Hagg Notation	Zhdanov Symbol
SiC I	15R	ABCBACABACBCACB	$(++---)_3$	$(23)_3$
SiC II	6H	ABCACB	++---	33
SiC III	4H	ABCB	++--	22
SiC IV	21R	ABCACBACABCBACB CABACB	$(+++----)_3$	$(34)_3$
SiC V	51R	ABCACBABCACBABCAC BCABACBCABACBCABA CABCBACABCBACABCB	$(+++--+++$ $---+++--)_3$	$(333332)_3$
-	2H	AB	+-	11

orientation of A,B,and C layers to each other.

The Hagg notation considers the layer orientation of a hexagonal unit cell to be of a cyclic nature. That is A -> B -> C-> A.. is positive stacking(+),and A -> C -> B-> A..is negative(-). Therefore, the above 15R sample is /++---++---++---/++-...= $(++---)_3$. An arithmetic relationship has been defined relating the number of plus and minus signs, within the brackets, to cell type:

$n^+ - n^- = 3r$ for hexagonal polytypes (r is any integer)

$n^+ - n^- = 3r +/- 1$ for rhombohedral polytypes

This method works because the number of plus and minus signs used to depict the stacking sequence is the same as the number of layers in the hexagonal unit cell. The rhombohedral polytype, expressed in hexagonal terms, is triply primitive, and the number of layers is three times the number of plus and minus signs. Similarily, the Zhdanov symbol gives the sum of +'s and -'s, so the above 15R is $(23)_3$. Ramsdell observed (33) that the Zhdanov symbol represented the zigzag sequence of silicon (or carbon) atoms in the (110) planes. Since an atom can not be stacked directly above another atom, the subsequent layer must be stacked either to the left or right of a representative atom in the layer; for example, if layer B is to the left of A then layer

Figure 1.5: Diagram of the Ramsdell zig-zag stacking sequence (25), viewed along the (110) plane. Black spheres represent carbon atoms, white spheres represent silicon atoms.

a) 6H SiC; 2 and not 1 is the end of the unit cell.

b) 15R SiC.

ZHDANOV

SYMBOL

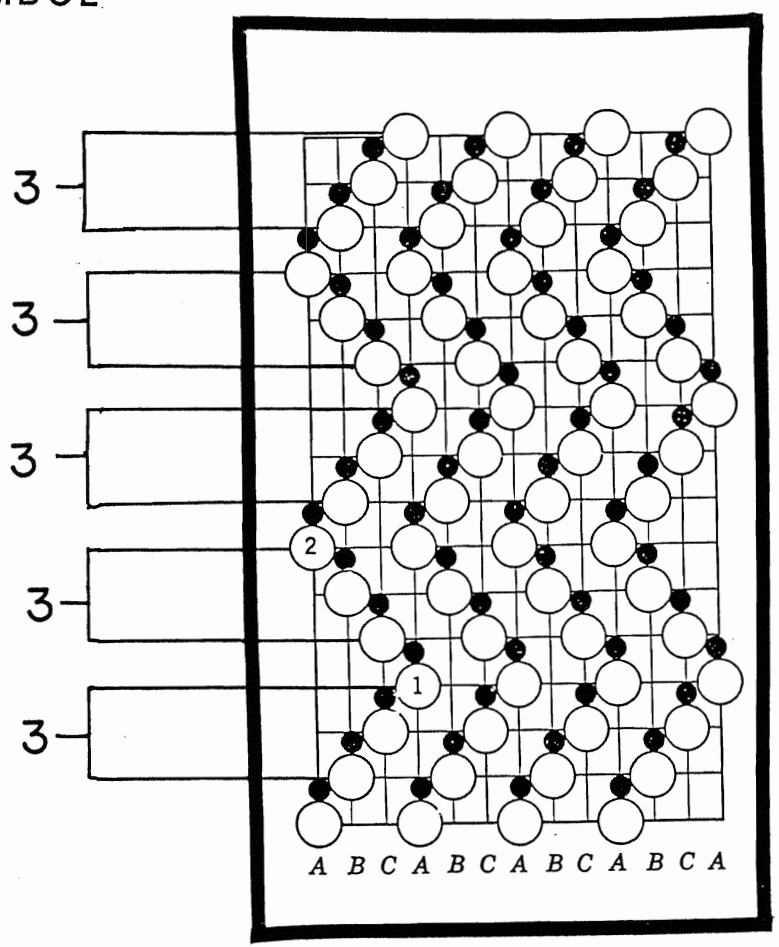

a)

ZDHANOV

SYMBOL

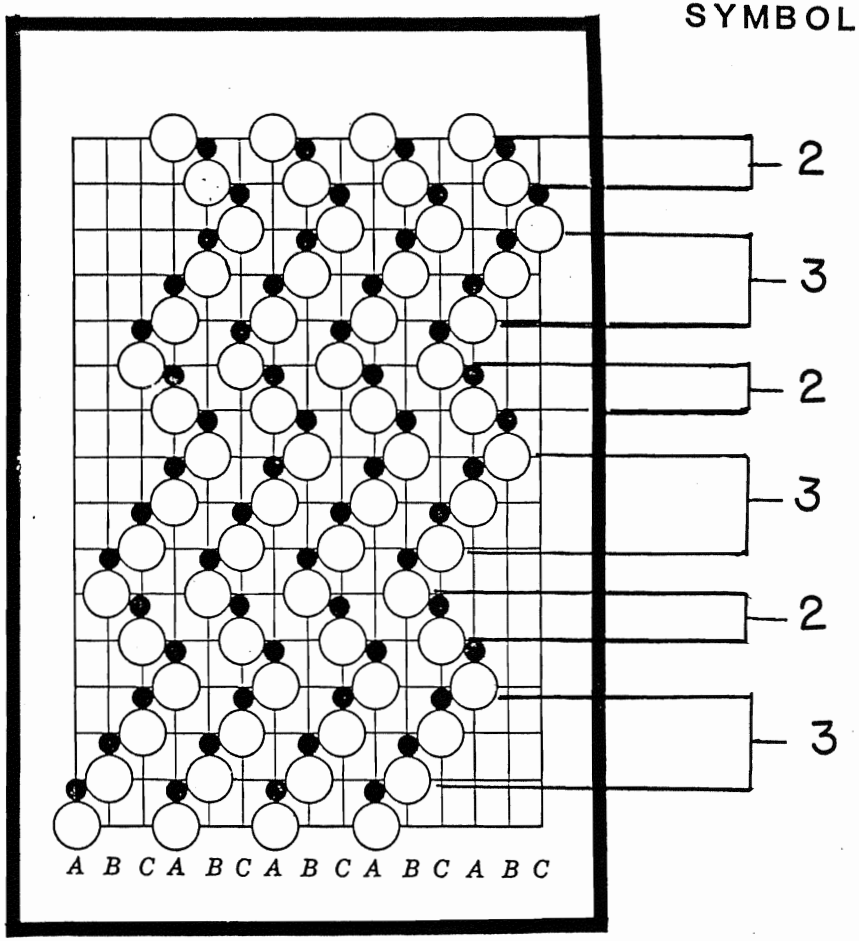

b)

C is to the right (Figure 1.5). This zigzag sequence is a simple method of visually describing a polytype. Table 1.2 summarizes some of the nomenclature systems (25).

E. Methods of Polytype Determination

There are a number of techniques available for differentiating between the various polytypes of SiC. These techniques include measuring the angles between external faces using an optical goniometer (28), and various microscopic techniques (36). However more detailed information can be obtained by the use of electron and x-ray techniques (25), which involve either diffraction or transmission of incident rays. X-ray diffraction techniques that are used most often for polytype determination of SiC are the oscillation, rotation, and Weissenberg methods (37). The Laue method is an x-ray technique that records transmitted light (38).

The Laue method and powder x-ray diffraction methods are not only useful for the identification of a single polytype but also for identifying individual polytypes in a mixed crystal. Powder methods give diffractions of many tiny crystals from a larger ground crystal. Statistically, the "tiny crystals" should contain a proportional mixture of polytypes present in the

original crystal. Since tha Laue method involves transmission of X-rays, detection of polytypes within the crystal is possible, so buried polytypes can be detected.

Recently, the solid state nmr technique, Magic Angle Spinning nmr (MAS nmr) has been used to study SiC structures (39,40). This technique is quite different from X-ray methods in many ways. The positions of X-ray diffraction maxima from any crystal depend only on the lattice type and parameters, while their intensities depend on the atomic structure represented by each lattice point. The chemical shifts of the SiC spectra depend on the silicon and carbon environments (see sections on chemical shift and MAS) and the peak intensities depend upon the relative abundance of the type of silicon (or carbon) site present in the particular SiC polytype sample. Hartman et al. (40) found that the 6H, 15R, and 3C SiC polytypes all gave different MAS nmr spectra. In order to explain such observations calculations from a chosen silicon (or carbon) to neighbours out to 5.00A apparently showed that there are three possible types of silicon (or carbon) sites in the above three polytypes, depending on the relative arrangement of layers. After more systematic and detailed consideration, it has been found that there are possibly four sites, when calculations are carried out to 5.00A. This will be shown later in the text (Chapter III).

F. Thesis Direction

The nmr chemical shift is both an analytical indicator of the presence of chemical species and a diagnostic indicator of electronic and physical interactions such species may experience in a given situation. With this in mind, silicon carbide will be studied in two perspectives, to obtain both sorts of information possible as stated above. Predominantly, the focus will be on the MAS nmr of SiC which characterizes chemical species by determining their isotropic chemical shifts. In an introductory capacity a second method will also be considered; single crystal nmr, which can give the CSA of the nuclear species studied. Once the CSA of the SiC nuclei is known, it should help one to visualize the SiC three dimensional environment and directional bonding capacity.

Chapter II

EXPERIMENTAL

A. SiC Samples

Most silicon carbide samples used were grown industrially by the Acheson method (41) whereby coke and silica sand are converted to SiC through the passage of an electric current. Other samples were obtained from personal collections. See Table 2.1 for the sample and donor, along with a summary of treatments and experiments performed on the samples.

All samples were ground, for powder pattern XRD and nmr work, using either a tungsten carbide shatterbox or a ball mill. Both apperati powder the material by crushing through shaking which produces grains that are finer than 150 mesh. The shatterbox is about 20 times the size of the ball mill and handles a greater amount of material in a shorter time. A hand magnet was used to remove any iron, which is a constant contaminant in industrially produced SiC. The samples were then washed with dilute hydrochloric acid to further remove any traces of iron.

Directory For Table 2.1.

A. Single Crystal X-Ray Structure Determination.

B. X-Ray Powder Pattern Structure Determination.

C. 1 Hour 3% Hydrofluoric Acid Wash.

D. 60-70 Hour 3% HF Acid Wash.

E. Preliminary Heating To Temperature Given, ^{o} C.

F. Heating To 1500^{o}C For 1 Hour.

G. 1 Hour HF Acid Wash After Heating To 1500^{o}C.

H. Heat To 1500^{o}C For 8 Hours Then HF Acid Wash.

I. Gamma-Ray Irradiation For Three Weeks.

J. Single Crystal NMR Study.

K. ^{29}Si MAS NMR Work Done.

L. ^{13}C MAS NMR Work Done.

Table 2.1 : Summary of SiC Samples Studied by NMR.

Sample	Donor	A	B	C	D	E	F	G	H	I	J	K	L
BGW1	GA											X	
" 2	"											X	
" 3	"											X	
" 4	"	6H	6H	X	X	950	X			X		X	X
" 5	N											X	
" 6	"											X	X
" 7	"											X	
" 8	"											X	
" 9	"		3C									X	
"10	"											X	
"11	"											X	
"12	"		3C			1150	X	X		X		X	X
"13	"		3C									X	
"14	"											X	
"15	"											X	
"16	"			X								X	
"17	"											X	
"18	"	6H										X	
"19	"											X	
20	"											X	
"21	"											X	
"22	"	6H	6H	X			X	X	X			X	X
"23	"	6H										X	
"24	"											X	
"25	"	Only one crystal.											
"26	RT		6H	X	X					X		X	
"27	RT	6H	6H	X	X							X	
"28 - 32 & 34		A variety of BGW4 and GA10, treatments listed.											
"33	XX					1150	X					X	X
"35	RT		6H									X	
"36	"		6H									X	
"37	"	-	3C+									X	
"38	"		6H									X	
"39	"		6H+	X								X	X
"41	GA											X	
"42	"											X	
"43	"											X	
"44	"											X	
"45	"											X	
"46	"											X	
"47	"											X	
"48A	"	6H										X	

Table2.1 continued

Sample	Donor	A	B	C	D	E	F	G	H	I	J	K	L
"48B	"	6H										X	
"48C	"											X	
"48D	"											X	
"48E	"											X	
"48F	"	6H										X	
"48G	"											X	
"49	"											X	
"50	"											X	
"51	"	6H									X	X	X
GA01	"											X	
"02	"											X	
"03	"											X	
"04	"											X	
"05	"												
"06	"												
"07	"											X	
"08	"												
"09	"											X	
"10	"	6H	6H	X	X							X	X
"11	"		6H										
"12	"		6H										
"13	"		6H										
"14	"		6H										
"15	"		15R									X	X
"16	"		6H										
"17	"		15R										
UCSiC	UC		AM									X	X
SiC01	GF		6H									X	X
" 02	"		3C									X	X
" 03	"		Not enough sample.										
" 04	"		"										
" 05	"		6H									X	X
" 06	"		6H									X	X

GA = General Abrasive, Division of Dresser Inc., N.Y.
N = Norton
UC = Union Carbide
XX = Nicalon ceramic fiber; from P.E.D.Morgan of Rockwell International; amorphous SiC.
GF = From the personal collection of G.R.Finlay.
RT = From the personal collection of N.W.Thibault.
AM = Amorphous
6H+= Powder pattern photo has 6H bands, and unidentified bands.
3C+= Powder pattern photo has 3C and unidentied bands.

B. Identification of Polytypes

1. X-Ray Powder Patterns

The powdered SiC material was loaded into thin-walled glass capillary tubes (.3 mm diameter) to a depth of about 2 cm.

X-Ray powder diffraction patterns were taken of SiC on a Picker X-Ray generator using a Charles Supper Co. Weissenberg Camera. Ni filtered CuK_{α} radiation was used. Two to six hour exposure times were used for all samples. The polytype of the sample was determined by comparing the resultant powder patterns with those of Thibault (43). Amorphous SiC was detected by the observation of very diffuse lines in the powder pattern. The results are listed in Table 2.1.

2. Diffractometer Studies

Plate-shaped crystals were selected for x-ray diffraction based on size and regularity of shape. Crystals are normally selected for such studies if they extinguish when the crystals are rotated in plane polarized light, which indicates that the crystal is not twinned (44). However, the SiC crystals are too

dark to detect such extinctions, so this criterion was not used.

Crystals were mounted on thin glass fibres with Lepage's Five Minute Epoxy cement. The dimensions of the crystals are roughly 0.5 x 0.2 x 0.2 mm for suitable x-ray diffraction studies.

Cell dimensions for SiC were measured with an Enraf-Nonius CAD-4 diffractometer using MoK_α radiation (λ = 0.71069 A). The methods of crystal alignment used are given in Stout and Jensen (42). The reciprocal unit cell parameters were calculated using 25 centered reflections; intensities were measured by the w/2θ scan technique (45). The formula used to calculate the reiprocal unit cell parameters is (46):

$$\frac{\sin\theta}{} = .5[h^2a^{*2} + k^2b^{*2} + l^2c^{*2} + 2hka^*b^*\cos\gamma^* + 2hla^*c^*\cos\beta^* + 2klb^*c^*\cos\alpha^*]^{1/2}$$

a^*, b^*, c^*, α^*, β^*, and γ^* are the reciprocal unit cell parameters which are used to calculate the direct cell parameters (47). The only polytype found was 6H. In general the unit cell parameters were:

a = 3.09 A; b = 3.09 A; c = nx2.518 A

α = 90.0 °; β = 90.0 °; γ = 120.0 °

The length of the c axis is a multiple of 2.518 A, n is the number of layers in the polytype. The results are given in Table 2.1, cell parameters and standard deviations are listed in Appndix I.

C. NMR Instrumentation

^{13}C, ^{29}Si, ^{111}Cd, ^{113}Cd, and ^{207}Pb MAS nmr spectra were obtained for powdered samples with home-built Magic Angle Spinning probes (48). The samples were packed into Delrin or Kel-F spinners which were spun at approximately 3300 Hz at an angle of 54.7^{o} to the applied magnetic field.

Most spectra were acquired on either a Bruker WH-400 or AC-200 multinuclear Fourier Transform (FT) nmr spectrometer. The former spectrometer, equipped with a 9.4 tesla superconducting magnet, is located at the South Western Ontario NMR Centre at Guelph University. The latter, at Brock University, has a 4.7 tesla superconducting magnet. The acquisition parameters employed with each instrument are listed in Tables 2.2 - 2.5.

^{13}C MAS nmr spectra of GA10 were obtained on a Bruker CXP-200 (4.7 tesla) multinuclear FT nmr spectrometer by E.C.Kelusky at Dupont, Kingston. A Doty Magic Angle Spinning probe was used, with alumina spinners, which gave excellent resolution. A Bruker AM-500 (11.8 tesla) multinuclear FT nmr spectrometer was also used to obtain ^{13}C MAS nmr spectra of GA15 and BGW39. The two spectra were obtained by B.Sayer at McMaster University.

The FID's were Fourier transformed to the frequency domain with a line broadening of 50 Hz and 25 Hz on the 9.4 and 4.7 tesla instruments, respectively. Relative peak positions for ^{13}C and ^{29}Si were measured in

Table 2.2 : Instrument Parameters for Carbon.

Acquisition Parameters for ^{13}C			
Instrument(Bruker)		AC-200	WH-400
Frequency,	MHz	50.32	100.57
Spec.Width,	Hz	12500.00	31250.00
Acq'n.Memory,	K	8	8
Working Memory,	K	16	16
Pulse Angle,	deg	30	30
30^{o}Pulse Width,	u	4.0	6.7
OperatingTemp.,	^{o}C	22.5	22.5

Table 2.3 : Instrument Parameters for Silicon.

Acquisition Parameters for ^{29}Si		
Instrument (Bruker)	AC-200	WH-400
Frequency, MHz	39.76	79.46
Spec.Width, Hz	15635.00	25000.00
Acq'n.Memory, K	8	8
Working Memory, K	16	16
Pulse Angle, deg	30	30
30^{o}Pulse Width, u	4.4	5.5
OperatingTemp., ^{o}C	22.5	22.5

Table 2.4 : Instrument Parameters for Cadmium.

Acquisition Parameters for Cadmium		
Instrument (Bruker)	AC-200	AC-200
Nucleus	^{111}Cd	^{113}Cd
Frequency, MHz	42.44	44.39
Spec.Width, Hz	50000.00	50000.00
Acq'n.Memory, K	8	8
Working Memory, K	16	16
Pulse Angle, deg	30	30
30^{o}Pulse Width, u	4.0	4.0
OperatingTemp., ^{o}C	22.5	22.5

Table 2.5 : Instrument Parameters for Aluminum and Lead.

Acquisition Parameters for ^{27}Al and ^{207}Pb		
Instrument (Bruker)	AC-200	AC-200
Nucleus	^{27}Al	^{207}Pb
Frequency, MHz	52.15	41.75
Spec.Width, Hz	15151.00	100000.00
Acq'n.Memory, K	8	8
Working Memory, K	16	16
Pulse Angle, deg	30	30
30^{o}Pulse Width, u	3.0	4.5
OperatingTemp., ^{o}C	22.5	22.5

ppm to low field with respect to the reference sample, tetramethylsilane (TMS) (which has a chemical shift of 0 ppm for both nuclei). The reference sample for both ^{111}Cd and ^{113}Cd was solid cadmium sulphate, $CdSO_4$ (49). For ^{207}Pb the reference sample used was solid lead (II) nitrate, $Pb(NO_3)_2$ (50).

D. Sample Treatment and NMR

1. Acid Washing

Selected samples of SiC were washed with hydrofluoric acid (HF) and/or heated in a muffle furnace (see Table 2.1). HF washing experiments were carried out on HCl-washed material, using either 3 or 48% aqueous HF containing a trace of nitric acid. The samples were stirred in Teflon beakers for one to 72 hours.

^{29}Si spectra were recorded on the WH-400 instrument, the samples were pulsed every .26 seconds. ^{13}C spectra were also recorded with pulsing every .26 seconds, the AC-200 instrument was used.

2. Heating

Powdered HCl-washed SiC samples and CH_2Cl_2-washed SiC fibres were heated, at atmospheric pressure, in a muffle furnace (PDL 50) by L.Wolfe of

General Abrasive, N.Y.. About one half of a gram of each sample was in an alumina boat for the heating; 1500°C for one hour. In addition, BGW12 and BGW22 were HF-washed after the one hour heating. Another .5 g sample of BGW22 was heated for another 8 hours at 1500 °C. The samples were weighed before and after heating to determine the percent weight gain associated with oxidation, the results are given in Table 4.2.

^{29}Si MAS nmr spectra were obtained on the WH-400 instrument, the samples were pulsed at both .26 and five seconds. To ensure that no aluminum from the alumina boats was transferred to the SiC, ^{27}Al MAS nmr experiments were run on the samples; no nmr signals were detected.

E. Observable Silicon Detected in the NMR Experiment

The aim in this experiment is to elucidate the percentage of observable silicon that is detected in the nmr experiment when SiC is the sample studied. The signal intensity of SiC is compared to that of a standard sample which has 100% of the observable silicon detected.

In order to select a standard for the experiment, several criteria had to be satisfied. The standard had to have a relatively short T_1 so that the nmr signal obtained would be at a maximum intensity and the time required to do so would not be unreasonable. The nmr signal should be one sharp peak to avoid any complication from minor component signals and to achieve a good signal to noise ratio. To maintain a consistent level of detection of SiC and standard, the concentration of Si in the standard

should be comparable to that of silicon in SiC.

After some consideration hexamethyldisiloxane (HMDSO), $(CH_3)_3Si\text{-}O\text{-}Si(CH_3)_3$, was selected to be the external standard. HMDSO has a T_1 of 20.4 seconds (Chapt.V), it has one nmr peak (6.8 ppm relative to TMS) and as a pure liquid the concentration of ^{29}Si is 0.44 M. The concentration of ^{29}Si in SiC is 3.8 M. The other single peak standard considered (aqueous sodium silicate) the ^{29}Si concentration was in the order of .1 M, also, the signal was very broad.

An internal standard was used by obtaining spectra of one of the samples (BGW12A) with only one half of the amount of sample in the nmr sample spinner (BGW12B). The 3C polytype has one nmr peak, which makes it an ideal candidate for an internal standard. Any relative effects on the SiC nmr signal due to experimental or instrumental conditions would most readily be detected by differences in the one peak of the internal standard.

Four SiC samples were studied: two 6H polytype samples, BGW4 and BGW26; one 3C polytype, BGW12; and one 15R polytype, GA15. Three recycle delay times were used; 5, 30, and 300 seconds with 300, 100 and 30 scans each, respectively. The recycle delay for the standard, HMDSO, was set at $6*T_1$, 120 seconds. Like the SiC samples, spectra were recorded after 300, 100 and 30 scans.

All spectra were obtained on the Bruker WH-400 nmr spectrometer tuned to ^{29}Si. Fourier transformation was done in the absolute intensity mode so that signal intensities were directly comparable between spectra.

A summary of the data is in Appendix II.

Signal intensities were measured by cutting around the peaks on a photocopied spectrum and weighing on an analytical balance (Mettler H20). This is of similar or greater accuracy to instrumental determination when peaks are not completely resolved since allowance can be made for noise, variations in the baseline and incorrect phase setting.

F. T_1 Studies

1. Methods and Samples

Hexamethyldisiloxane (HMDSO), forsterite, Mg_2SiO_4 (RLM77), and 3C SiC (BGW12) were all used to study the ^{29}Si spin-lattice relaxation time (T_1). Two methods were used; the conventional inversion-recovery method (6) and a variation on the steady state method, Driven Equlibrium Single-Pulse Observation of T_1 or DESPOT (51). All inversion recovery and DESPOT experiments were conducted on the Bruker AC-200 instrument.

2. DESPOT

DESPOT (51) requires a series of non-sampling pulses followed by sampling pulses:

$$(\theta\text{-ti})_I\text{-}(\theta\text{-A-ti})_N$$

where I and N are the number of non-sampling and sampling scans, respectively. θ is the pulse angle to be used. The experimental delay time, ti, was chosen using an approximated T_1 value such that:

$$ti/\ T_1 = .1 \text{ to } .5.$$

The required number of non-sampling or dummy scans for an experiment were determined using the equation:

$$\ln(M_o - M_z) = -ti/T_1 + \ln(M_o - M_i \cos\theta)$$

to satisfy the equality:

$$M_z = 0.995\ M_i$$

Where M_z is the magnetization in the z direction of the applied magnetic field, M_o is the equilibrium magnetization and M_i is the magnetization at the start of the i^{th} cycle, starting from M_o.

Delay times used for HMDSO were two or four seconds, with 20 dummy scans, 100 sampling scans, and eight to ten different pulse angles a typical experiment took no longer than 80 minutes. A similar number of scans were used for RLM77 but delay times were either 0.8 or 1.6 seconds, therefore an experiment would only take about 20 minutes. A number of different delays were used for the SiC sample, BGW12, ranging from 30 to 1200 seconds. The number of scans used were appropriate to give a good

signal to noise ratio. An experiment using the former delay would last about two hours, the latter lasted four days.

3. Inversion-Recovery

^{29}Si inversion-recovery (180-T-90) experiments were run on RLM77 and BGW12 to test the use of the method in studying the T_1's of solids and the reliability of DESPOT. The T_1 of HMDSO was also determined for use in the study of the percentage of observable silicon detected.

Bracketing T values of 0.05 to 60 seconds with a delay of 300 seconds was initially used for HMDSO. A focusing experiment was set up with bracketing T values from 15 to 30 seconds, with a delay of 120 seconds.

A number of inversion-recovery experiments were run on RLM77 with T values ranging from 0.05 to 120 seconds and a delay time of 300 seconds. One inversion-recovery study was carried out on BGW12 bracketing T values were 1 and 600 seconds, the delay used was 900 seconds. The study on BGW12 took 96 hours (4 days), a typical RLM77 experiment would take 3 days.

G. Single Crystal NMR

A single crystal nmr study of both the ^{13}C and ^{29}Si chemical shifts

Figure 2.1: Diagram of a glass insert as used in the single crystal nmr experiment to set the orientation angle, θ.

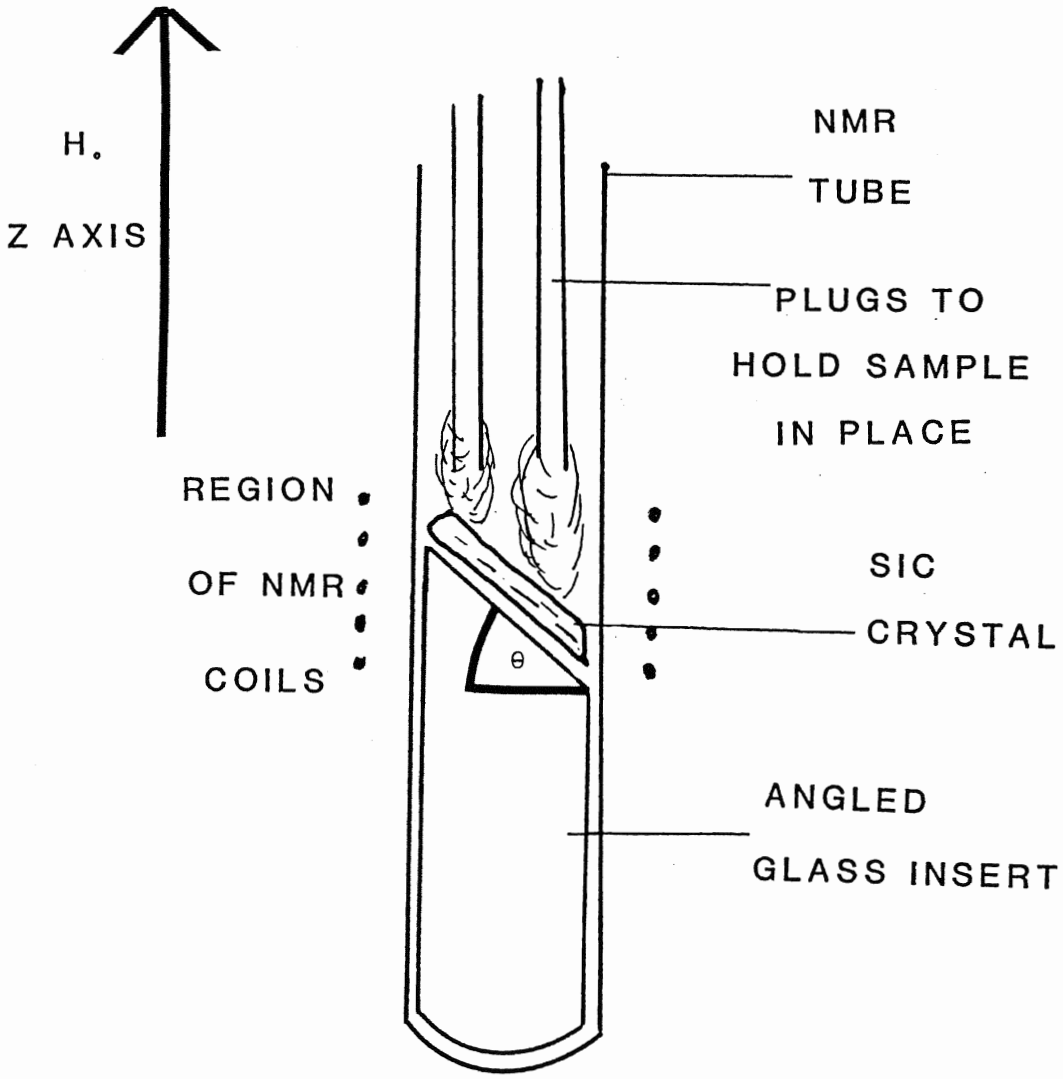
H.
Z AXIS
REGION
OF NMR
COILS
NMR
TUBE
PLUGS TO
HOLD SAMPLE
IN PLACE
SIC
CRYSTAL
θ
ANGLED
GLASS INSERT

of 6H SiC was performed on BGW51. The nmr experiments were done using the Bruker AC-200 instument and the standard Bruker broad brand probe (non-Magic Angle Spinning).

The blue-black plate-like crystal of dimensions 10 x 5 x 3 mm was selected for size and shape. Single crystal XRD analysis identified the sample to be the 6H polytype (Table 2.1). The crystal was oriented with the six-fold axis of rotation (the c axis, perpendicular to the flat face) relative to the z axis of the applied magnetic field. Spectra were acquired with the crystal oriented at 15^{o} intervals, from 0 to 105^{o}, using angled glass inserts in a 10mm nmr tube (Figure 2.1).

For ^{13}C nmr spectra, the sample was given pulsed every five seconds, 11,700 transients were acquired. To circumvent the probe background interference while running ^{29}Si nmr spectra (quartz, -110 ppm) the sample was pulsed every 30 seconds, 1800 transients were acquired. ^{13}C and ^{29}Si MAS nmr spectra were also obtained of the powdered HCl-washed sample, to obtain the experimental isotropic chemical shifts of BGW51.

H. Investigation of Other Material for Further Studies On Polytypism

Using the Bruker AC-200 nmr instrument, an MAS nmr study was conducted on some inorganic material. ^{111}Cd and ^{113}Cd MAS nmr spectra of the following materials were obtained; $CdCl_2$, $CdBr_2$, CdI_2. ^{207}Pb MAS nmr spectra of $PbCl_2$ and $PbBr_2$ were also obtained. Unsuccessful attempts were

made to record the MAS nmr spectra of PbI_2. All of the chemicals were from Aldrich Chemical Co..

Chapter III

NMR OF BULK SILICON CARBIDE

A. Introduction

As previously mentioned, the nmr chemical shift of a species is dependant upon its local environment (see section I.B.2). Due to the rigid nature of the lattice of a crystalline network system, it can be very straight forward to understand the local environment of the nuclei in a solid as opposed to a solution. There are many examples of MAS nmr and crystallographic determinations being used jointly to study the structure of crystalline material. This is a logical union of the two techniques because information is mutually useful in both studies. Such applications were alluded to earlier (section I.A); zeolite and glass studies, for example.

Where crystallographic data were lacking in the identification of Si/Al ratios in zeolite A, a particular zeolite modification, C.S.Blackwell *et al* (52) used ^{29}Si MAS nmr to decidedly solve the problem. Aluminum was used to replace silicon in the silicate structure, the degree and manner of silicon replacement was a source of much debate. Both

aluminum and silicon have similar scattering factors, limiting x-ray determinations. However, silicon and aluminum can be studied independently by nmr. From the nmr data specific silicate sites in the zeolite lattice were identified and the Si/Al ratios were easily calculated.

There are many models proposed for the structure of silicate glasses; the random network theory (53), discrete ion theory (54), and the strained-mixed-cluster model (55). Combined ^{23}Na and ^{29}Si MAS nmr and XRD studies by R.Dupree *et al* (56) were used to show that the addition of cations to silicate glasses stoichiometrically randomizes the silicate tetrahedra. This work provided evidence in support of the random network model and showed, in this case, that cations do not cluster. Later work by C.M.Schramm *et al* (57) came to similar conclusions using ^{29}Si MAS nmr to study lithium silicates.

Prior work by Hartman *et al* (39, 40) used ^{13}C and ^{29}Si MAS nmr spectra of various polytypes of SiC (3C, 6H, and 15R) to study the polytypic nature of SiC. Three silicon (and carbon) sites in SiC were characterized using next-nearest neighbour calculations from a chosen atom. These sites were then used to explain the ^{13}C and ^{29}Si nmr spectra of the SiC samples studied. Upon further consideration, using layer models with the next-nearest neighbour calculations it can be shown that there are in fact four sites, and even more are possible (58). More

samples have been studied to test the concept of peak correlation with the silicon/carbon site calculations.

B. Results

Long pulse delay MAS nmr spectra have been obtained (or attempted) for a number of SiC polytypes and samples; two amorphous, two 3C polytype, six 6H polytype, and one 15R polytype. The results of the long pulse delay acquisitions are shown here because they best represent the bulk sample; the delays used are 5 and 15 minutes between pulses, the amorphous samples were pulsed every five to thirty seconds. No further increase in delay time was attempted for the ^{13}C or ^{29}Si MAS spectra due to the limited instrument time available.

The ^{29}Si MAS nmr spectra of the 6H samples all had three peaks that were equal in intensity, indicative of three Si sites. The 6H chemical shifts are; -14.3 $\pm$ 0.4, -20.4 $\pm$ 0.3, -24.7 $\pm$ 0.2 ppm. Similarily, the ^{13}C MAS nmr signals are of equal intensity. The 6H ^{13}C MAS nmr chemical shifts are; 23.3 $\pm$ .4, 20.4 $\pm$ .2, and 15.4 $\pm$ .2 ppm. The best example of a ^{13}C and ^{29}Si spectrum, which is representative of all of the 6H samples is given in Figure 3.1.

Figure 3.1: MAS nmr spectra of GA10, 6H silicon carbide.

a) ^{13}C, 100.57 MHz. Recycle delay, 15minutes.

b) ^{29}Si, 79.46 MHz. Recycle delay, 5 minutes.

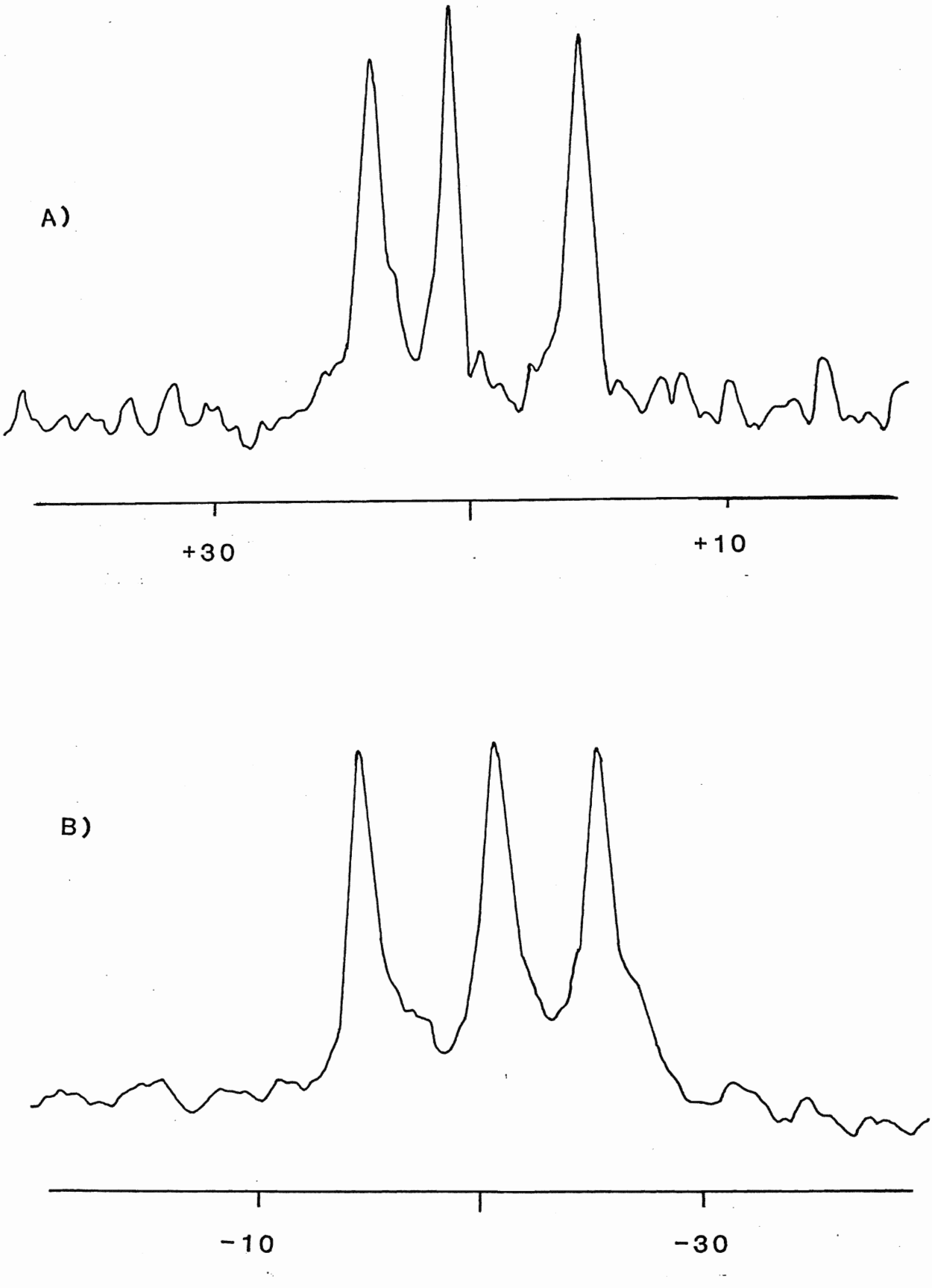
A)
+30
+10
B)
-10
-30

There was only one 15R polytype sample available which gave clean nmr spectra (Figure 3.2). The ^{29}Si MAS nmr spectrum has three peaks with similar shifts to those of the 6H samples (-15.3, -21.0, -24.7 ppm), the peak intensities are 1:2:2. The ^{13}C MAS nmr spectrum has four signals, the lowfield peaks have approximately the same chemical shifts as the 6H polytype (22.7, 20.7, 16.0). The species that is characterized by the upfield peak, 13.3 ppm, as yet has not been identified. The peak intensities are 1.9 : 1.5 : 1.5 : 1 (low to high field).

The spectra in Figure 3.3 are of BGW39 which, according to its powder pattern photograph, is predominantly 6H with weak bands that may correspond to 15R. However, BGW39 does not have a 2.11 A band which appears in the 15R powder pattern. Figure 3.3a is the ^{29}Si MAS nmr spectrum and Figures 3.3b and c are the ^{13}C MAS nmr spectra. Figures 3.3a and b were taken on the 4.7 Tesla instrument and the confirmatory spectrum, Figure 3.3c, was obtained on the 11.7 Tesla instrument.

The shifts of the three peaks that seem to be 6H in the ^{29}Si spectrum are -14.7, -20.8, and -24.7. Due to overlap the exact intensities of the peaks are not ascertainable. The relative intensity of the peak at -14.7 ppm to the cluster of highfield peaks is 1 : 4.8. The ^{13}C spectrum obtained on the 11.7 Tesla magnet shows six peaks; 23.8, 22.9*, 22.1*, 21.0, 16.0 and 14.8*. (The asterisked peaks appear to be less intense and are likely 15R peaks). As in the ^{29}Si spectrum, the peak intensities can not be determined; however, the relative intensity of the low to

Figure 3.2: MAS nmr spectra of GA15, 15R silicon carbide.

a) ^{13}C, 125.76 MHz. Recycle delay, 15 minutes.
b) ^{29}Si, 79.46 MHz. Recycle delay, 5 minutes.

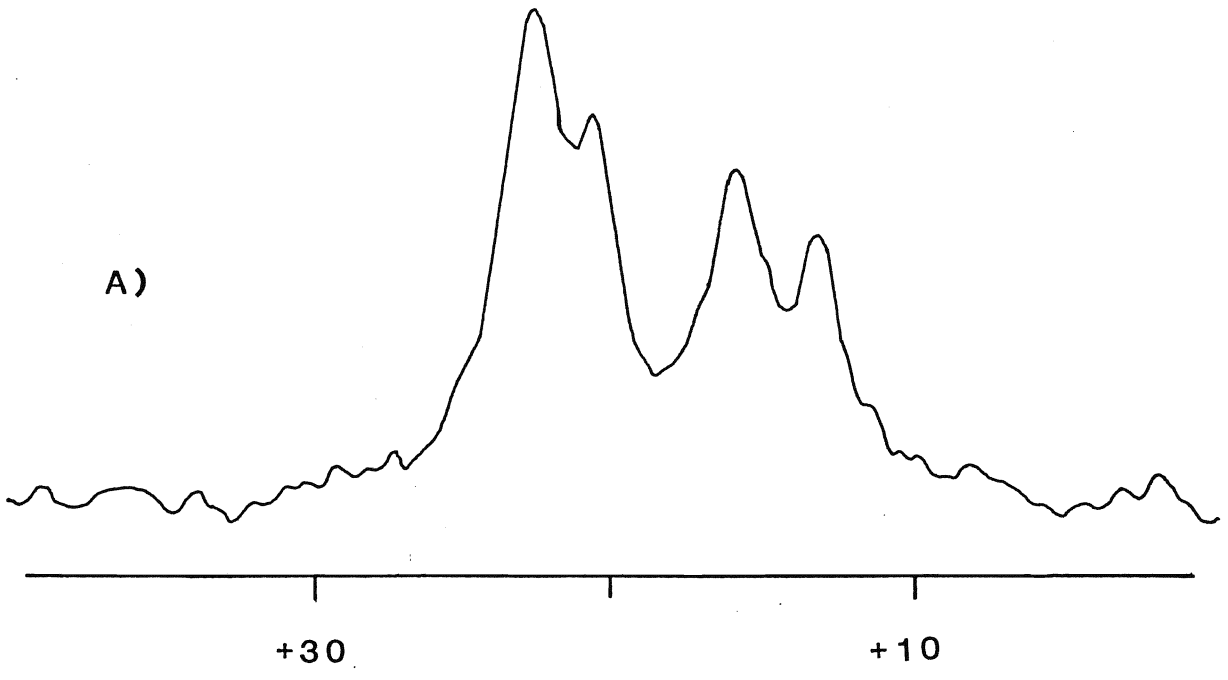
A)
+30
+10

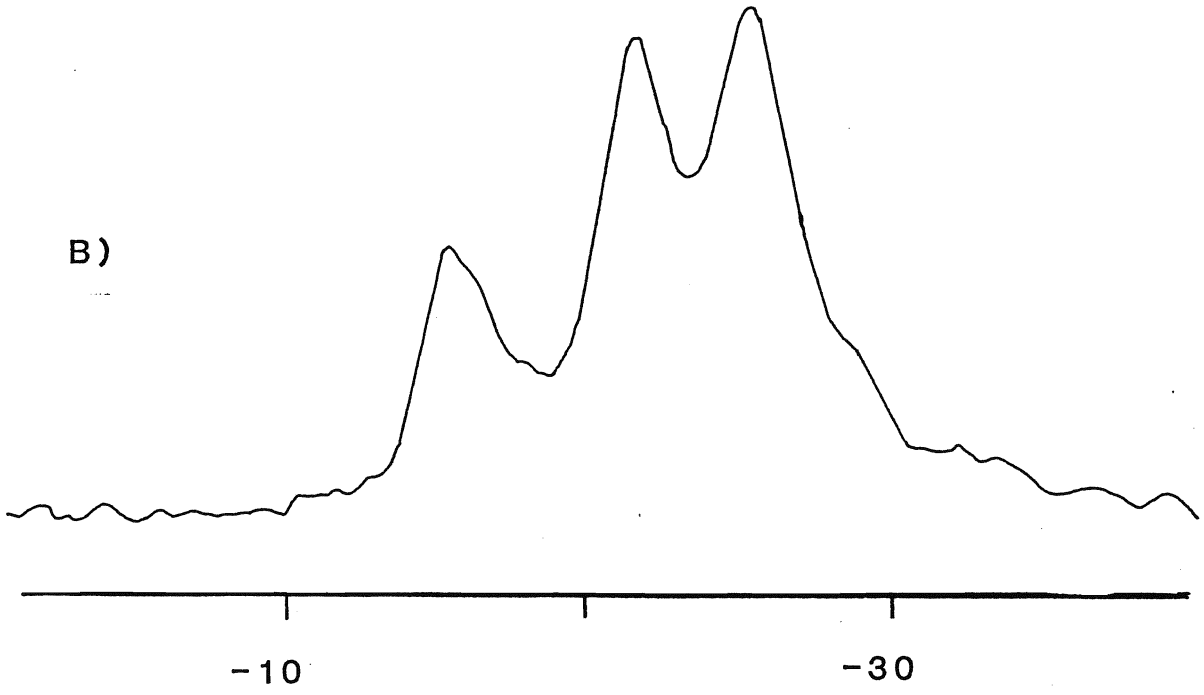
B)
-10
-30

Figure 3.3: MAS nmr spectra of BGW39, 6H silicon carbide with some other polytype impurity.

a) ^{13}C, 50.32 MHz. Recucle delay, 5 minutes.

b) ^{13}C, 125.76 MHz Recycle delay, 15 minutes.

c) ^{29}Si, 79.46 MHz. Recycle delay, 5 minutes.

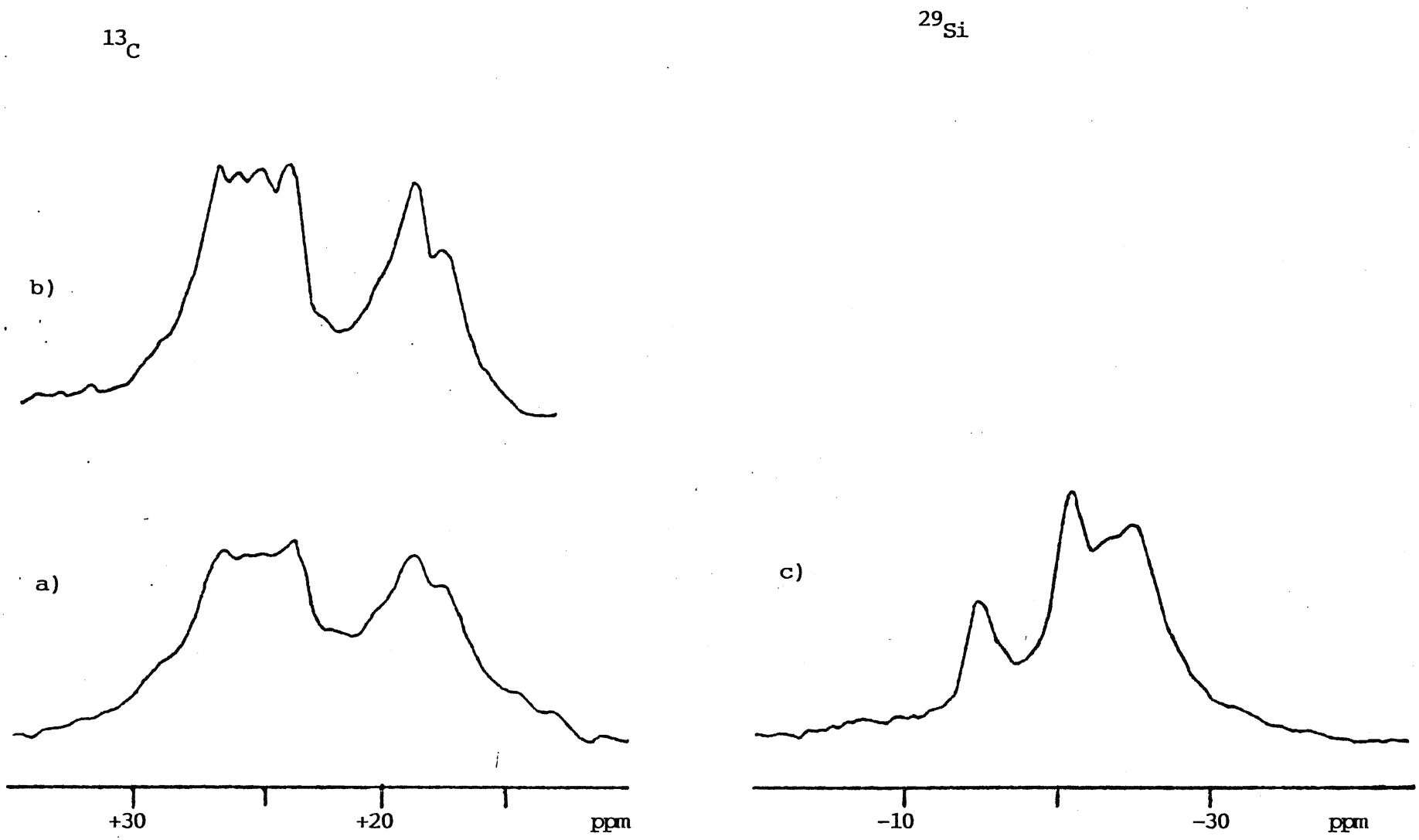
^{13}C
b)
a)
+30
+20
ppm
^{29}Si
c)
-10
-30
ppm

high field clusters of peaks is 1.4 : 1.

The 3C polytype ^{29}Si spectrum (Figure 3.4) has only one peak at -18.8 ppm. No ^{13}C MAS nmr spectrum has been recorded as yet, despite many attempts. Some of the acquisition conditions were: multiple 30° pulse accumulations over 12 hours with 5, 300, and 900 second delays between pulses (9.4 tesla instrument), a single 90° pulse after 12-16 hours in the magnetic field (9.4, and 11.7 tesla instruments) as well as 16 and 62 hours in the 4.7 tesla magnetic field.

The ^{13}C and the ^{29}Si MAS nmr spectra of the amorphous SiC (Figure 3.5) both have only one broad featureless signal. The ^{29}Si shift is -14.5 and the ^{13}C shift is 25 ppm for the Nicalon ceramic fibres (BGW33). The Union Carbide sample (UCSiC) has ^{29}Si and ^{13}C chemical shifts of -15.9 and 19 ppm, respectively. The ^{29}Si peak width at half height of BGW33 and UCSiC is 18 ppm (9.4 tesla instrument) and 16 ppm (4.7 tesla instrument) for the ^{13}C signal. When the sample is pulsed very rapidly, every .26 seconds, the ^{13}C signal broadens to 58 ppm. Given the linewidths of these peaks, the difference in peak positions between the two amorphous samples is not significant.

The chemical shifts and powder patterns are summarized in Tables 3.1 and 3.2, respectively.

Figure 3.4: ^{29}Si MAS nmr spectrum of BGW12, 3C silicon carbide; 79.46 MHz. Recycle delay, 5 minutes.

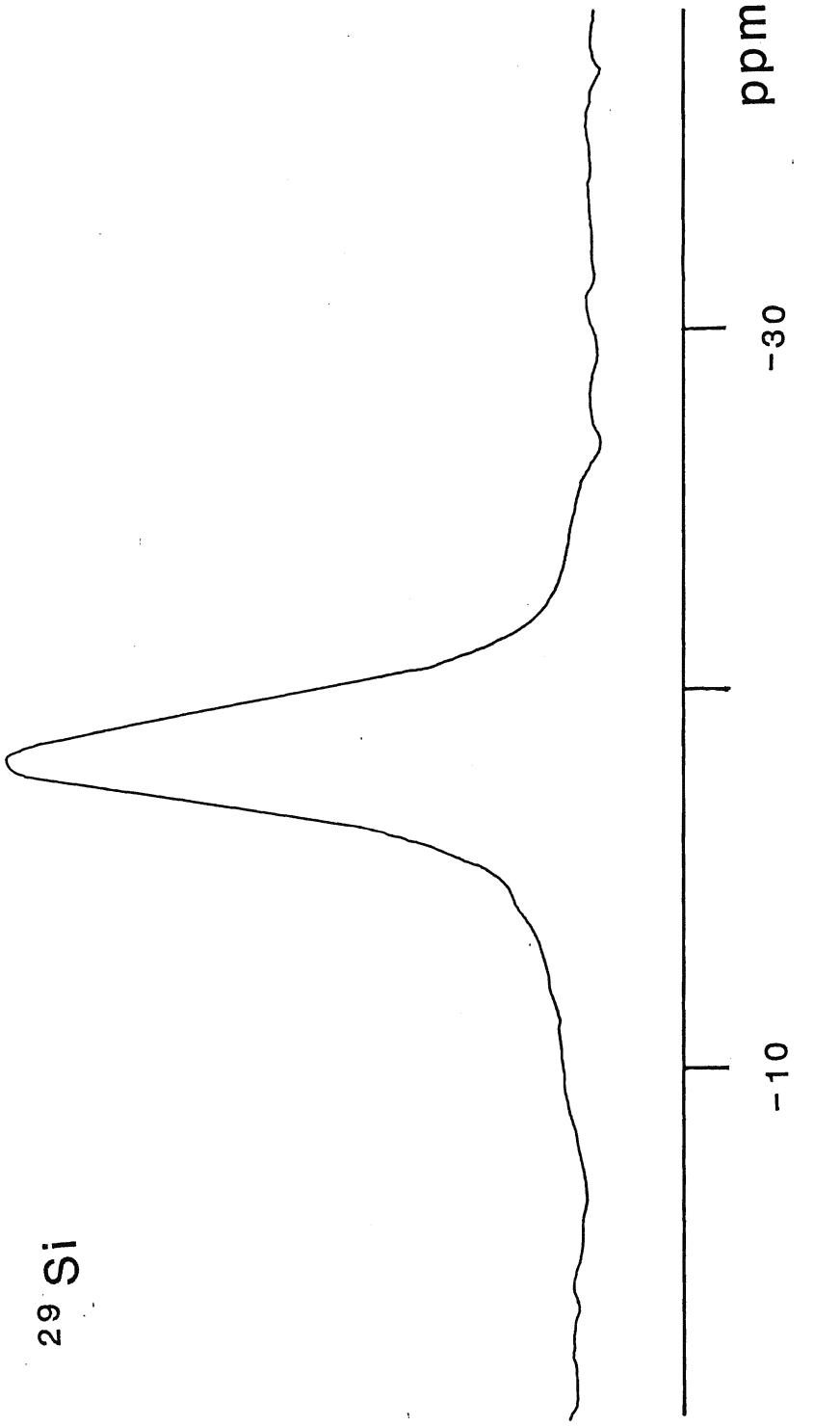
^{29}Si
-10
-30
ppm

Table 3.1 : Chemical Shift Summary.

Sample	Poly-type	^{29}Si Chem.Shifts	Rel. Int.	^{13}C Chem.Shifts	Rel. Int.
SiC1	6H	-13.9,-20.1,-24.5	1:1:1	23.2, 20.2, 15.2	1:1:1
SiC5	6H	-13.9,-20.4,-24.6	1:1:1	22.9, 20.5, 15.2	1:1:1
SiC6	6H	-14.2,-20.4,-24.6	1:1:1	23.3, 20.2, 15.2	1:1:1
BGW39	6H	-14.7,-20.8,-24,7	a	23.8, 21.0, 16.0[b]	a
BGW48	6H	-14.7,-20.7,-24.9	1:1:1	23.6, 20.6, 15.5	1:1:1
GA10	6H	-14.2,-20.2,-24.8	1:1:1	23.7, 20.7, 15.7	1:1:1
GA15	15R	-15.3,-21.0,-24.7	1:2:2	22.7,20.7,16.0,13.3	c
SiC2	3C	-18.8		-	
BGW12	3C	-18.8		-	
BGW33	AM	-14.5 ($W_{1/2}$ 18 ppm)		25 ($W_{1/2}$ 16 ppm)	
UCSiC	AM	-15.9 ($W_{1/2}$ 19 ppm)		19 ($W_{1/2}$ 12 ppm)	

a = Poorly resolved peaks.

b = There are also three other minor peaks; 22.9, 22.1, 14.8.

c = Intensity is 1.9 : 1.5 : 1.5 : 1.0

AM = Amorphous

Table 3.2 : d Spacings For Various SiC Polytypes.

3C*		6H*		15R*		BGW39	
d (A)	I	d (A)	I	d (A)	I	d (A)	I
				2.66	45		
				2.58	80	2.59	S
		2.61	75				
2.51	100	2.51	80	2.51	80		
				2.40	65		
		2.36	60			2.36	S
				2.32	55		
2.17	20	2.19	50	2.19	10	2.18	VW
				2.11	35		
		2.00	35				
				1.97	10		
				1.70	20		
		1.67	35			1.68	W
				1.59	55	1.60	VW
1.54	63	1.54	100	1.54	100	1.54	S

Table 3.2 continued

3C*		6H*		15R*		BGW39	
d (A)	I	d (A)	I	d (A)	I	d (A)	I
				1.44	55	1.45	VW
		1.42	60			1.42	M
				1.40	45	1.41	VW
		1.33	35				
				1.32	20		
1.31	50	1.31	100	1.31	90	1.31	S
				1.30	20		
		1.29	35			1.29	W
				1.28	20		
1.26	5			1.26	20		
		1.25	35	1.25	10	1.25	W
		1.22	25				
				1.14	10		

* = From reference 64.

Figure 3.5: MAS nmr spectra of BGW33, amorphous silicon carbide.

a) ^{13}C, 100.57 MHz. R.D., 30 seconds.

b) ^{29}Si, 79.46 MHz. R.D., 30 seconds.

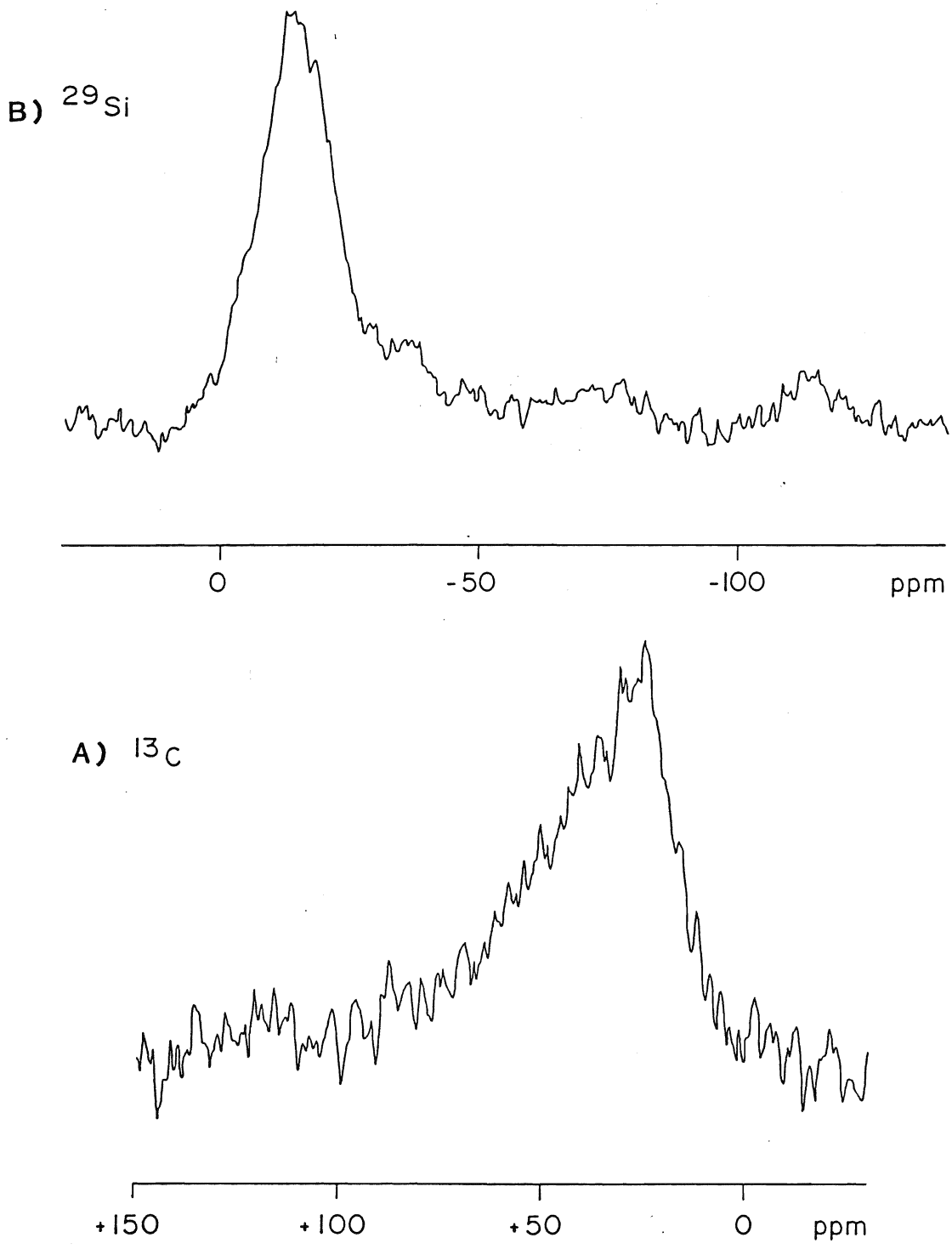
B) 29Si
0
-50
-100
ppm
A) 13C
+150
+100
+50
0
ppm

C. Discussion

1. SiC Geometry

Since the chemical shift of a nucleus is dependent upon its local environment, the analysis of the chemical shifts of SiC must therefore begin with an understanding of the SiC crystal structure. A lot of crystallographic data has been published on SiC (25) and an especially detailed x-ray structure determination of the 6H polytype was done by A.H.Gomes de Mesquita (59).

For simplicity, the focus will be on silicon, with the understanding that the same holds true for carbon because of the one to one silicon to carbon relationship in SiC. By using the SiC unit cell dimensions ($\underline{a}$ = $\underline{b}$ = 3.08 A), layer spacings (2.52 A), and the lattice point coordinates of the different polytypes (60 and Table 1.1), the number and distances of the next nearest neighbours from a chosen central silicon can be calculated.

The first co-ordination sphere around each silicon has four carbon atoms. According to Gomes de Mesquita (59) there are actually three silicon sites in the 6H polytype, each site has three shorter Si-C bonds (1.885 - 1.886 $\pm$ 0.002 A) and one longer Si-C bond parallel to the stacking, $\underline{c}$, axis (1.891 - 1.894 $\pm$ 0.002 A). The Si-C-Si bond angles are in the range 109.4 - 109.5 ^{o}. The nmr chemical shift is not accurate to

distinguish between such small differences in distance (61,62) so at the first co-ordination sphere all silicon sites are considered to be equivalent and Si-C bond lengths are taken, within experimental error, to be 1.89 A apart.

Consider Table 3.3 where the next nearest neighbours of a central silicon have been calculated out to 5.00A. With three possible layers or hexagonal close packed structures (A,B,C) stacked, in the allowed positions (no like layers adjacent), there are eight possible silicon sites. The primed types have the same distances and neighbours as the unprimed types, and are related by a 60 degree rotation about an axis parallel to the hexagonal c axis (the six-fold axis of rotation). So there are in fact only four silicon sites to 5.00A (Figure 3.6). Each silicon in a layer is of the same type, the asterisked B layer in the table is the layer for which the calculations are carried out. For the calculations, the standard orientation was with the corresponding carbon layer directly above the silicon layer. (The neighbours and distances are the same for carbon, switch carbon for silicon and vice versa.) To obtain the same neighbours and distances for the A and C layers, accordingly substitute using the cyclical ABC relationship ie. BCBA = ABAC = CACB.

The assumption here, is that the shielding effect of the neighbouring atoms in the nmr experiment does not go past the outer layer of carbon atoms at 4.75 A. It is interesting to see

Table 3.3: Silicon Surroundings in SiC Polytypes; Out to 5 A.

Layer Type & Sequence	Neighbours	Geometry	Distance to Central Si
a' = CB*AC	4 C	Tetrahedron	1.89 A
a = AB*CA	12 Si	Cuboctahedron	3.08
	12 C	No Established Name	3.61
	6 Si	Octahedron	4.36
	12 C	No Established Name	4.75
b' = CB*CA	4 C	Tetrahedron	1.89
b = AB*AC	12 Si	Eclipsed 3:6:3	3.08
	12 C	No Established Name	3.61
	6 Si	Trigonal Prism	4.36
	12 C	No Established Name	4.75
c' = CB*AB	4 C	Tetrahedron	1.89
c = AB*CB	12 Si,1 C	Capped Cuboctahedron	3.08, 3.15
	9 C	No Established Name	3.61
	6 Si	Octahedron	4.36
	6 C	Hexagon	4.40
	9 C	No Established Name	4.75
d' = CB*CB	4 C	Tetrahedron	1.89
d = AB*AB	12 Si,1 C	Eclipsed 3:6:3,capped	3.08, 3.15
	9 C	No Established Name	3.61
	6 Si	Trigonal Prism	4.36
	6 C	Hexagon	4.40
	9 C	No Established Name	4.75

Figure 3.6: Diagram of the first and second neighbour layers about each of the four site types of silicon and carbon in silicon carbide, (58).

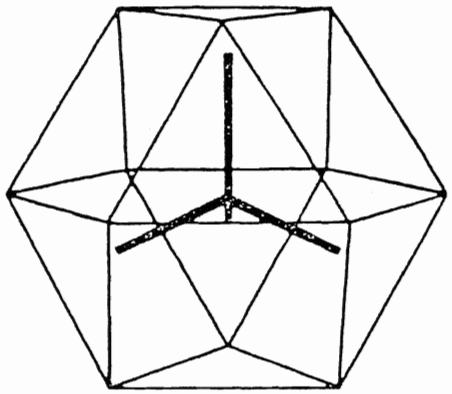

TYPE a

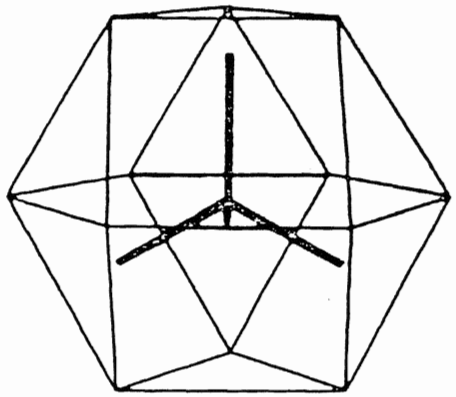

TYPE b

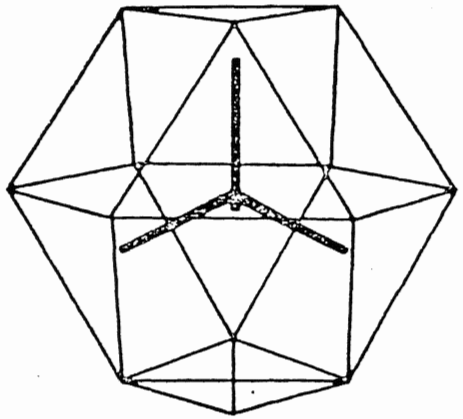

TYPE c

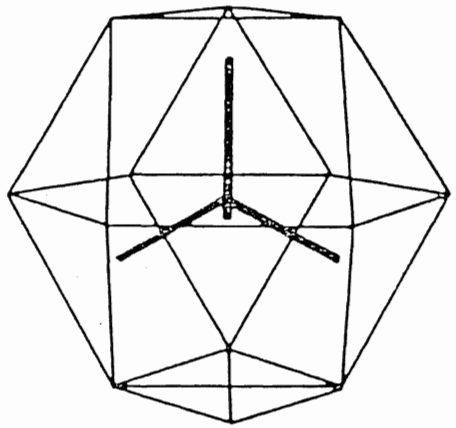

TYPE d

how the site types differentiate as layers farther away from the central silicon are taken into consideration. An additional silicon layer on either side of the central silicon atom is within 5.02 A of the atom. At that point the neighbour geometries of types c and d have two possibilities ; there are then six possible silicon sites. At 5.60A a carbon layer is also within range of the central silicon atom and types a and b are each split into two geometries; the total number of possible silicon sites is now eight. Finally, at 7.50A all of the eight sites further branch into two geometries, 16 possible silicon sites (Figure 3.7) (58).

Using the Table 3.3 nearest-neighbour stacking sequence, the number of crystallographically independent silicon sites in the given polytypes can be determined (Table 3.4). Also listed are the expected number of nmr peaks (based on silicon type regardless if primed or not) and corresponding relative intensities (using relative abundance). Note that site type d is the only silicon type in the 2H polytype, and site type a is the only one in the cubic polytype.

Another important feature to note is that for each b site in a polytype there is always a c site. Consider the Ramsdell zig-zag sequence (33), which is viewed along the (110) plane, in Figure 3.8. Silicon site b four layer sequence involves a clockwise "zig" and the c site four layer sequence involves a

Figure 3.7: Layers surrounding an arbitrary central layer of silicon atoms (58). The 5A sphere does not quite reach the silicon layers at $\pm$ 5.04 A. The 5.6 A sphere stops short of the carbon layer at $\pm$ 5.67 A, and the 7.5 A sphere stops short of the silicon layers at $\pm$ 7.56 A.

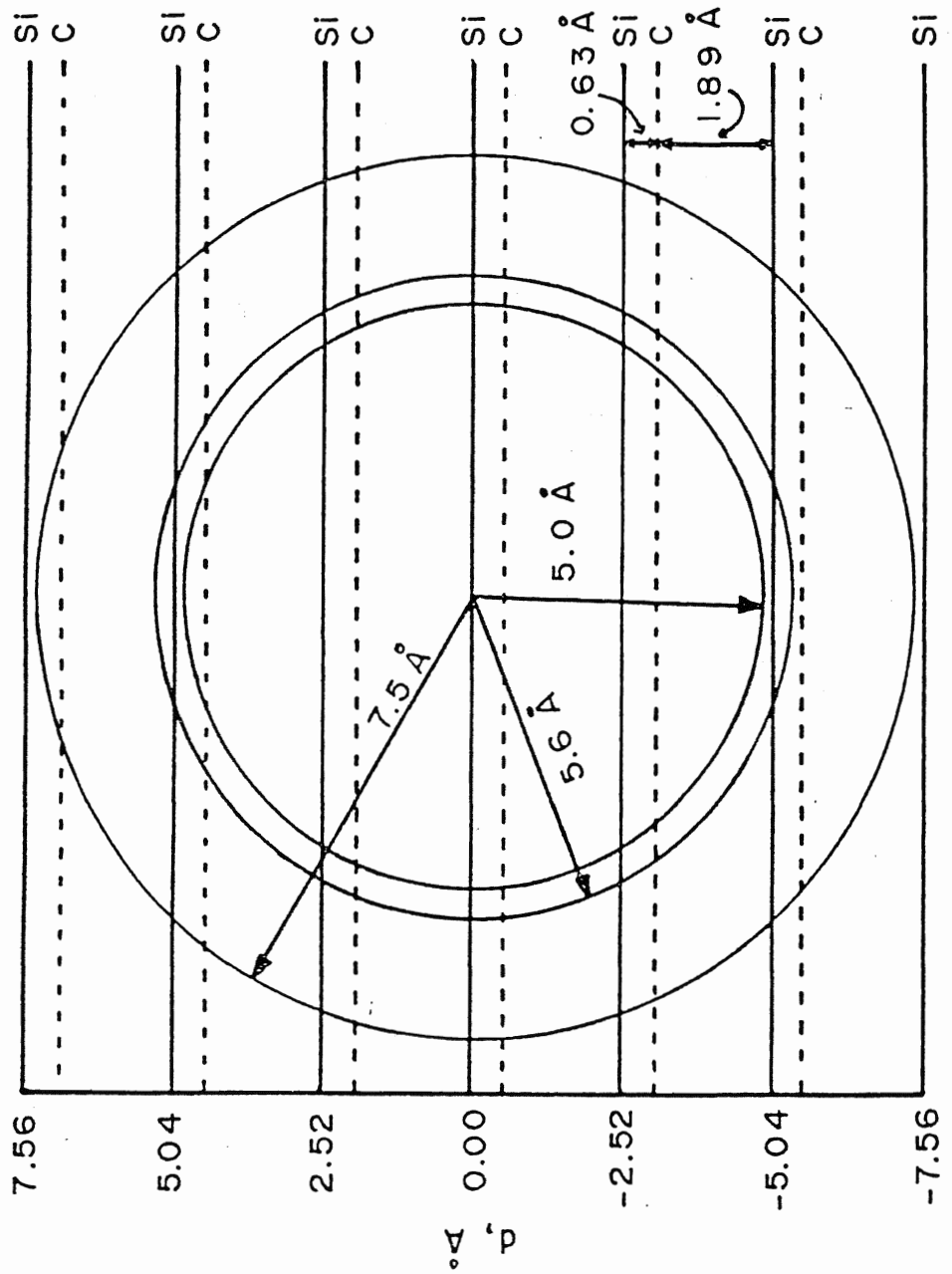
Si
C
0.63 Å
1.89 Å
5.0 Å
7.5 Å
5.6 Å
7.56
5.04
2.52
0.00
-2.52
-5.04
-7.56
d, Å°

Table 3.4 : Categorized Types of Si Sites In Some SiC Polytypes

Polytype	Sequence	Si Type	#cryst. indep. Si in polytype	#equivalent nmr types (rel.abun)
2H	/AB/AB..	dd'	1	1
3C	/ABC/AB...	aaa	1	1
4H	/ABAC/ABA..	cb'c'b	2	2 (1:1)
6H	/ABCACB/ABC..	b'acba'c'	3	3 (1:1:1)
9R*	/ABCBCACAB/AB..	b'cdb'cdb'cd	3	3 (1:1:1)
15R	/ABCBACABACBCACB/	b'cba'c'b'cb' a'c'b'cba'c'	3	3 (1:2:2)

* = From reference 65.

Figure 3.8: Zig-zag sequences for the four possible types of silicon (and carbon) sites in silicon carbide (58). Carbon atoms have been omitted for simplicity.

Type a: BCAB

Type b: CBAB

Type c: ACAB

Type d: ABAB

Type a

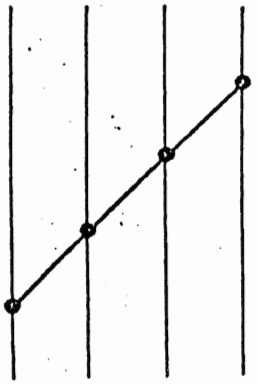

Type b

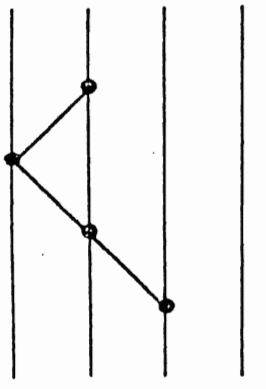

Type c

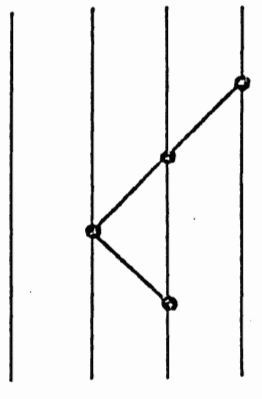

Type d

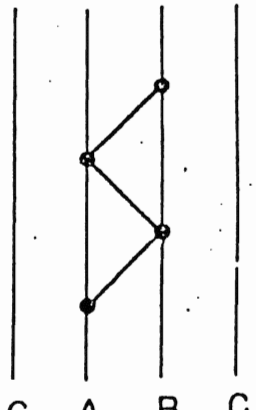

concommittant counter-clockwise "zag". The two four layer sequences are needed to be paired in order to maintain the polytype sequence. A further treatment of this uses Zhdanov symbols to explain the b and c site relationship (58).

2. NMR

Note that the ^{13}C and ^{29}Si MAS nmr spectra are mirror images of eachother, almost exactly to the chemical shift. Recall that the reference sample for both nuclei is tetramethylsilane, $Si(CH_3)_4$ (TMS). Structurally TMS is similar to SiC, which is a tetrahedral arrangement of sp^3 hybridized carbon atoms about an sp^3 hybridized silicon atom. The SiC has a network of alternating silicon and carbon atoms in place of the TMS hydrogens. The heavier, more shielded silicon nuclei will appear upfield of TMS, and the lighter, less shielded carbon, will be to lower field in the nmr spectrum. Since silicon is isostructural with carbon in SiC, any effects on shielding should be observed for both nuclei in the chemical shift in their respective nmr spectra.

Both the ^{13}C and ^{29}Si MAS nmr spectra of the amorphous SiC samples have one very broad featureless signal. As the term amorphous implies, there is no regular structure in the SiC

sample. The peak widths of the SiC signal for both nuclides is roughly 18 ppm; representative of a distribution of a number of silicon/carbon environments. This is analagous to glasses which are considered to be fast frozen liquid (57). During the SiC synthetic process, if the sublimated carbon and silicon atoms condense too quickly, the conditions will not be conducive of proper crystal formation. Hence, random bond lengths and angles of linked silicon and carbon tetrahedra will be produced. Therefore, the nmr spectra are a representation of a large number of silicon (and carbon) sites which have different environments because the number of next nearest neighbours and their distances all vary.

Consider the information available for the 15R polytype. The ^{29}Si spectrum has three peaks 1:2:2 and the ratio of silicon sites in 15R is 1:2:2 for a:b:c (Table 3.4). Quite reasonably, from these observations, the two more intense peaks to higher field in the ^{29}Si nmr spectrum can be designated as the b and c silicon sites and the low field peak as silicon site a.

The chemical shift for the site a peak is -14.9 ppm. As a comparison, the 6H polytype the chemical shift for the corresponding lowest field peak is -14.3 $\pm$ .4 ppm. Since the chemical shifts of the 6H and 15R polytypes are similar, it is feasible to label the peaks in the 6H spectrum in the same way; the lowest field peak as site a and the two higher field peaks as

sites b and c.

Further evidence for the identification of the silicon sites comes from the ^{29}Si nmr spectrum of the 3C polytype. The only silicon site in the 3C polytype is site a; less than coincidentally the ^{29}Si nmr spectrum has only one peak, at -18.8 ppm. This chemical shift is to higher field than the other a site peaks for the other two polytypes. This is not unexpected and indicates that a different shielding anisotropy is experienced by the 3C polytype nuclei. The 3C polytype, which is the cubic polytype, is the only SiC polytype with all four Si-C bonds equidistant in the first co-ordination sphere, whereas there are three short and one long Si-C bonds in the other polytypes (59). Such a difference in bond lengths will have a marked effect on the chemical shift, as observed (61).

As for the silicon b and c sites, they are identified as the two high field peaks in the ^{29}Si 15R nmr spectrum because their relative intensities are equivalent, as earlier proposed. The chemical shifts are -20.8 and -24.4 ppm. With the thought that the chemical shifts for silicon sites do not grossly change with polytype, the 6H chemical shifts for the b and c silicon sites are designated as $-20.4 \pm .3$ and $-24.7 \pm .2$ ppm.

Contrary to the ^{29}Si nmr spectrum, consistent with the mirror image relationship, the ^{13}C nmr spectrum of 15R has the least intense peak at highest field. This would most likelybe the

carbon a site, as in silicon. The chemical shifts of the high field peaks for the 6H and 15R polytypes are 15.4 $\pm$ .2 and 16.0 ppm, respectively. The highest field peak in the 6H spectrum is probably also representative of the carbon a site. No ^{13}C nmr spectra have been obtained for the 3C polytype so confirmation of this assignment is still needed.

It is understandable that the 3C ^{13}C nmr signal is very difficult to observe. The spin-lattice relaxation time, T_1, of SiC is very long (see Chapter V). In agreement with this, the carbon T_1 of diamond is about 6 hours (63). The significance of this is the similarity in structure between SiC, 3C in particular, and diamond. SiC is often described as a diamond structure, which is cubic, with half of the carbon atoms replaced by silicon atoms.

Comparison of the 6H and 15R lower field peaks in the ^{13}C nmr spectra further indicates the similarities between the nmr spectra of the two polytypes. The chemical shifts are 23.3 $\pm$ .4 and 20.4 $\pm$ .2 ppm for the 6H polytype and 22.7 and 20.7 ppm for the 15R polytype. Like the silicon spectra, these peaks are considered to represent the carbon b and c sites.

Unfortunately, there is no readily obvious means of differentiating between the b and c sites in either the ^{13}C and ^{29}Si nmr spectra. Up to 4.75 A from a central atom calculations show that there are only four sites. However, at 5.02 A the c

sites branch to two different geometries. If resolution was good enough or the nmr instrument more sensitive (use a larger magnet) perhaps a broadening or splitting of the c site peak could be observed.

Another thought towards the identificaton of the specific b and c sites involves the use of Table 3.3. Sites a and b are the most similar with respect to next-nearest neighbour relationships, as sites c and d are to each other. This may be the basis for suggesting that the peak next to the a site peak is the b site peak.

Finally, consider the fourth peak at highest field in the ^{13}C nmr spectrum of the 15R sample (13.3 ppm). The original thought was that this peak is the 15R c site where the two different geometries are possible if detection is out to 5.02 A from the observed nucleus because the 20.7 ppm peak seems to be at a weaker intensity than expected. If this were true, it would mean two things. First, the proposal that the peak at 20.7 is site b is incorrect. Second, a nucleus that had a chemical shift at 20.7 ppm should now be detected at 13.3 ppm (a difference of 6.9 ppm !) simply because a geometrical difference at 5.02 A could be detected.

If this peak is not a "branched" c site, then there are two possible explainations for the peak; it is either an impurity or a new carbon site, independent of the other sites. The peak

may be an impurity, but it seems, from experience, that impurities are detected at short delays and with many scans, where the SiC signal is weak because of its long T_1. There are only 61 scans for the 15R sample with 15 minutes between pulses, the extra peak is observed only under these conditions of long recycle delay between pulses in the ^{13}C nmr spectrum. This indicates that the species corresponding to this peak has a long T_1 as in an ordered crystalline sample, which may be due to a separate crystal or a stacking fault in the SiC sample.

This may only be circumstantial evidence, but the apparent loss of intensity in the 20.7 peak in the 15R ^{13}C nmr spectrum may be an indicator of crystal defects. Crystallographic data seems fine; there are no apparent distortions or extra bands in the x-ray powder pattern photograph of GA15 to indicate the presence of impurities. The extra peak is most likely due an entirely separate crystalline entity.

In the case of BGW39, Figure 3, it appears that there is a mixture of polytypes present in the sample; major component 6H and a minor unidentified component. The latter appears to be SiC from the crystallographic and nmr data. It is somewhat distressing to learn that the chemical shifts are not superimposable between polytypes. Perhaps the nuclei are more sensitive to neighbour effects than originally thought.

As an aside, if the difference between the a and b peaks is roughly six ppm then the d peak, present in 2H and 9R

polytypes, could be six ppm from the c peak (site a is to b is as site c is to d). This would be -31 and 29 ppm in the ^{29}Si and ^{13}C nmr spectra, respectively. Before any inferences can be made more samples and work are required.

Chapter IV

MINOR SiC COMPONENTS

A. Introduction

There are normally three peaks (Chapter III) in the ^{29}Si MAS nmr spectrum of SiC. In earlier work by Hartman et al (40) it was observed that the peaks in the ^{29}Si MAS nmr spectra of an industrially produced 6H SiC sample were significantly broadened when the sample was pulsed rapidly (.5 and 5 seconds) in the nmr experiment. This was attributed to detection of amorphous components in the SiC, but recent work shows that more discrete species are likely to be present that are the cause of this effect. The following is an investigation of the rapid pulsing ^{29}Si MAS nmr spectrum of SiC.

B. Results

Figure 4.1 shows the high field peaks that are resolved when industrial 6H SiC (BGW4) is pulsed rapidly (.26 seconds) in a ^{29}Si MAS nmr experiment. The chemical shift of these upfield peaks are -32.4, -44, -49, -56, and -97 ppm. Peaks that are

Figure 4.1: Rapid pulsing ^{29}Si MAS nmr spectrum of BGW4; a depiction of the extra peaks observed in the spectra of some 6H samples.
79.46 MHz , recycle delay is .26 seconds.

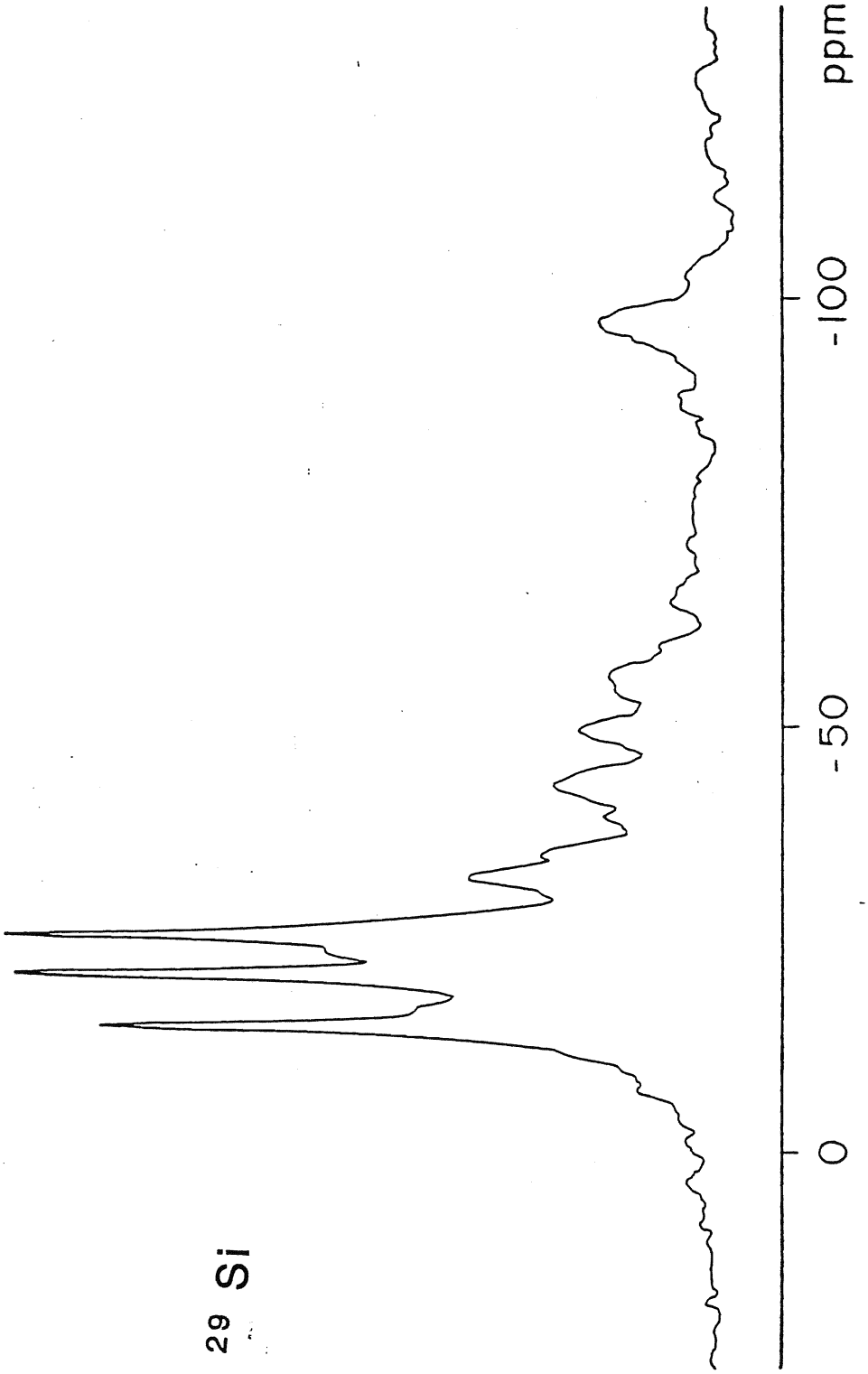
^{29}Si
0
-50
-100
ppm

regularly observed in other samples are at -31.8, -79 and -86 ppm.

Washing with 3% HF for one to 64 hours shows a removal of the impurities in the series of ^{29}Si MAS nmr spectra of an industrial 6H SiC sample, GA10, Figure 4.2. ESCA analysis, Table 4.1, done by J.Elman of Eastman Kodak, Rochester, indicates the presence of oxygen, nitrogen and fluorine on the SiC surface. However, ^{19}F MAS nmr does not detect any signals which may be due to fluorine species bonded to the surface after HF-washing.

Preliminary heating to 1100^{o}C showed that SiC could be oxidized. Five samples were heated to 1500^{o} C; gravimetric work shows that only a small fraction of the sample was oxidized (Table 4.2). Their ^{29}Si nmr spectra (.26 seconds between pulses) have a new peak at -110 ppm which is indicative of SiO_2 (3). Figure 4.3 shows the effect on one of the samples, BGW4. The most interesting feature of this figure is the fact that the spectrum taken at 5 seconds delay does not show any distortion of the SiC peaks as observed in the short recycle delay spectrum. Also, the SiO_2 peak is not as intense relative to the SiC signal. These trends are observed in the spectra of all of the other four samples that were treated in the same manner. Since the 5 second recycle delay spectra typically represent only 8 to 13% of the entire sample (Chapter V), then the .26 second delay spectra must represent an even smaller amount of the entire sample. This suggests that the oxidation is occuring at the surface because a

Table 4.1: ESCA Results, Analysis of HF-Washed 6H SiC. *

	Stoichiometric Mole %	
Element	Virgin Surface	5 A Inside
F	0.6	1.5
O	12.4	6.8
Na	0.3	0.4
N	1.6	0.4
Ca	0.2	0.3
C	64.4	49.1
Si	20.5	40.6
Ar	-	0.9

* results reported by J.Elman, Eastman Kodak, Rochester.

Table 4.2 : Heat Treatment Gravimetric Analysis Summary.

Sample	Poly-type	Temp. (°C)	Heating Time(Hr)	% Wt. Gain	Further Treatment
BGW4	6H	1500	1	8.6	-
BGW12	3C	1500	1	20.0	HF-wash
BGW22	6H	1500	1	0.9	HF-wash
BGW22	6H	1500	8	8.4	-
BGW33	AM	1500	1	1.2	-
GA10	6H	1500	1	1.9	-

Amorphous = AM

Figure 4.2: ^{29}Si MAS nmr spectra, 79.46 MHZ, of 3% aqueous hydrofluoric acid washing treatments on GA10, 6H silicon carbide. .26 seconds between pulses.

a) no HF wash

b) 1 hour wash

c) 65 hour wash.

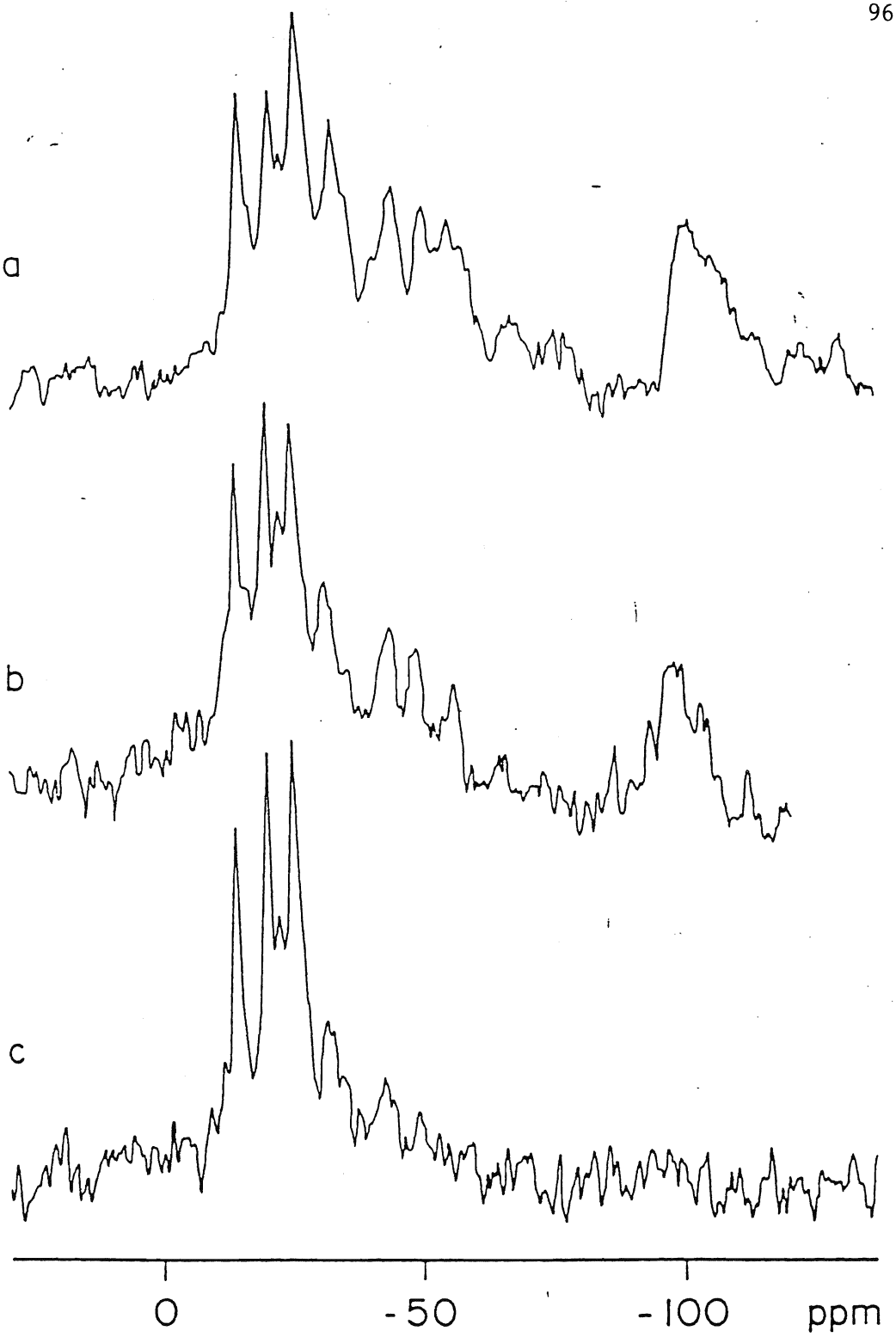
a
b
c
0
-50
-100
ppm

Figure 4.3: ^{29}Si MAS nmr spectra showing the effect of heating silicon carbide; BGW4, 6H SiC. 79.46 MHz.

a) .26 sec between pulses; no heating

b) .26 sec between pulses; 1 h 1500^{o} C

c) 5 sec between pulses; 1 h 1500^{o} C.

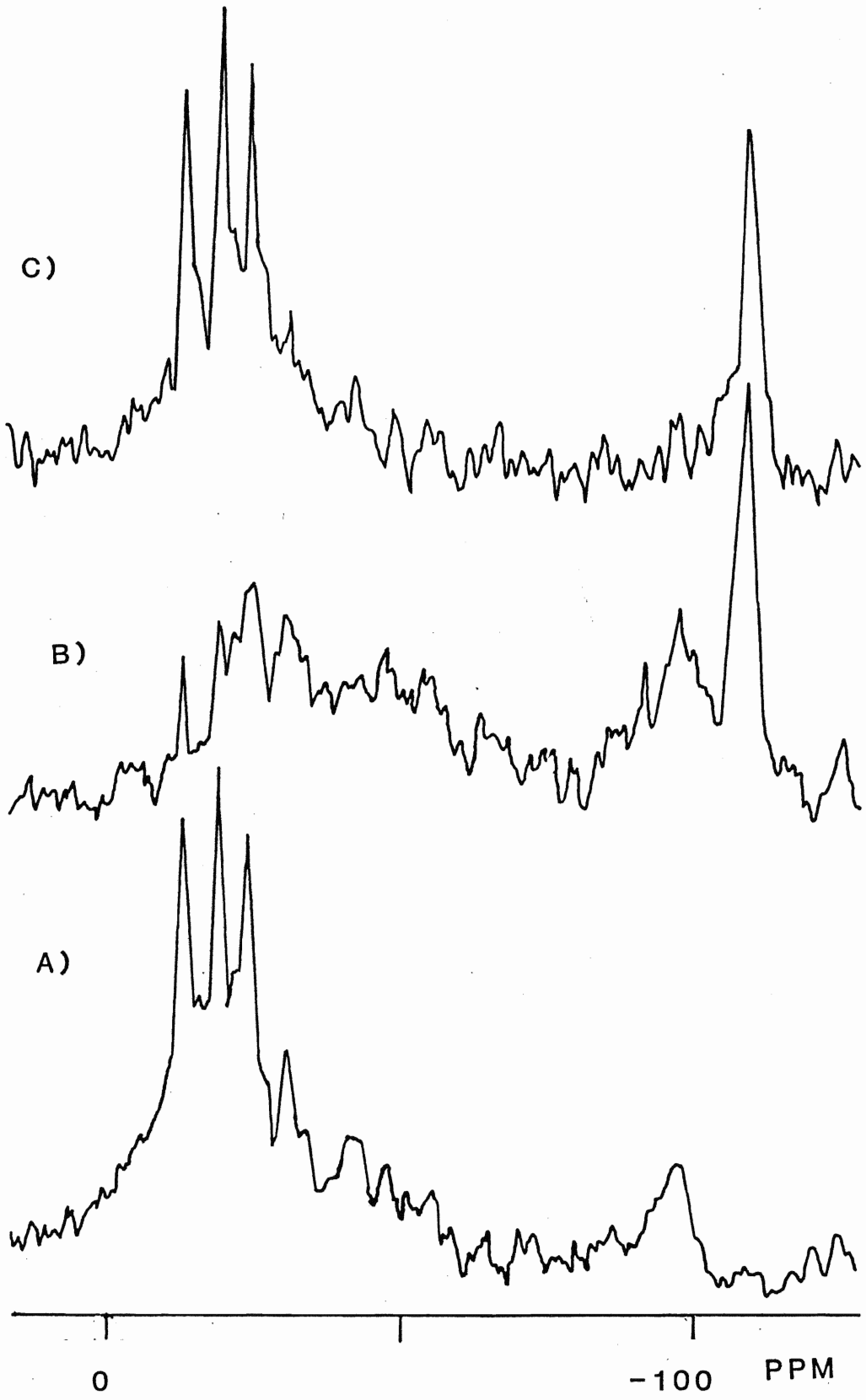
C)
B)
A)
0
-100
PPM

minor amount of the sample is affected.

Figure 4.4 is another representation of a heat treatment series, the heated sample is also treated with hydrofluoric acid to determine what part of the sample is being oxidized (HF is a surface etchant). Washing the cubic and a green 6H sample (not industrially produced), BGW22, with HF shows that this species can be removed without any effect on the rest of the nmr spectrum. This result proves that the oxidation observed is a surface phenomenon. Further heating and washing of the 6H sample, BGW22, shows a linear increase in oxidation with heating time and again removal of the -110 ppm peak. One also observes the low field of -14 ppm peaks, resolved after HF-washing, in the ^{29}Si MAS nmr spectrum, .26 seconds between pulses (Figure 4.4). This result is contrary to extra peaks viewed in other 6H samples, which appear to high field. Figures 4.5a and b show the two types of "extra peak" ^{29}Si MAS nmr spectra possible for 6H SiC at rapid pulsing rates (.26 seconds); peaks to low and high field, respectively, of the standard three SiC peaks.

Unlike the ^{29}Si nmr spectrum, only one low field peak (in keeping with the mirror image ralationship) is observed in the ^{13}C MAS nmr spectrum of industrial SiC. Figures 4.6 a and b, respectively, shows the ^{13}C and ^{29}Si MAS nmr spectra (.26 seconds between pulses) of an industrial SiC sample. The only low field peak to the SiC peaks in the ^{13}C nmr spectrum is at 30 ppm. This corresponds to the ^{29}Si peak at -31.8 ppm.

Figure 4.4: ^{29}Si MAS nmr spectra showing the combined effects of heating and washing BGW22, 6H silicon carbide.
79.46 MHz

a) .26 sec between pulses, no treatment
b) .26 sec between pulses, 1500^{o}C 1 h heating
c) 5 sec between pulses, 1500^{o}C 1 h heating
d) .26 sec between pulses, 1 h HF wash after heating
e) .26 sec between pulses, 8 h 1500^{o}C heating
f) .26 sec between pulses, 1 h HF wash after heating.

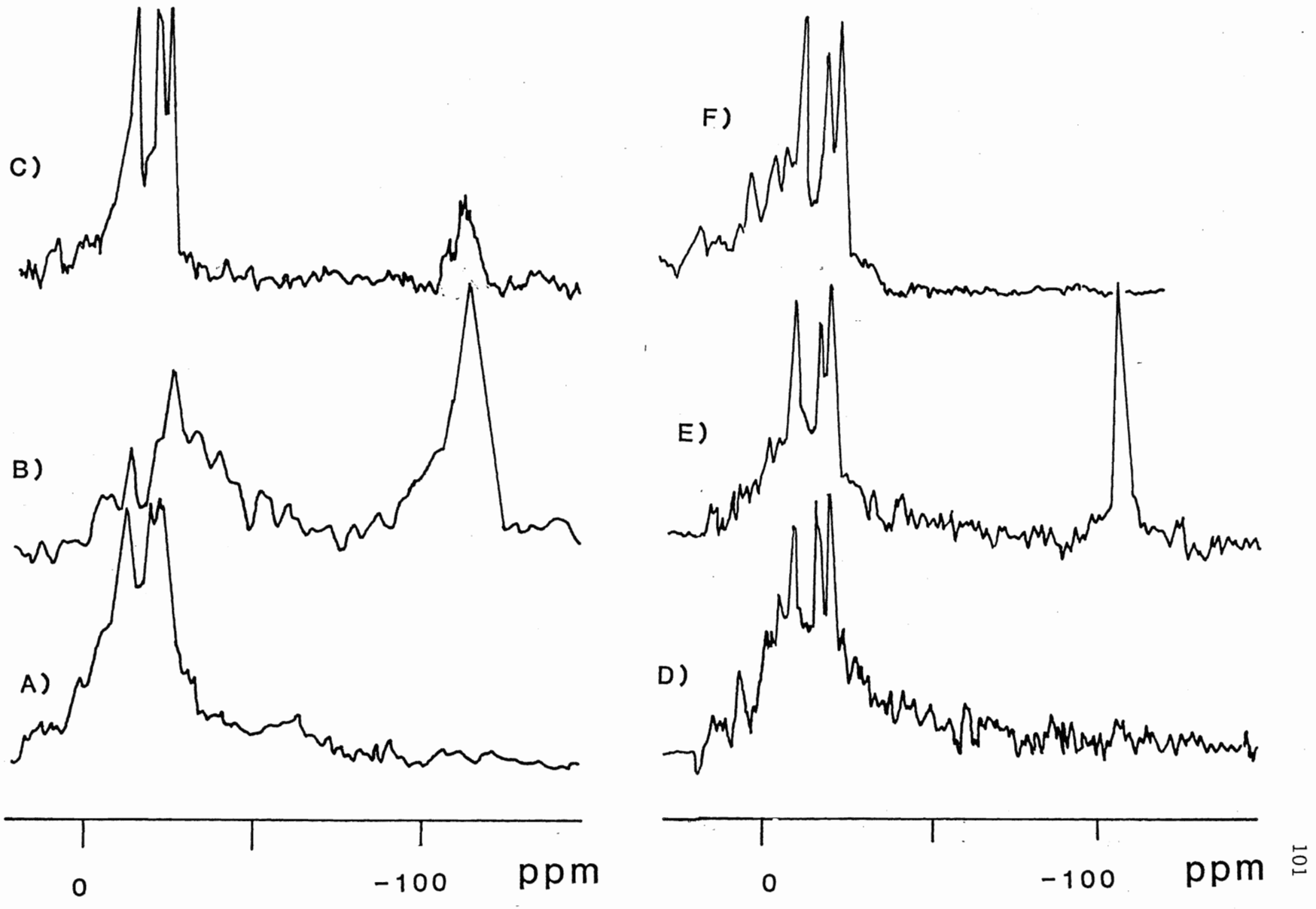
C)
B)
A)
0
-100
ppm
F)
E)
D)
0
-100
ppm

Figure 4.5: ^{29}Si MAS nmr spectra showing the two types of extra peaks observed in rapid pulsing MAS nmr spectra of some 6H SiC samples. 79.46 MHz, .26 seconds between pulses.

a) BGW4

b) BGW22, only occurence

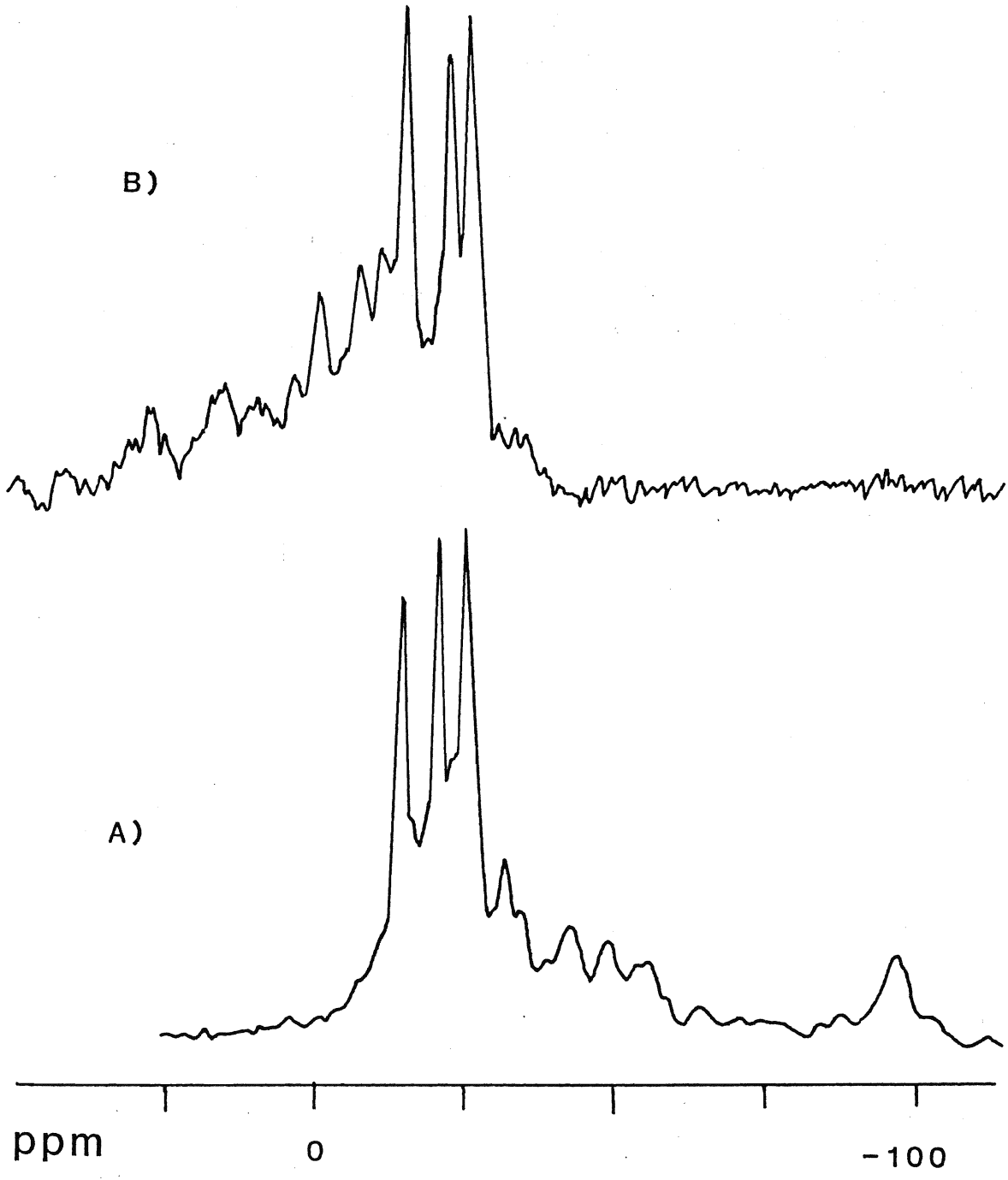
B)
A)
ppm
0
-100

Figure 4.6: MAS nmr spectra (HF washed) of GA10, 6H silicon carbide, showing the extra peak that is observed in both ^{13}C and ^{29}Si spectra (this sample only).

a) ^{13}C, 50.37 MHz; 354,000 scans, recycle delay 1 second (acquired over Christmas).

b) ^{29}Si, 79.46 MHz. 19,000 scans, .26 seconds between pulses.

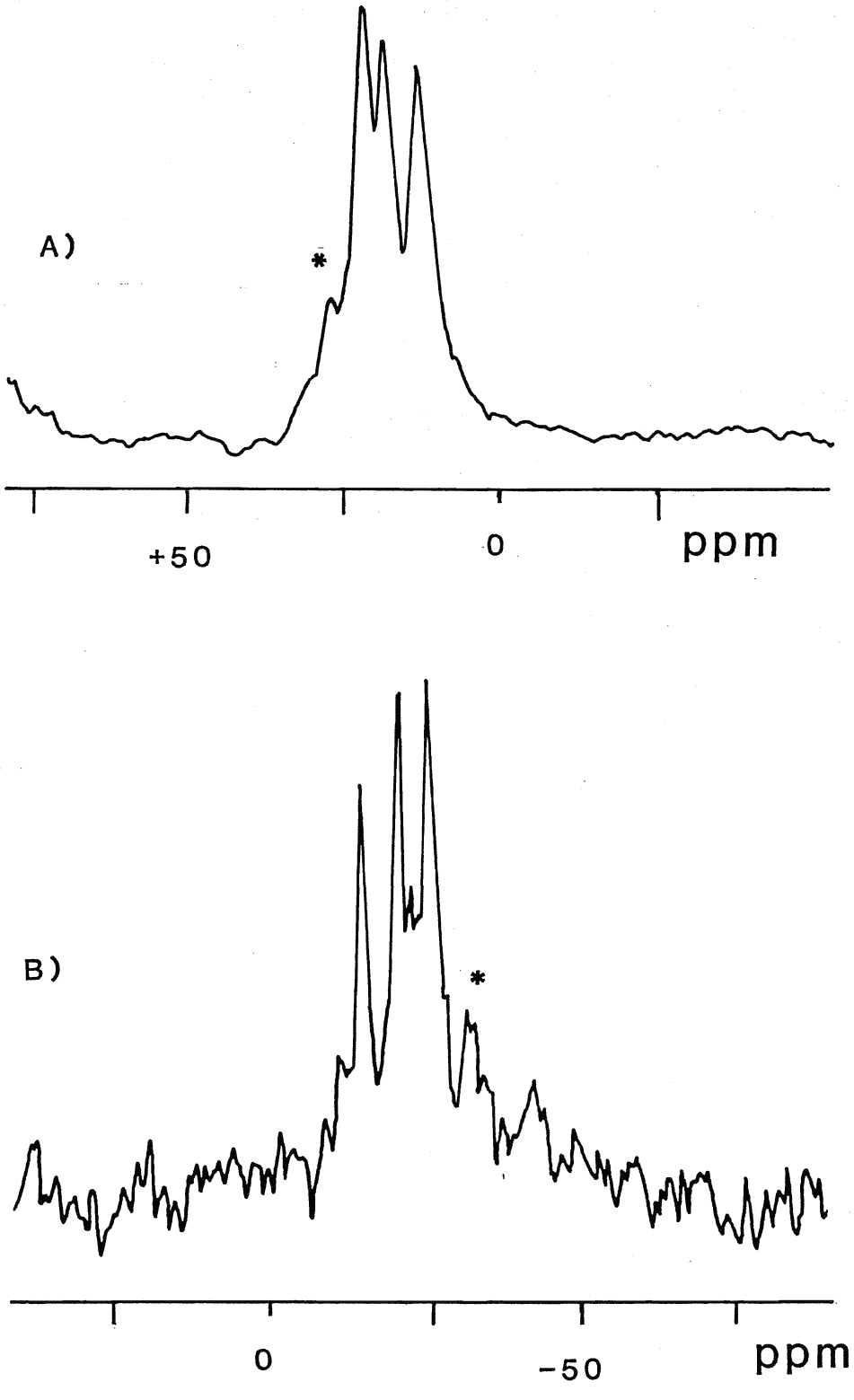
A)
*
+50
0
ppm
B)
*
0
-50
ppm

C. Discussion

Prior ^{29}Si MAS nmr spectra, pulsed rapidly (.5 to 5 seconds), of industrial batch production SiC showed severe broadening of the SiC peaks (40). The thought was that amorphous impurities were being detected. However, with rapidly pulsing (.26 seconds) a great number of times, discrete peaks can be resolved, high field of -25 ppm in the ^{29}Si MAS nmr spectrum (Figure 4.1).

This method of rapid pulsing is crudely analogous to the cross polarization/magic angle spinning (CP/MAS) technique. CP/MAS uses polarization transfer from an abundant nucleus (hydrogen, usually) to a magnetically dilute nucleus (i.e., carbon or silicon), which enhances the signal of the dilute signal and shortens the delay time between pulses. With this technique better resolved and more intense signals can be detected in a much shorter time frame. The method used in these experiments pulses the sample so quickly that the bulk SiC nuclei do not have time to relax, their magnetizations become saturated, and only a minor component of the signal is observed. On the other hand, any sites or impurities that have a much shorter T_1 will be detected more readily.

The chemical shifts of these peaks do not change with

spectral frequency or spinning rate; therefore, they are real and not spinning sidebands. They constitute less than 5% of the observable silicon in SiC, which suggests that they may be due to impurities or irregularities in the crystal. To further indicate that these peaks may be due to impurities, they only appear in the ^{29}Si spectra of black/grey industrial SiC and not in the purer light green crystals.

Batch production of SiC involves the heating of unreacted silica sand, petroleum coke, and frac. Frac is known in the abrasive indusry as unreacted material, taken from the previous SiC production run. Frac can consist of silica sand, petroleum coke, graphite, SiC, oxides and metals. The SiC ingot is ventillated from underneath to prevent excessive over heating during the reaction process by sucking air in through the top of the ingot to the vents below.

There are two basic means in this process whereby impurities can be incorporated into the SiC. Firstly, the frac will contribute many metallic impurities. Second, as air is sucked through the ingot, atmospheric gaseous species and oxygen can react with the SiC. Many of these impurities are visually detected as colourful bands in the SiC.

The range of upfield peaks in the ^{29}Si nmr spectrum of SiC is -30 to -100 ppm, sometimes a peak at -110 ppm, SiO_2 (66), is also observed. These upfield peaks coincide with the shift region of several Si-X systems, whereby X can be a number of

functional groups; OH, O, N, F, Al and OR (67-71).

The silicate chemical shift range extends from -60 to -120 ppm; depending on the degree of polymerization Q^0 to Q^4(3). Q^0 are monosilicates, Q^1 are disiicates and end chain groups, Q^2 are mid-chain groups, Q^3 are chain branching groups, and Q^4 are three-dimensional crosslinked framework silicates. Each silicate in the above groups therefore has no, one, two, three, and four Si-O-Si bridging bonds, respectively. With increased polymerization the ^{29}Si chemical shifts move to higher field, due to increased shielding of the silicon nuclei.

The Si-N system also appears in the chemical shift region upfield of -25 ppm (72). Each silicon is bonded to four nitrogen atoms in Si_3N_4. The chemical shift is -48 to -50 ppm, depending on the "polymorph" (this term should probably be polytype in keeping with proper crystallographic terminology). Another species is Si_2N_2O which has a chemical shift of -63 ppm (73). Incorporation of aluminum into any of the above systems invoves further differentiation of the signal in the chemical shift region of interest (74,75).

Two groups (67,76) have used ^{29}Si CP/MAS to study silica gel surfaces. Peaks at -90 and -100 ppm have been selectively detected which are characterized as geminal silanol groups. By all indications, a sure means of identifying the peaks at -86 and -98 ppm in the ^{29}Si nmr spectrum of SiC would be to run a CP/MAS experiment on the SiC samples. A positive result would confirm

that there are terminal hydroxyl groups on the SiC surface.

A final system which also has chemical shifts in the ^{29}Si -25 to -100 ppm chemical shift range is the $SiR_3(OR)$ system. The R and OR groups are alkyl and alkoxy groups, respectively. These systems have been studied extensively and chemical shifts are well defined (70).

Surface etching experiments (HF-washing) on 6H sample, GA10, showed a definite cleaning up of the upfield of -25 ppm peaks in the ^{29}Si nmr spectrum. The only upfield peak that was still present is the -31.8 ppm peak (Fig 4.2). This apparent removal of peaks is indicative of surface SiC impurities, however, this phenomenon is only observed for one sample (out of five).

Assuming that these impurities are on the surface consider the possibility of layered oxidation. If SiC_4 has a ^{29}Si chemical shift of about -20 ppm and "SiO_4" (SiO_2) has a shift of -110 ppm, then a set of intermediate chemical shifts can be approximated for the SiOC system. If there is a linear relationship betwoon the substitution of oxygen for carbon and chemical shift, then SiC_3O, SiC_2O_2, and $SiCO_3$ would be expected to appear around -42, -64, and -86 ppm, respectively. The SiC_3O and $SiCO_3$ species can be present on the surface of SiC if the outermost silicon layer is oxidized, depending on which face is showing. Remember that silicon in SiC is tetrahedrally bonded to carbon, and vice versa. If the carbon layer that is directly

beneath the silicon layer (orthogonal to the SiC *c* axis) is replaced by an oxygen layer then the surface species will be SiC_3O. However, if the carbon layer above the silicon layer (silicon fits into a three atom hole) is replaced by an oxygen layer, then the surface species will be $SiCO_3$. It is not likely that a layer would be partially oxidized to produce the SiC_2O_2 species.

The samples that were heated to 1500° C under normal atmospheric conditions all showed signs of oxidation with the appearance of a separate single peak at -110 ppm (Figure 4.3), this would correspond to SiO_2 (3). The only sample that showed any other changes is BGW22 which is green, not industrially produced 6H. With oxidation, the SiC peaks in the rapid pulse ^{29}Si nmr spectrum become better resolved. But this result may be due to a difference in the spinning angle, the spinner may have been wobbling during the acquisition of the nmr spectrum of the untreated sample, or other experimental differences.

There is only a minor fraction of the material that was oxidized, the percent of weight gain ranged from 0.9 to 8.6 % for the 6H samples. The 3C sample showed the most dramatic increase in weight, 20%. This certainly confirms that 6H is much more resistant to modification than the 3C polytype (26). In all cases the effect of heating SiC is most dramatically observed in the short recycle delay spectra. At a longer delay of five seconds (Figures 4.3c and 4.4c) the SiC peaks are unaffected and

the SiO_2 peak is weak.

When samples were earlier washed with HF very little change in the upfield of -25 ppm peaks was noted for all but one of the samples treated (Figure 4.2). If the impurities were all at the surface, they should have been removed with HF-washing. These observations suggest two possible explainations; the HF is not an effective etchant, as was earlier believed (77), or the impurities are not at the surface. HF-washing of the 3C and green 6H samples, after they were heated to 1500°C for one hour, shows that HF is indeed an effective surface etchant. The ^{29}Si nmr spectra show a complete removal of the SiO_2 species which has a chemical shift at -110 ppm.

Further heating of the green 6H sample, BGW22, to 1500°C for eight hours gives a proportional eight fold increase in percent weight gain. Recently, the oxidation kinetics of SiC have been studied (78) it was found that in the 1200 to 1500 °C range oxidation was linear with time. They describe the oxidation using the linear-parabolic model of Deal and Grove (79) which is basically a model to explain active oxidation.

The oxidation of SiC can occur by two means; active and passive oxidation (27). In the case of active oxidation, a coherent layer of silicon dioxide is formed on the surface which suppresses further oxidation. Passive oxidation occurs under either gentler or very extreme conditions, the result is a migration of oxygen into the crystal lattice. The evidence from

the above experiment strongly suggests that the other upfield peaks are not due to surface impurities, but rather impurities within the crystal. Oxygen may be included into the lattice as the SiC is produced because simple heating does not seem to induce passive oxidation which allows the migration of oxygen into the crystal lattice.

The only observable differences in the ^{29}Si nmr spectrum of BGW22 after heating is the increased intensity of the -110 ppm peak, and a decrease in intensity of the middle SiC peak, at -20.7 ppm. However, after HF-washing this sample, peaks are resolved that are low field of the SiC peaks and the -110 ppm peak is gone. The observation of low field peaks came as a total surprise; normally, only high field of -25 ppm peaks are observed.

Upon reconsideration of the BGW22 short delay spectra, one can see a hint of the low field peaks noted earlier, in some cases it appears asthough the SiC peaks are on top of an amorphous SiC peak which is observed in the short delay spectra of other samples. There are no other indications of this phenomenon in other 6H samples, but perhaps it is linked with the upfield peaks observed in the ^{29}Si nmr spectra of the other samples.

SiC is well known for its semiconducting properties (27,80). Depending on the metal that is used to dope a semiconductor, the semiconductor can be made into two types; N

and P-type. An N-type semiconductor has an abundance of electrons and a P-type semiconductor has a lack of electrons (or abundance of holes)(81). If a nucleus was in an environment with an abundance of electrons it would be more shielded. Perhaps the peaks that appear to high field of the SiC peaks are due to greater shielding by an abundance of electrons. This implies that the SiC with high field peaks has N-type semiconducting properties or regions. Similarily, electron defficient dopants in SiC may cause deshielding of proximal silicon sites. This would cause a down field shift, implying that low field peaks are indicative of P-type characteristics in the SiC.

Aluminum, phosphorous, galium, germanium and arsenic are regularly used to dope silicon in the production of semiconductors (27). Aluminum is a common contaminant in industrial SiC, ^{27}Al MAS nmr analysis does detect any aluminum in the SiC. One must remember that the high and low field peaks only represent less than 5% of the total observable silicon. So, this result does not mean that there is no aluminum in SiC because nmr is not sensitive for trace impurity detection in solids. In agreement with the above proposal, industrial SiC crystals do have random spots that conduct a current from one wire to another which are touching the crystal. This finding is certainly a good incentive for further work along these lines.

ESCA (electron spectroscopy for chemical analysis) analysis of the HF-washed industrial 6H sample shows that there

are a number of impurities present on the surface of SiC. The results, given in Table 4.2 show two interesting features. First, the mole percent of carbon is much greater than silicon at the surface. Second, fluorine is present at the surface, which does not come as a surprise since this was found in another surface study of HF-washed SiC (82).

The abundance of carbon atoms at the surface may be due to dirt and oils from handling the SiC samples. There may also be alkyl groups on the SiC surface. Alkyl and alkoxy species may bond to the surface during SiC production; the carbon atoms could be oxidized and/or reduced during cooling after SiC condensation. Apparently HF does not cleave Si-C bonds (26) which would explain why HF-washing does not seem to be effective as an etchant.

^{19}F MAS nmr analysis of the HF-washed samples does not detect any signals. If fluorine co-ordinates with silicon upon washing, it is undetected in the nmr experiment. The surface study of SiC, mentioned above (82), shows that the fluorine and oxygen impurities on SiC are trace amounts only, which is not easily detected using solid state nmr.

Perhaps a definate means of characterizing the species that cause the high field and BGW22 low field peaks would be to reductively heat the SiC. In this way, if the species are surface bonded, heating in a hydrogen atmosphere would remove surface species and replace them with hydrogen atoms. The hydrogen atoms would definitely have a different shielding effect

and the associated silicon atoms would have a different chemical shift.

Minor peaks in the ^{13}C MAS nmr spectra of SiC that would correspond to the ^{29}Si extra peaks should appear to low field of 25 ppm. Unfortunately, the signal of the sample spinner, -60 ppm region, interferes. The only low field peak that was detected is at 30 ppm in the short delay (.26 to 1 second) ^{13}C spectrum of GA10 (Figure 4.6). It is especially interesting to note that there is a corresponding peak in the ^{29}Si nmr spectrum of GA10 and most of the other industrial 6H SiC samples. This peak may be the predicted d site (see I.C.2) or it may be a site that is due to stacking irregularities in the samples.

Chapter V

SPIN-LATTICE RELAXATION CONSIDERATIONS

A. Introduction

1. Potential Problems in Spectral Interpretation

The preferred approach to the analysis of SiC MAS nmr spectra is to consider the crystal structure of each SiC polytype. This method (Chapter III) considers the number of possible silicon (carbon) sites in SiC on the basis of calculations of the distance of neighbouring atoms from a central atom. It is critical when relating the crystal structure of SiC to its nmr spectrum that the observed nmr spectrum is representative of the bulk sample. There is evidence (see section IV.B, Figure 4.1), and therefore concern, that when shorter delays between pulses are used in the nmr experiment, the results are not representative of the entire sample.

Furthermore, the relative intensities of the SiC peaks in both the ^{13}C and ^{29}Si MAS nmr spectrum may vary depending on the recycle delay (39, Figure 5.1). This signifies that some of the nuclei in the sample are not allowed to completely relax to

Figure 5.1: ^{29}Si and ^{13}C MAS nmr spectra of SiC5, 6H silicon carbide, acquired at various delays between pulses.

15 minutes	a) ^{29}Si, 79.46 MHz	d) ^{13}C, 50.37 MHz
5 minutes	b) ^{29}Si	e) ^{13}C
5 seconds	c) ^{29}Si	f) ^{13}C.

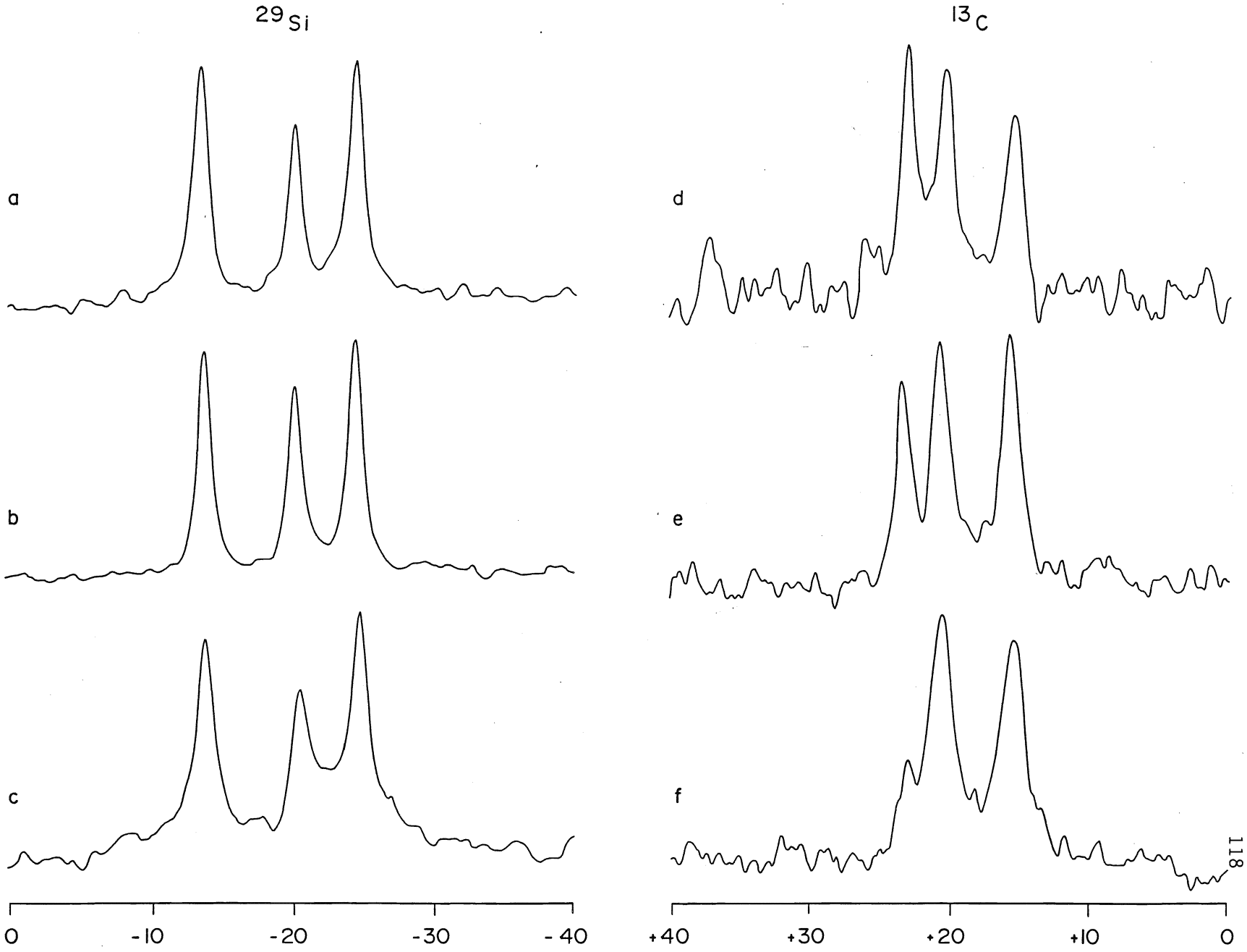
29Si
13C
a
b
c
d
e
f
0
-10
-20
-30
-40
+40
+30
+20
+10
0

equilibrium before they are pulsed again, therefore the signal intensity is weaker than that observed at longer pulse delays.

The following work is an attempt to understand the relaxation process of the silicon nuclei in SiC during a pulsed nmr experiment and to ascertain whether or not ^{29}Si nmr spectra are representative of the bulk sample. This will be approached in two ways. First, the percent of observable silicon detected will be determined at different pulse recycle delays for various samples. This should show whether or not the asssumptions made in Chapter III, concerning the observation of bulk sample, are valid. Second, attempts will be made to learn the T_1 of silicon in SiC.

2. Theoretical Considerations

a. Inversion-Recovery

There are three commonly used pulse techniques for the determination of T_1; inversion-recovery (83), saturation-recovery (84), and progressive saturation (85). Inversion-recovery $(180\text{-}\tau\text{-}90\text{-}Aq\text{-}D)_m$ is the more common method. A 180° pulse inverts the spin population, the spins begin to relax during the time τ, then the spectrum is recorded (Aq) after the 90° pulse (depicted in Figure 5.2). This experiment is repeated a number of times for a different τ value. The T_1 of the species of interest is

Figure 5.2: Diagrams of the inversion-recovery pulse sequence.

a) 180° pulse; spin initialization

b) τ evolution time

i) less than $T_1/\ln 2$

ii) equal to $T_1/\ln 2$

iii) greater than $T_1/\ln 2$

c) 90° pulse; spin modulation

d) Fourier Transformed FID.

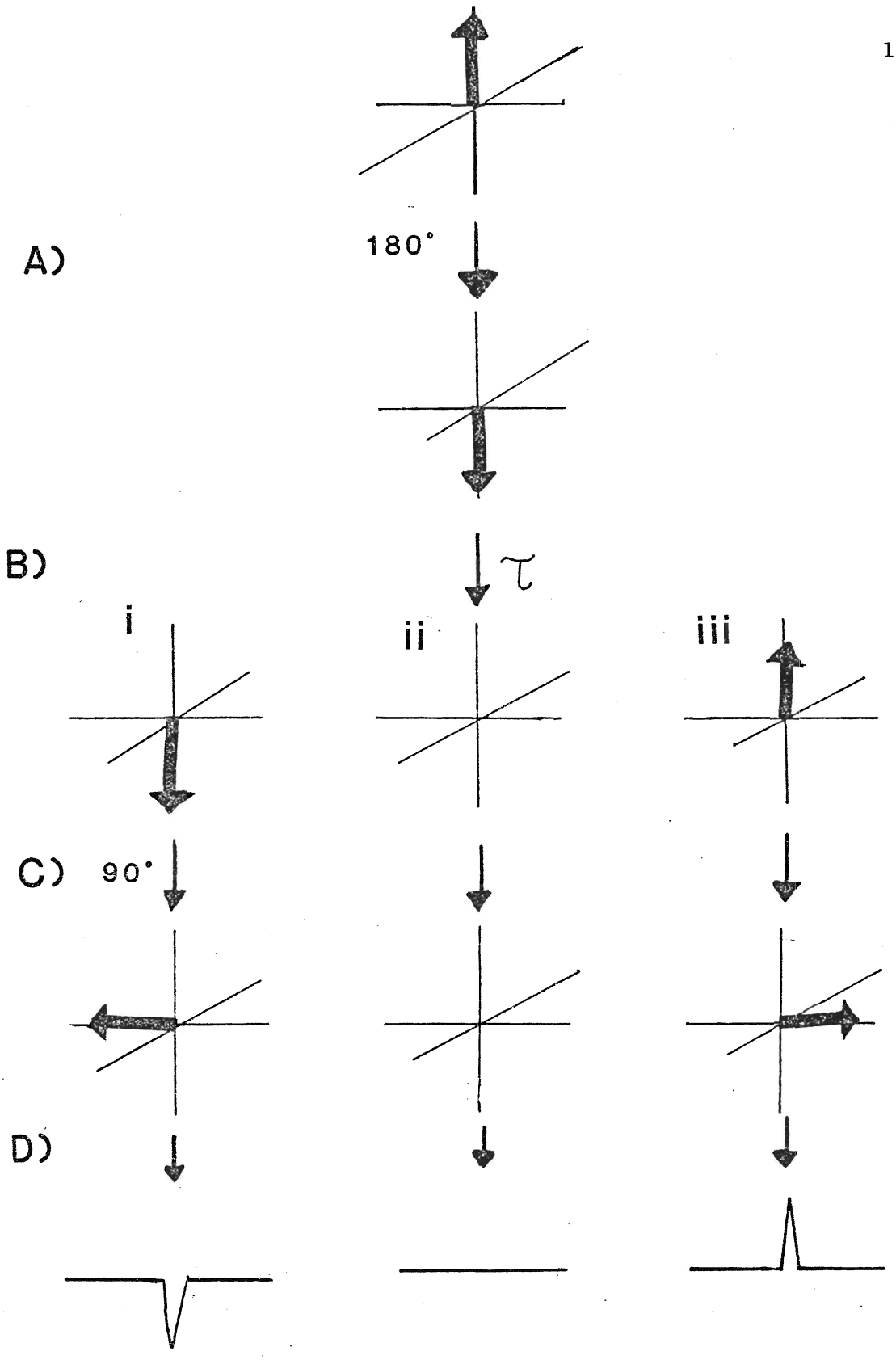
A)
180°
B)
τ
i
ii
iii
C)
90°
D)

approximated and τ values are selected to bracket it. To ensure that the system is at full equilibrium, a delay (D) equal to at least five times the estimated T_1 is required after the pulse sequence which is repeated m times before changing τ values.

In the inversion-recovery experiment the first pulse initializes the spin population and the second pulse measures the magnetization after the waiting period, τ. The actual magnetization after waiting for a time T is:

$$M(\tau)/M_o = 1 - 2 \exp(-\tau/T_1)$$

where $M(\tau)$ is the observed magnetization and M_o is the equilibrium magnetization.

Signal detection is normal to the applied magnetic field; detection of the magnetization after a 180° pulse will produce a null signal and the positive and negitive signal maxima appear after 90° and 270° pulses, respectively.

Essentially, when the τ value is less than the T_1, then the effect of the (180-τ-90) sequence will be less than a 270° pulse but greater than a 180° pulse and the resultant signal will be negative. Conversely, a positive signal will be detected if the τ is greater than the T_1 because the effective pulse is somewhere between 180° and 90°. Finally, if τ is in the T_1 range, then no signal will be observed. Therefore, the T_1 of the species can be visually detected by a null signal, or estimated

by bracketing positive and negative signals. The exact T_1 is obtained by analysis of the above equation.

b. DESPOT

If the T_1 of the species is long then the inversion-recovery experiment can be quite time consuming. A method that is like the progressive saturation method is also considered in some detail; the variable nutation method (86). This method has been recently revived and has been called the driven-equilibrium single-pulse observation of T_1 relaxation method (DESPOT) (51).

Unlike most other T_1 determining methods, the duration of the DESPOT experiment does not depend on the T_1. The sample is pulsed repeatedly at a fixed angle, θ, until an equlibrium cycle is attained (n pulses, dummy scans). Then the pulse sequence is repeated with the acquistion (Aq) of the signal after each pulse, m times. To remove any T_2 relaxation influences, a field gradient is applied (FS, field spoiling pulse) if the T_2 is greater than the experimental delay time, ti. The DESPOT pulse sequence is:

$$(\theta - FS - ti)_n - (\theta - Aq - FS - ti)_m$$

The resultant magnetization, M_z, which reflects the T_1 is tilted θ degrees away from the H_o z axis (direction of the applied magnetic field) and will relax back towards the z axis during the time period ti. See Figure 5.3a for a depiction of the cycle to set up the equilibrium, and Figure 5.3b for the acquisition cycle. The perturbation-recovery cycle has been shown (86) to obey the following relationship:

$$M_z = M_o[1 - \exp(-ti/T_1)] \; / \; [1 - \cos\theta \exp(-ti/T_1)]$$

M_o is the initial magnetization before the experiment. This equation can be rearranged to (51):

$$M_z = M_z \cos\theta \exp(-ti/T_1) + M_o[1 - \exp(-ti/T_1)].$$

A linear regression of M_z on $M_z \cos\theta$ will yield a linear plot with slope $\exp(-ti/T_1)$. M_z can be determined because the intensity, I, of the signal measured in the DESPOT experiment is proportional to M_z:

$$I \propto M_z \sin\theta$$

In fact, the linear regression analysis is then of $I/\sin\theta$ versus $I \cos\theta/\sin\theta$. Therefore, the T_1 can be determined without having

Figure 5.3: Diagram of the DESPOT pulse sequence.

a) variation of the magnetization vector during the DESPOT initializaton sequence. In this case i=3 for the number of dummy scans, i, used to attain equilibrium.

b) the equilibrium cycle for M_z.

a

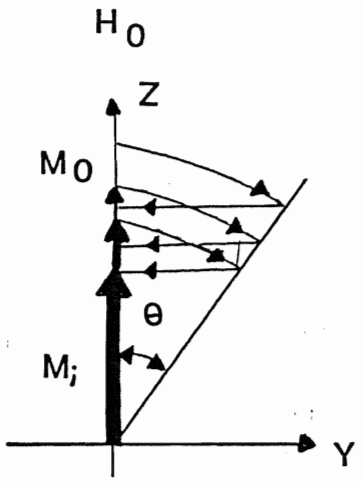

b

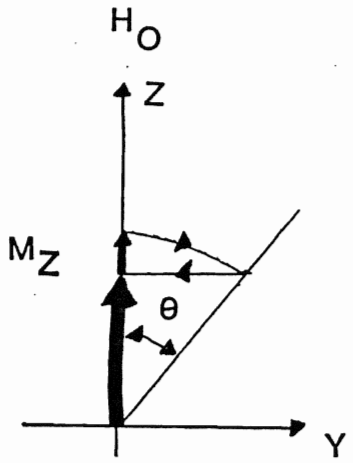

to measure the M_o which is the bottle neck to the inversion-recovery method because M_o is T_1 dependent. Instead of time, the pulse angle is the variable in the DESPOT experiment, which potentially makes this method at least 10 times faster than the inversion-recovery method.

B. Results

The inversion-recovery experiments on hexamehtyldisiloxane ($(Me_3Si)_2O$), HMDSO, gave a silicon T_1 value of 20.4 seconds; the chemical shift is 6.8 ppm. When this sample is pulsed every two minutes, greater than $5*T_1$, it is assumed that 100% of the detectable silicon is being observed. It was used as the standard to determine the amount of silicon detected in SiC at various pulse recycle delays.

Tables 5.1 to 5.3 list the percent of observable silicon detected for 5, 30 and 300 second delays between pulses, respectively. On the average, with five seconds between pulses, only 10 % of the observable silicon was detected. Increasing the delay time, a concommitant increase in observable silicon is detected; 15 - 33 % at 30 seconds and 42 - 56 % at five minutes delay.

A comparison of the DESPOT and inversion recovery T_1 analysis (Figure 5.4) for forsterite, a chain silicate, is listed

Figure 5.4: ^{29}MAS nmr spectra, 39.76 MHz, of an inversion-recovery experiment on forsterite which shows the inconsistency of the longer τ values (60 and 120 second spectra should be of equal intensity).

$(D - 180 - \tau - 90 - FID)_{64}$ D = 5 minutes

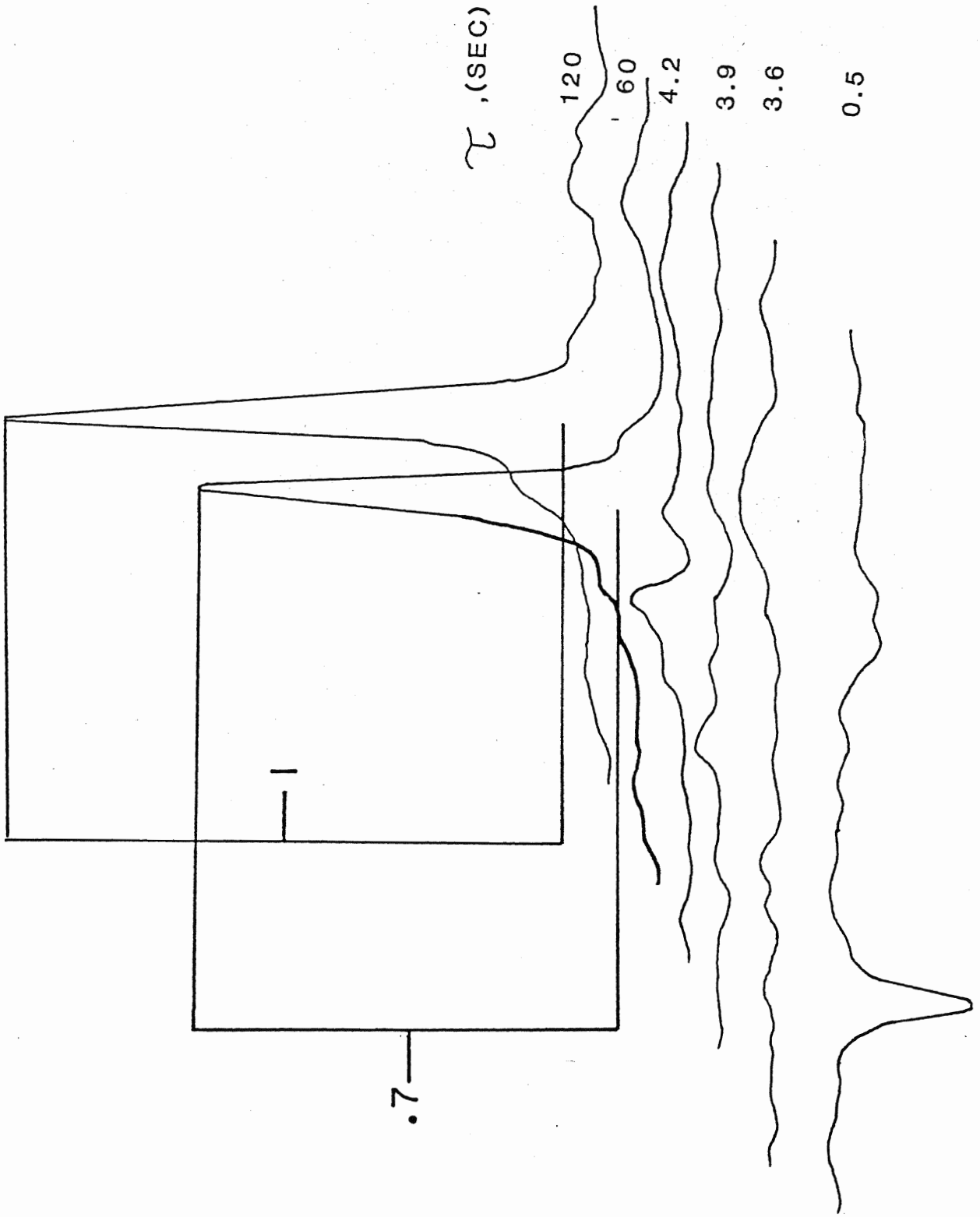
τ ,(SEC)
120
60
4.2
3.9
3.6
0.5
1
.7

Figure 5.5: ^{29}Si MAS nmr spectra of the inversion-recovery experiment on BGW12, 3C silicon carbide. Peak intensities should be equivalent from 30 to 600 sec, if the experiment is correct.

$(D - 180 - \tau - 90 - FID)_{48}$. D = 15 minutes.

The apparent T_1 is about 2 seconds, however this experiment is not considered to be valid. Note that the shortest τ value of 1 second does not invert. It was reasonable to expect inversion since the T_1 of SiC seems to be so long. Due to time limitations more experimentation was not possible.

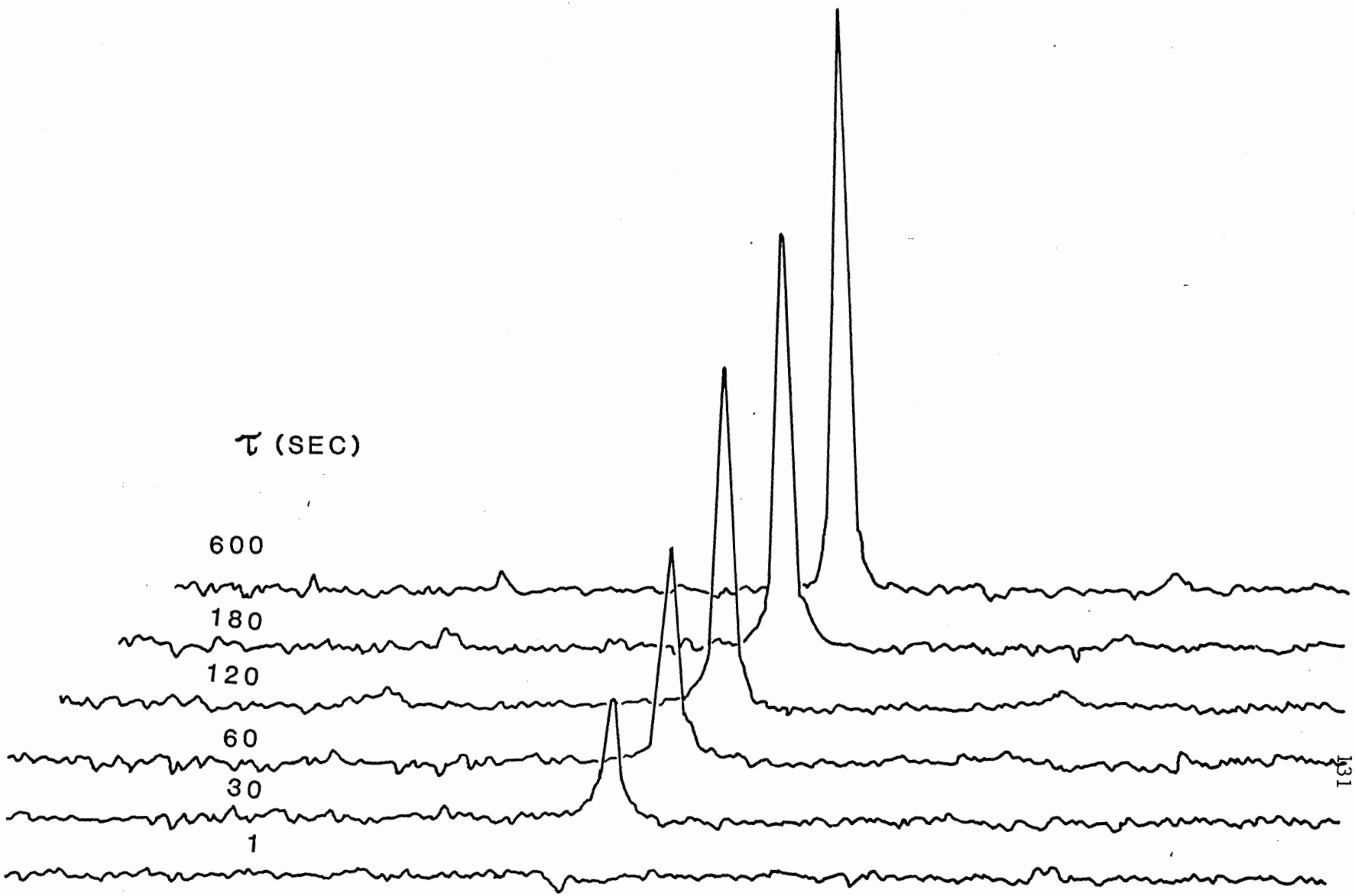
τ (SEC)
600
180
120
60
30
1

Table 5.1: Percent Silicon Detected; Spectra Acquired at a Five Second Recycle Delay.

Sample	Polytype	Recycle Delay (sec.)	Number of Scans	% Observable Silicon Detected
HMDSO		120	300	100
BGW12A	3C	5	300	11.64
BGW12B	3C	"	"	13.01
BGW4	6H	"	"	4.78
BGW26	6H	"	"	10.80
GA15	15R	"	"	8.29

Table 5.2 : Percent Silicon Detected; Spectra Acquired at a 30 Second Recycle Delay.

Sample	Polytype	Recycle Delay (sec.)	Number of Scans	% Observable Silicon Detected
HMDSO		120	100	100
BGW12A	3C	30	100	32.73
BGW12B	3C	"	"	33.56
BGW4	6H	"	"	14.87
BGW26	6H	"	"	23.37
GA15	15R	"	"	17.38

HMDSO = Hexamethyldisiloxane; $O(Si(CH_3)_3)_2$.

Table 5.3: Percent Silicon Detected; Spectra Acquired at a 300 Second Recycle Delay.

Sample	Polytype	Recycle Delay (sec.)	Number of Scans	% Observable Silicon Detected
HMDSO		120	30	100
BGW12A	3C	300	30	56.07
BGW26	6H	"	"	43.16
GA15	15R	"	"	42.46

HMDSO = Hexamethyldisiloxane; $O(Si(CH_3)_3)_2$.

Table 5.4: Forsterite[@] ^{29}Si T_1 Results.

	DESPOT				180-T-90	
	ti = .96s		ti = 1.3s		dT = 3s	dT = .3s
		*		*		
1	4.6	3.2 - 7.7s	3.8	2.9 - 5.4s	2 - 5s	3.0 - 4.2s
2	3.9	3.2 - 4.9	5.4	4.0 - 7.9		
3			5.4	4.5 - 6.6		

* 95 % Confidence Limit; Student's t Test.

@ $O(Si(CH_3)_3)_2$.

Table 5.5: 3C SiC (BGW12) DESPOT Results For ^{29}Si.

Run	Dummy Scans	ti (s)	T_1 (s)	95% Confidence
1	15	1200	676	597 - 757
2	15	143	219	179 - 305
3	20	60	141	114 - 197
4	40	60	203	160 - 294
5	20	30	72	64 - 84
6	20	30	86	66 - 114
7	40	30	83	73 - 98
8	40	30	66	61 - 72

in Table 5.4. Results from both methods indicate that the forsterite silicon site (-61.6 ppm ^{29}Si MAS nmr peak) has a spin-lattice relaxation time, T_1, between 3.5 and 5.5 seconds.

According to the inversion-recovery results for BGW12, 3C SiC, the silicon T_1 is about two seconds. However, this result is suspect because at T greater than $5*T_1$ the peak intensities should plateau, which they do not do (Figure 5.5). Using the DESPOT method on the same sample a large range of T_1 values were determined. The 3C silicon site (-18.8 ppm ^{29}Si MAS nmr peak) T_1 can be from 66 to 676 seconds, depending on the ti value used, Table 5.5.

C. Discussion

1. Determination of Observable Silicon Detected

As can be seen, in Tables 5.1 to 5.3, the percentage of silicon detected for SiC is similar for the three polytypes; 3C, 6H, and 15R. However, the 3C polytype consistently appears to have the highest percentage of silicon detected. This can be due to two factors. First, the 3C silicon nuclei relax faster than the other nuclei. This is not likely because the structures of the polytypes are very similar to each other and relaxation mechanisms would be expected to be related. Second, spectral information of weaker signals may be lost into the baseline.

There is only one peak in the ^{29}Si nmr spectrum of the 3C polytype, -18.8 ppm, which will contain all of the silicon information. The 6H and 15R polytypes have three or more peaks in their ^{29}Si nmr spectra; the silicon information will be distributed amongst these peaks. When the spectra are Fourier Transformed relative to HMDSO, the signal to noise of the SiC spectra will decrease if the intensity of the HMDSO peak is that much greater than that of the SiC peaks. Hypothetically, if 10 % of one peak is not detected because of the above effect, then 10% of the 3C SiC will not be detected. Similarly, 30% of the 6H or 15R spectra will not be detected because they both have three peaks and more if there are more than three peaks at shorter delays (Chapter IV). The result is that the 3C SiC appears to relax faster at shorter recycle delays because more signal is detected than the 6H or 15R polytypes.

As has been suspected (58), the spectra acquired at long recycle delays are representative of the bulk sample. The spectra obtained with a five minute delay or longer represent at least 50 % of the observable silicon, and should be used when correlating crystal structure to the nmr spectrum.

The time required for longitudinal relaxation is an exponential function (6) so a delay longer than two times five minutes is required to see 100% of the detectable silicon. If it were desired to detect 100% observable silicon, then longer delays would have to be attempted. There will be a rather large demand

on instrument time, which is not always possible.

The spectra obtained at short delays, five seconds or less, are only representative of a small fraction of the sample, 10% or less. This is a point where the crystallographic determination becomes limited in its usefulness, and the MAS nmr experiment continues. A great deal of information about small domains in heterogeneous samples and/or their surfaces can be studied by nmr; see Chapter IV for the study of SiC samples at short delays. Such aspects of the crystal can not be studied by crystallographic structure determinations.

2. T_1 Studies

From the spectra in Figure 5.1 and the observable silicon calculations, done earlier in this chapter, it seems that the T_1 of SiC can be quite long. A preliminary attempt of the inversion-recovery experiment on SiC took four days. Forsterite, synthesized by R.Millard, Brock Chemistry Department, is a silicate mineral and its ^{29}Si MAS nmr spectrum has a well resolved peak at -61.6 ppm which is readily observed with few scans and a short recycle delay. It has been used as a test sample for both the inversion-recovery and DESPOT methods.

The forsterite silicon T_1 appears to be between 3.0 and 4.2 seconds in the inversion-recovery experiment. However, it is

disconcerting to note that the signal with τ equal to 60 seconds is less intense than that at 120 seconds (Figure 5.4). The delay between cycles is five minutes, allowing plenty of time for the system to relax if the T_1 is less than 4.2 seconds. After the initial 180° pulse, the magnetization should relax back to full equilibrium with τ equal to 60 or 120 because both are more than five times longer than the apparent T_1. The subsequent 90° pulse should then produce a signal of equal intensity for both τ values, which it does not. This indicates that the system has not competely relaxed; either the 90° pulse is incorrectly set or the inversion-recovery experiment is not effective for this sample. The 90° pulse was rechecked many times, so it is most likely to be set correctly. It seems as though the five times T_1 delay for complete relaxation pattern is not followed by this sample nor the 3C SiC sample (Figure 5.5).

The inversion-recovery result for BGW12, 3C SiC, is not considered to be correct. According to Figure 5.5, the silicon T_1 is about two seconds. However, if this were true then the intensities of any of the positively phased peaks should be equal because the corresponding τ value is more than 5 * 2 seconds.

The DESPOT sequence was set up for liquid samples, this is the first incidence of an attempt of DESPOT on solids, and some differences were noted. To begin with, the field spoiling pulse was not required in the runs with solid forsterite and SiC.

The T_2 for solids is so short (I.B.3) that the spins dephase without requiring any field gradient, like the solution samples do. The other difference between solids and liquids, is that it seems as though the solid samples need more dummy scans than calculated to attain the equilibrium cycle. If future work is to be done with DESPOT one should keep these comments in mind.

The results of the DESPOT experiment on forsterite give slightly higher results than the inversion-recovery experiment. The forsterite T_1 is calculated to be between 3.8 and 5.4 seconds by DESPOT, within experimental error. The T_1 values calculated from both methods are close enough to eachother to show that DESPOT may be a technique that will work efficiently to give the T_1 of solids. The time required for the typical inversion-recovery experiment on forsterite was two and a half days, whereas with DESPOT it was 20 minutes.

A 3C SiC sample, BGW12, was chosen for DESPOT because of the simplicity of its ^{29}Si MAS nmr spectrum, one peak. The difficulty with setting up DESPOT for this sample was in choosing the correct ti. The incorrect choice of ti could affect the results in two ways; the ti/T_1 ratio may not be optimized, and the equilibrium cycle may not be fully attained before acquisition.

According to Homer and Beevers (51), the ti/T_1 ratio should be between .05 and unity; if not the results will be inaccurate. Since the 3C T_1 can only be crudely estimated, it is

not certain whether the ti/T_1 ratio is within the optimal region. Also, to determine the number of dummy scans required (see II.F.2), one needs to have an idea of the ti/T_1 ratio. If the ti/T_1 value is overestimated, not enough dummy scans will be used, and the equilibrium cycle will not be correctly set up. Despite all of these potential quirks, it is still worthwhile to try DESPOT on the 3C SiC.

For the first run it was assumed that the T_1 was six hours, and a ti of 1200 seconds was used (ti/T_1 = .06). The corresponding T_1 was found to be 676 seconds (11.3 minutes). For verification, the second run the T_1 was chosen to be 676 seconds and the ti was set to 143 seconds (ti/T_1 = .21). The T_1 obtained was not 676 seconds but rather 219 seconds (3.7 minutes).

In a cascade approach, the ti was then set at 60 seconds (T_1 = 219, ti/T_1 = .27) for run 3. The resultant T_1 is 140 seconds which is just outside the 95% confidence range (student's t test) of run 2. This exeriment was then repeated, run 4, but the number of dummy scans were doubled to be sure that the full equilibrium cycle was attained. The T_1 was found to be 203 seconds; runs 2 and 4 are well within the 90% confidence range of each other.

For further verification, the ti was halved to 30 seconds (ti/T_1 = .14), runs 5 - 8. The calculated T_1's are all within the 95% confidence range of each other, averaging to 76 seconds. These results do not seem to agree with the previous results,

which suggests at least three things; one set of results is inaccurate, both sets of results are inaccurate, or there are several T_1 relaxation times for the silicon sites that have the same chemical shift. If runs 2 and 4 are in agreement with eachother, it is not likely that these results are inaccurate. The ti/T_1 ratio (0.14) for runs 5 to 8 may be too short or not enough dummy scans were used. If 40 dummy scans were successfullly used for ti equal to 60 seconds, then perhaps 80 dummy scans should have been used for ti equal to 30.

During the MAS nmr experiment of coal samples it has been found that there are some regions in the coal which relax faster than others, due to sample inhomogeneity (12). Most of the SiC samples studied are industrially produced; a number of impurities may be randomly incorporated into the material which may give rise to sample inhomogeneity.

One can not rule out the final possibility; there are several relaxation times for the silicon sites with the same chemical shift. The assumed relaxation mechanism for network solids is by means of spin diffusion (see I.B.3). These potentially inhomogeneous regions may be the cause of the inconsistencies in the SiC spectra obtained at different pulse recycle delays perhaps this is also reflected in the DESPOT and inversion-recovery experiments. The DESPOT results seem to point out the same problem that the inversion-recovery experiment does; it is difficult to determine the T_1 of solids if a range of T_1's

are possible for sites having the same chemical shift.

Chapter VI

SiC Shielding Tensors: A Single Crystal NMR Study

A. Introduction

A principal aim of this work has been in the identification of the silicon and carbon sites in SiC by the isotropic chemical shifts observed in the MAS nmr spectrum (Chapter III). MAS nmr works to remove the effects of chemical shift anisotropy (CSA) inherent in the nmr spectrum of powder solid samples by averaging the shielding tensors. The concepts of chemical shift, shielding tensors and CSA were introduced earlier (I.B.2 and I.C).

The shielding tensor, σ, is affected by the electronic environment around the nucleus which is governed by three basic factors (4):

$$\sigma = \sigma^{d} + \sigma^{p} + \Sigma\, \sigma^{nb}$$

The diamagnetic shielding term, σ^{d}, is due to spherically circulating electron currents (electrons are paired). In contrast, the paramagnetic shielding term, σ^{p}, is a result of

non-spherical electron motions from unpaired electrons. Finally, the neighbouring shielding anisotropy term, σ^{nb}, is a sum of the induced currents on neighbouring atoms.

A wealth of information can be learned about a molecule by studying its CSA. The shielding tensor which describes the CSA is dependent upon its orientation with respect to the applied magnetic field, H_o. The tensor is represented by a 3X3 matrix (87):

$$\sigma = \begin{vmatrix} \sigma_{xx} & \sigma_{xy} & \sigma_{xz} \\ \sigma_{yx} & \sigma_{yy} & \sigma_{yz} \\ \sigma_{zx} & \sigma_{zy} & \sigma_{zz} \end{vmatrix}$$

With some symmetrical molecules the tensor can be reduced to its three diagonal elements when the principal axis system is used; σ_{xx}, σ_{yy}, σ_{zz}. Furthermore, the directions of the principal axes are dependent upon the molecular symmetry. Determination of each of these three principal elements will provide information about the magnetic field generated by electron currents at the nucleus considered (while in an applied magnetic field), along each of its principal axes. Each independent nucleus has its own set of principal elements.

It has been verified using shielding tensor calculations that the induced electronic currents about a nucleus are not spherical but instead elipsoidal (88, 89). From this perspective, the bonding characteristics of the nuclei considered

can be better understood because the local magnetic environment is represented in a three dimensional manner.

It is interesting to consider the ^{13}C shielding tensors of other molecules (90-93). The general trend is that aliphatic carbons are more axially symmetric and therefore have smaller shielding anisotropies than aromatic or carbonyl carbons. Little ^{29}Si shielding tensor information is available (94), but the same shielding trends might be considered as for carbon where similar hybridized bonding orbitals are used.

Much recent work has been focused on the study of shielding tensors. A two-dimensional spectral technique has been used to directly correlate nmr lines obtained for each unique carbon at two different crystal orientations (95). More detailed theoretical work involves ab initio calculations of magnetic susceptibilities and chemical shifts based on localized molecular orbitals (95-98). Such calculations fit theoretical spectra to experimental nmr data in order to select the set of crystal orientations over which the spectral frequencies are calculated. In other words, theoretical calculations and 2-D nmr are also used to characterize the nuclear shielding along the principal axes of a given nucleus.

CSA studies of solids involve the use of powder samples or single crystals. This work uses a SiC single crystal to study the nature of the magnetic environment about the carbon and silicon nuclei. Comparisons will also be made between the

isotropic shielding tensors (σ_i) determined using the two techniques of single crystal and MAS nmr. To obtain the isotropic shifts for each nucleus with the single crystal method, the following formula is used (89):

$$\sigma_i = (\sigma_{xx} + \sigma_{yy} + \sigma_{zz}) * 1/3.$$

Results

Figure 6.1 shows the ^{13}C non-MAS nmr spectra of a single crystal of SiC, BGW51, with its c axis oriented a range of angles (0° to 105°) to the applied magnetic field, H_o, z axis. The same is shown for the ^{29}Si non-MAS spectra of BGW51 in Figure 6.2. The corresponding chemical shifts for Figures 6.1 and 6.2 are given in Table 6.1. The plots of chemical shift versus c axis orientation are given in Figures 6.3a and 6.4a for the ^{13}C and ^{29}Si non-MAS nmr spectra, respectively. The crystal is a flat plate and the c axis is normal to the plate. The spectrum with the c axis oriented 75° to the H_o z axis is identical to that at 105°; the points from 124° to 180° are then extrapolated on a symmetry basis about the 0° and 90° orientations.

For a more accurate plot, data points should be acquired for different angles and each experiment should be replicated at least three times, to do an error analysis. However, it takes about 12 hours to obtain one data point and it was not possible

Figure 6.1: ^{13}C single crystal nmr spectra of BGW51, 6H silicon carbide oriented at various angles to the applied magnetic field, H_o. Recycle delay was 5 seconds.

The orientation angle, θ, is with the crystal $\underline{c}$ axis relative to the H_o z axis.

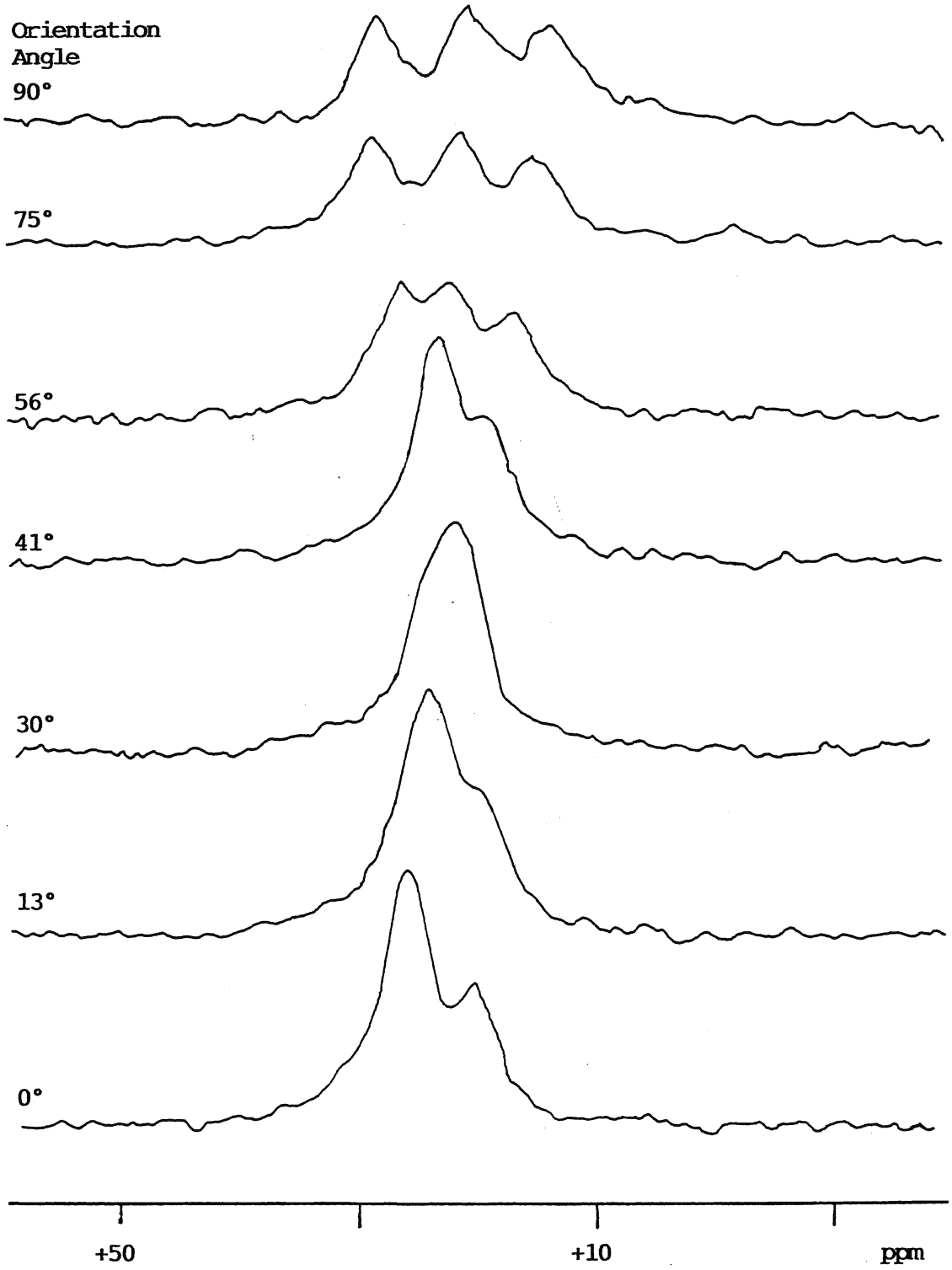
Orientation
Angle
90°
75°
56°
41°
30°
13°
0°
+50
+10
ppm

Figure 6.2: ^{29}Si single crystal nmr spectra of BGW51, 6H silicon carbide, oriented at various angles to the applied magnetic field, H_o. Recycle delay was thirty seconds (to overcome probe background). The orientation angle, θ, is with the crystal $\underline{c}$ axis relative to the H_o z axis.

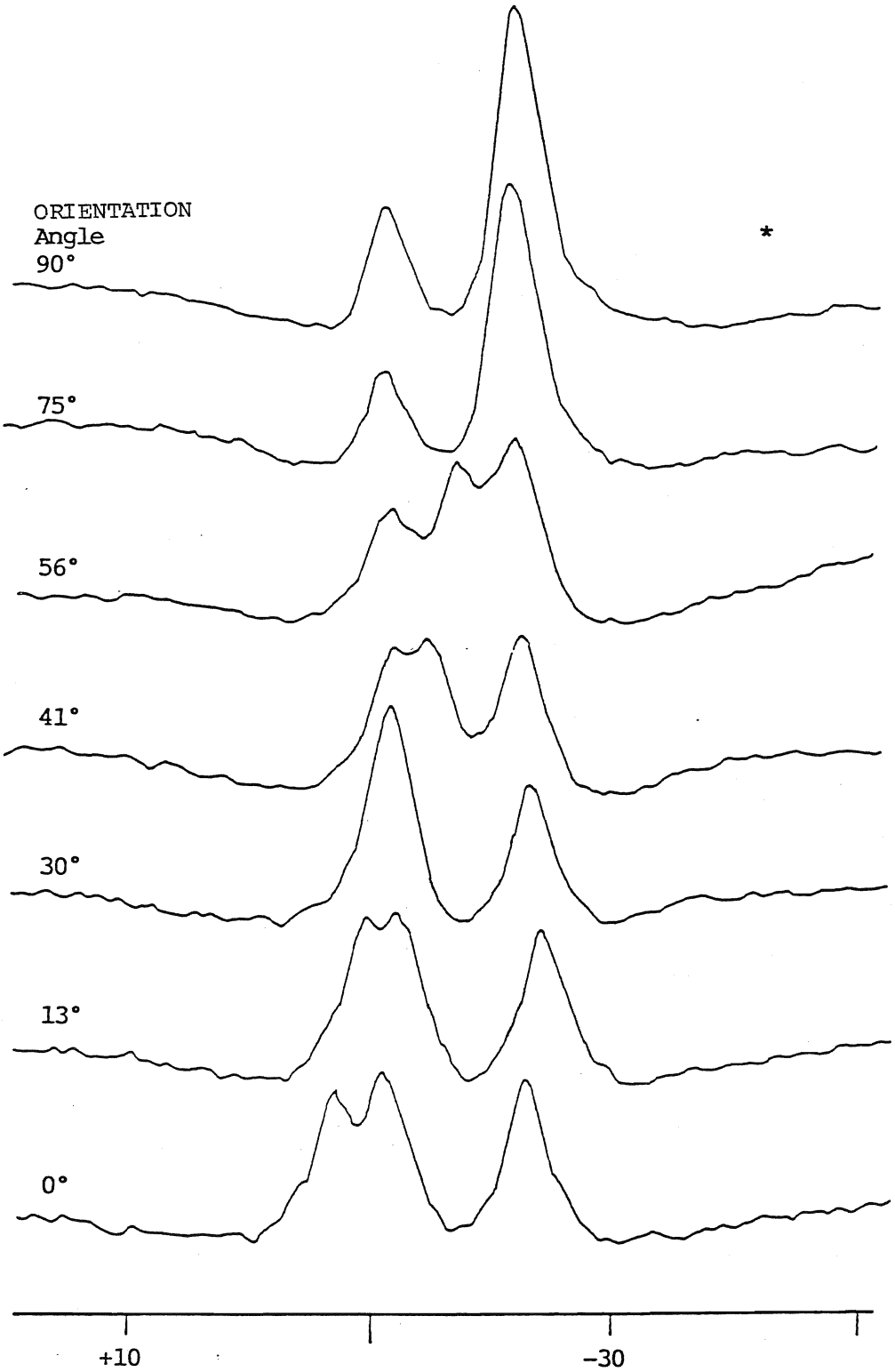

*rolling baseline due to probe signal (Quartz) interference

Figure 6.3: Plots of ^{13}C chemical shift versus orientation angle, θ.

a) results fron the single crystal nmr experiment; slashed lines are symmetry based exptrapolations.

b) calculated sinusoidal curves expected for the amplitude found (0° and 90° experimental points).

B)

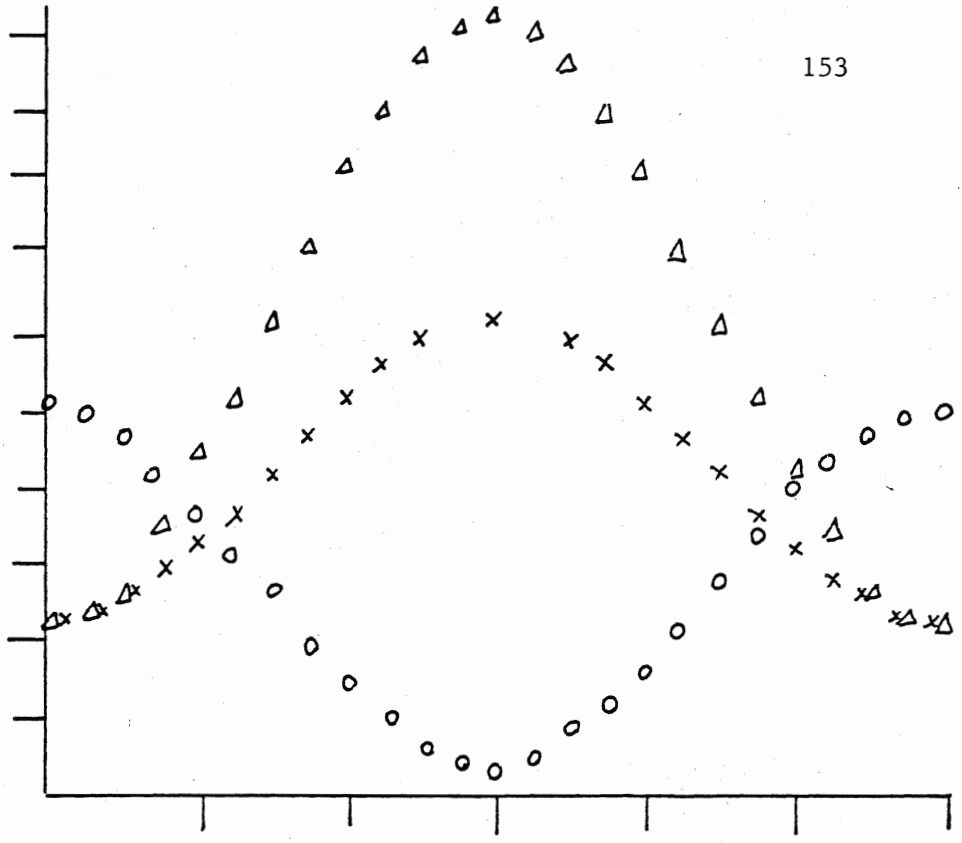

A)

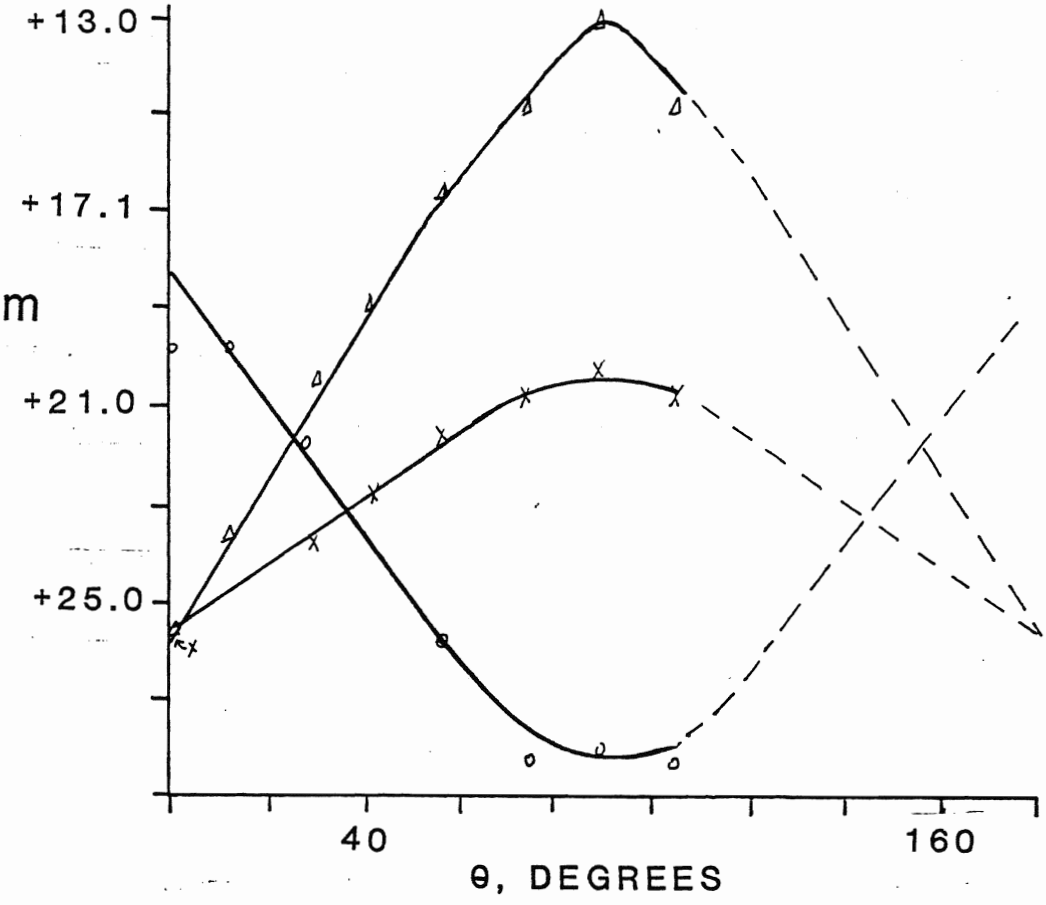

Figure 6.4: Plots of ^{29}Si chemical shifts versus orientation angle, θ.

a) results fron the single crystal nmr experiments; slashed lines are symmetry based extrapolations

b) calculated sinusoidal curve expected for amplitudes found (0^{o} and 90^{o} experimental points).

B)

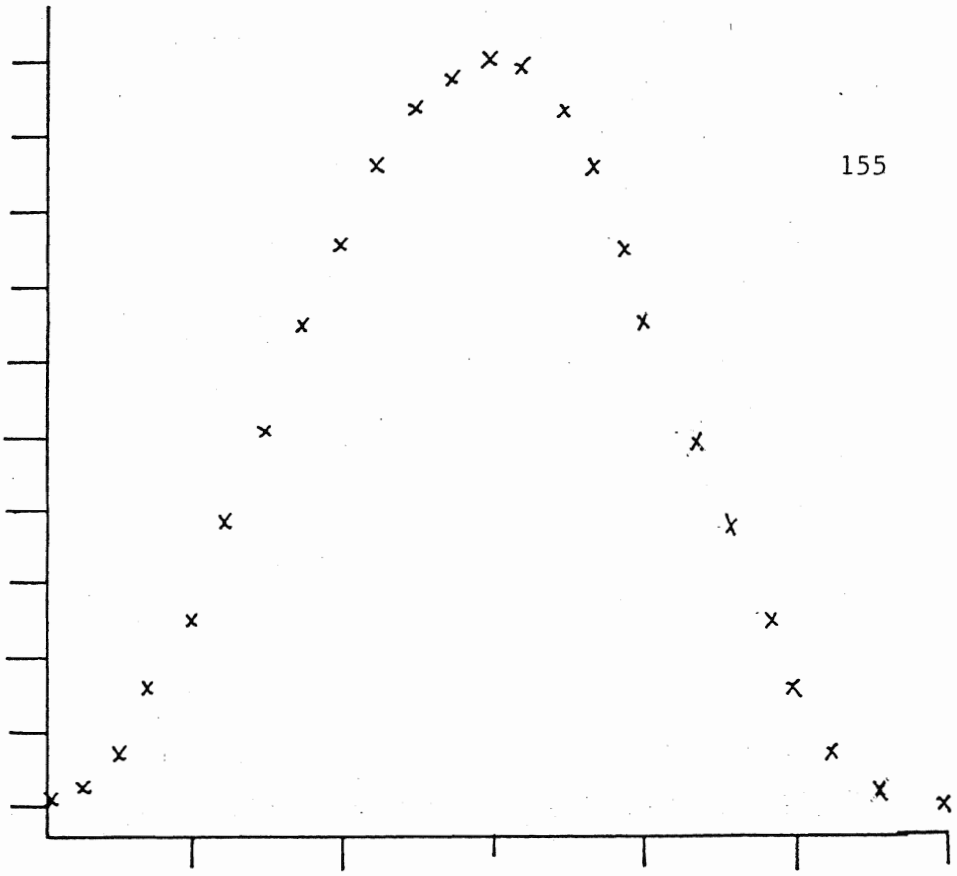

A)

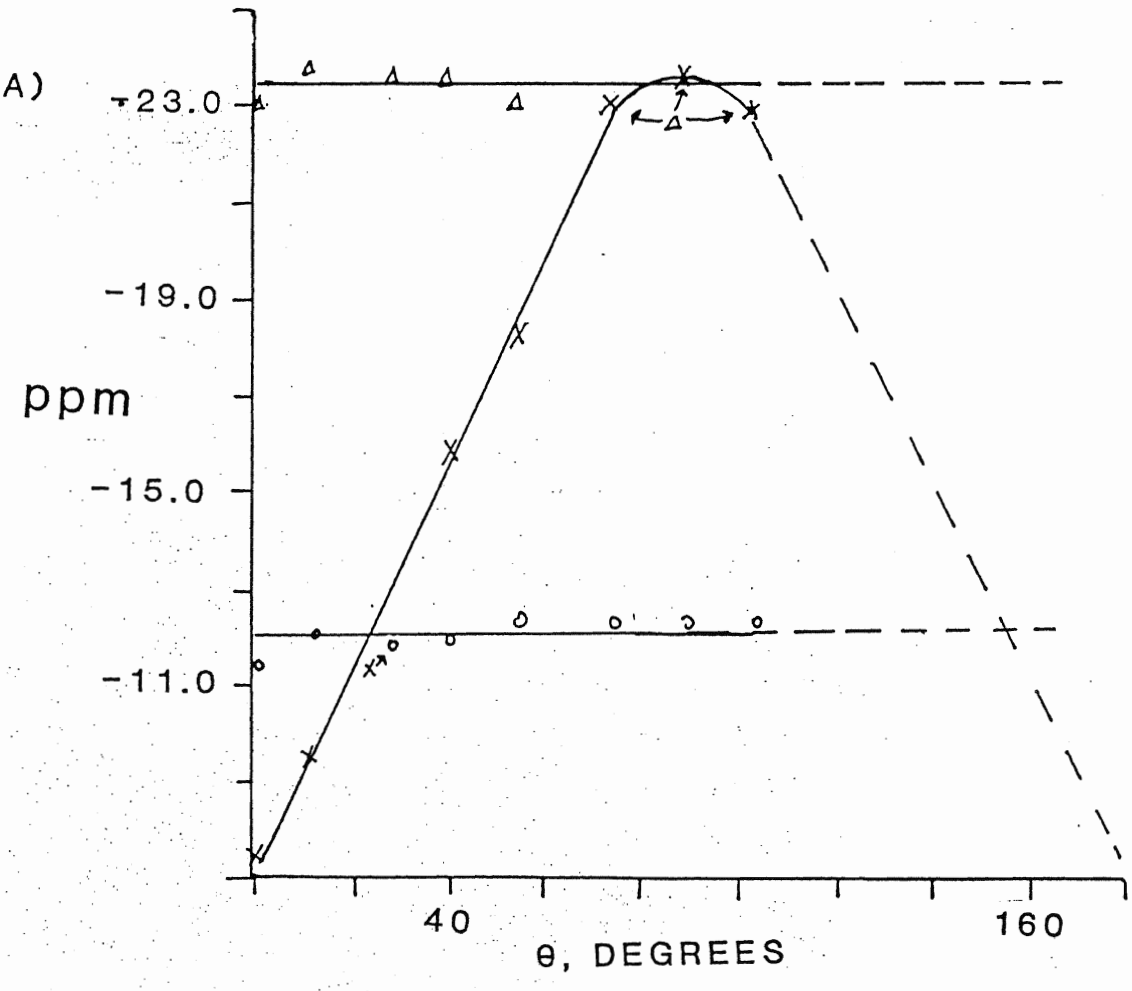

Figure 6.5: MAS nmr spectra of BGW51, 6H silicon carbide.

a) ^{13}C, 50.37 MHz, recycle delay was 5 seconds.
b) ^{29}Si, 39.76 MHz, recycle delay was 30 seconds.

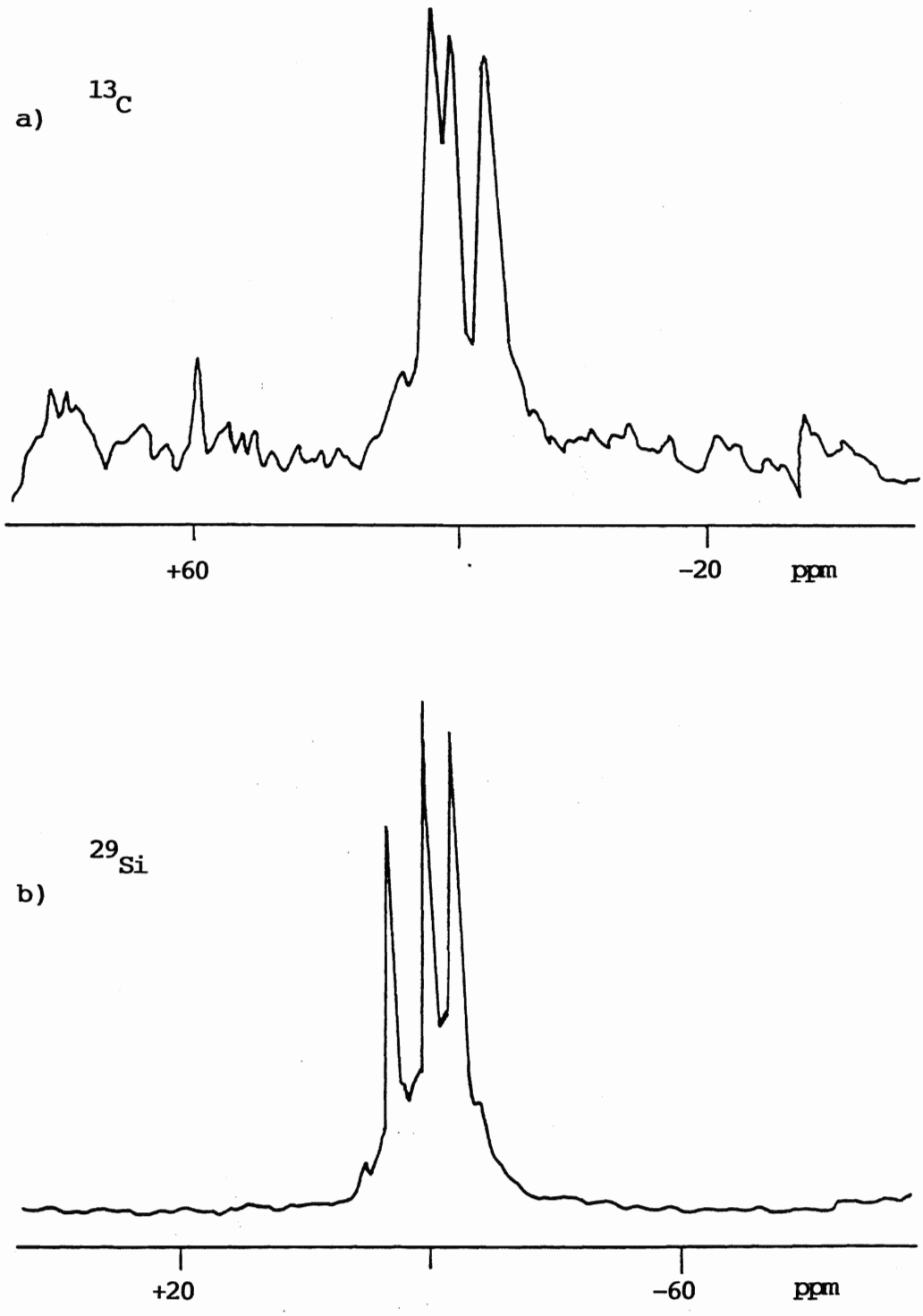
a)
^{13}C
+60
-20
ppm
b)
^{29}Si
+20
-60
ppm

Table 6.1 : Summary of Single Crystal NMR Chemical Shifts.

Orientation Angle	^{13}C (ppm)	^{13}C Int.*	^{29}Si (ppm)	^{29}Si Int.*
105	28.3, 21.0, 14.9	1:1:1	-12.3, -23.0	1:2
90	27.9, 20.2, 13.1	1:1:1	-12.4, -23.6	1:2
75	28.3, 20.8, 14.8	1:1:1	-12.4, -23.0	1:2
56	25.8, 21.8, 16.4	1:1:1	-12.6, -18.2, -23.1	1:1:1
41	22.7, 18.8	2:1	-12.0, -15.8, -23.6	1:1:1
30	24.0, 21.6	1:2	-11.9, -23.6	2:1
13	23.6, 19.6	2:1	-9.5, -12.1, -23.1	1:1:1
0	25.6, 20.1	2:1	-7.6, -11.5, -23.1	1:1:1

* = Intensities are approximate.

Table 6.2: ^{13}C Single Crystal and MAS nmr results.

Single Crystal						MAS
curve type	amplitude (ppm)	σ_{xx} ppm	σ_{yy} ppm	σ_{zz} ppm	σ_i ppm	σ_o ppm
max 90°	12.5	13.0	13.0	25.6	17.2	15.1
max 90°	5.5	20.1	20.1	25.6	21.9	20.4
min 90°	8.5	28.0	28.0	20.1	25.4	23.4

σ_o = Corresponding shift observed.

Table 6.3: ^{29}Si Single Crystal and MAS nmr results.

Single Crystal						MAS
curve type	amplitude (ppm)	σ_{xx} ppm	σ_{yy} ppm	σ_{zz} ppm	σ_i ppm	σ_o ppm
m = 0	-	-11.5	-11.5	-12.5	-11.8	-14.5
max 90°	15.5	-23.6	-23.6	-7.6	-18.3	-20.6
m = 0	-	-23.5	-23.5	-23.0	-23.2	-25.1

σ_o = Corresponding observed shift.

to collect more data. Also, the angles should be accurately set with a goniometer head. This facility is not available at Brock University, the glass inserts used seem to work well for this preliminary study.

Since the chemical shift is dependent upon angle, the plot of chemical shift versus crystal orientation angle should take on a sinusoidal curve (4,91). The expected curve has been calculated for carbon and silicon, Figures 6.3b and 6.4b, respectively, using the chemical shifts from the 0° and 90° orientations as the peak maxima or minima (whatever the case). Since the SiC crystal is a flat plate, the symmetry is such that the 180° to 360° orientations are not necessary. Therefore, only one half of a sinusoidal plot was drawn, 0 to 180°.

The ^{13}C and ^{29}Si MAS spectra of ground BGW51 are given in Figures 6.5a and b, respectively. Tables 6.2 and 6.3 summarize the single crystal and MAS data.

C. Discussion

Next nearest neighbour calculations have shown that the nmr spectra of SiC may be interpreted on a geometrical basis (39,58). Also, the ^{13}C and ^{29}Si MAS nmr spectra appear to be mirror images of each other, reflecting the reciprocal

silicon-carbon relationship of the SiC structure (Chapter III). Like the MAS nmr spectra, the single crystal experiment can be used to identify three sites with similar isotropic shifts to those of the MAS nmr experiment. However, the results from the two techniques differ in other ways. The only mirror image relationship observed in the single crystal nmr spectra may be coincidental; the ^{13}C 0^{o} spectrum versus the ^{29}Si 90^{o} spectrum and the ^{29}Si 0^{o} spectrum versus the ^{13}C 90^{o} spectrum (Figures 6.1 and 6.2).

Single crystal work on 6H SiC is simplified by the fact that it is readily obvious where the cell axes are within the crystal, on the basis of crystal shape and symmetry. In this way it is straightforward to identify the shielding tensor elements that correspond to the different cell axes.

The symmetry of the SiC 6H polytype is such that the a and b axes are identical and they lie in the plane of the SiC layer structure, the c axis is perpendicular to this. A six-fold axis of rotation is parallel to the c axis. The shielding tensors do depend upon the symmetry of the crystal so the tensor elements are considered to align with the SiC cell axes. Therefore, the symmetry of the crystal requires that the c_{zz} tensor be aligned with the c axis and that $\sigma_{xx} = \sigma_{yy}$.

Orientation of the crystal c axis parallel to the H_o z axis (the crystal is lying flat in the nmr tube) will produce an nmr spectrum of the σ_{zz} element. On the other hand, if the

crystal is vertical in the nmr tube, the $\underline{c}$ axis will be normal to the H_o z axis and the $\bar{\sigma}_{xx}$ and $\bar{\sigma}_{yy}$ elements will be recorded in the nmr spectrum.

Due to the symmetry of the crystal and the tensors, the environment of the nuclei with the $\underline{c}$ axis tilted $\pm\ \theta^o$ away from the H_o z axis will be the same and the corresponding nmr spectra will be identical (as observed with the 75^o and 105^o spectra). The resultant shift tensors will then display a sinusoidal response to orientation about the H_o z axis with a period of π (87). The maximum nuclear shielding will be with the $\underline{c}$ axis either 0^o or 90^o to the H_o z axis (vice versa for minima). The amplitude of the sinusoidal curve will be dependant upon the anisotropy of the induced electron currents about the nucleus. This is very useful because the electronic environment of the nucleus of interest can now be visualized in three dimensions and the bonding capabilities along each axis can be considered.

Comparison of Figure 6.3a with 6.3b and 6.4a with 6.4b shows that the experimental curves are not exactly sinusoidal. However, they are very close, within experimental error. A perfect SiC crystal would have a hexagonal face which is smooth on both sides. The face of the crystal used had only three sides of a hexagon. Irregularities in the crystal shape may cause the nmr line to broaden which makes it difficult to determine the exact peak position. Also, these broadened lines converge in

some spectra and at times it is impossible to distinguish between peaks. This apparent anisotropy is observed when the isotropic chemical shifts from the single crystal and MAS nmr experiments are compared. In both the ^{13}C and ^{29}Si cases the single crystal isotropic shifts are about 2 ppm to lower field than the MAS isotropic shifts. Bulk anisotropies in the magnetic susceptibility may be a factor in this discrepancy; it is not certain all of the factors that need to be considered without more data.

At this point, the single crystal data can be studied even further. The behavior of each nucleus is considered individually as the single crystal is rotated through 105° in H_o. It becomes immediately clear that the behavior of silicon is unlike that of carbon, plus each site has its own characteristic pattern, in the single crystal nmr experiment. This is not expected when only MAS nmr results are taken into account.

Two of the silicon sites seem to have very little anisotropy in the magnetic field. That is, the chemical shift does not change much with the angle of orientation. This suggests that two sites have a near isotropic local magnetic environment or field about the nucleus. The layer sequence for 6H is not cubic (/ABC/A..) but this sort of result would be expected for a cubic structure. The cubic layer sequence is identified as site type a (Chapter III), perhaps one of the nuclei is site a and the other site is very similar to site a (either site b or c).

The third silicon site has a large shielding anisotropy,

the amplitude is 16 ppm. The most shielded element (most negative chemical shift) is the one that corresponds to the σ_{xx} and σ_{yy} elements which are in the plane of the SiC crystal. The least shielded element is σ_{zz} which lies along the _c_ axis. A simplified picture of the electron currents about the nucleus would then be an elipsoid with its long axes in the _a_ - _b_ plane, and the short axis along the _c_ axis.

Unlike the silicon results all three carbon sites show anisotropy to orientation, to different extents. The site of least anisotropy has an amplitude of 5.5 ppm. The site with the most anisotropy has an amplitude of 12.5 ppm. Both sites have the σ_{xx} and σ_{yy} components maximally shielded and the σ_{zz} component minimally shielded. In contrast, the site that has the intermediate anisotropy ($\cong$ 8.5 ppm amplitude) has maximal shielding for the σ_{zz} element and minimal for the σ_{xx} and σ_{yy} elements.

Unfortunately only one SiC single crystal experiment was done. Before any correlations can be made more work as above is required. Some questions that can be asked now and hopefully answered with more work are:

1. Why don't the silicon and carbon shielding tensors have a mirror image relationship? Can this difference be because carbon is a second row element and silicon a third row element in the periodic table?

2. Why do two silicon sites seem to be insensitive to the angle of orientation?
3. Why does one carbon site behave in an opposite manner to the other two sites? Why would orthogonal axes in different carbon sites have greater CSA when all sites seem to be similar structuraly?
4. To what distance from a central site are neighbouring atom differences important?
5. How valid are the geometric considerations of Chapter III?
6. If they are valid, does the silicon site that is affected most by orientation correspond to the same site type as the carbon mentioned above in 3? Hence, can the silicon (carbon) sites be identified on the basis of layer stacking sequences and shielding tensors?

It seems as though the single crystal approach is more apt to answer the above questions than MAS nmr. This is in no way suggesting that MAS nmr is not useful, but rather the two techniques are complementary to each other. Single crystal work will give a better three dimensional picture of the local magnetic field at the nucleus, whereas MAS nmr results give the isotropic shifts realatively quickly which are useful in characterizing the samples studied.

The critical point in single crystal work is to get a large enough crystal and to correctly orient the crystal in the magnetic field (best done with a goniometer head). Otherwise inaccurate crystal orientation and broadened lines, due to shape anisotropy, will make it difficult to analyse data. Also, much care has to be taken in selecting the single crystal for size and shape, such stringent requirements are not necessary for MAS nmr studies.

In both single crystal and MAS nmr studies it is important to get more polytypes to better correlate structure to nmr spectra. Especially in the case of single crystal studies it is best to obtain polytypes with only one geometrical site type, so that the CSA pattern can be monitored without interference.

Chapter VII

A PRELIMINARY STUDY OF OTHER POLYTYPIC MATERIAL

A. Introduction

In addition to SiC there are other polytypic substances; alloys, organic compounds, mixed crystals and so on (25). One polytypic class that is well studied is MX_2 (99, 100); a metallic cationic layer is sandwiched between two anionic layers (X-M-X). Like SiC it is a layer structure, which grows along the c axis, but there are three monoatomic layers not two. The metallic ions lie in octahedral holes formed by hexagonally packed anionic X layers. The isotypic materials considered here are $CdBr_2$, CdI_2, and PbI_2.

The Ramsdell notation (see I.D.2) is also used to classify the MX_2 polytypes. In these cases if the symbol is 6H, the six represents six repeating MX_2 layers. The following are the observed polytypes of the matrials considered:

$CdBr_2$: 4H, 6R (100)

CdI_2 : 2H, 4H (100)

PbI_2 : 2H, 4H, (6H, 8H, 12H), 12R (99, 100)

The bracketed PbI_2 polytypes are not common (99).

Preliminary next nearest neighbour calculations (by M.F.Richardson, Depatment of Chemistry, Brock University) like those done for SiC (III.C.1) show that the Cd and Pb sites in the 2H, 4H, and 12R polytypes are all different. There is one different site in each of the 2H and 4H polytypes and two in the 12R polytype.

Both cadmium and lead nuclei have I = 1/2 isotopes. It is feasible that polytypism in $CdBr_2$, CdI_2, and PbI_2 could be studied by MAS nmr in the same fashion that SiC has been. One advantage of studying these samples as compared to SiC is that they can be grown from saturated gels or solutions (99, 103), which makes one independent of sample donors (i.e. samples are more accessible than SiC samples).

B. Results

Table 7.1 is a list of the ^{111}Cd, ^{113}Cd, and ^{207}Pb MAS nmr chemical shifts for the MX_2 halide compounds of these metals. All of the compounds are taken from reagent bottles and are probably a mixture of polytypes.

Table 7.1: Chemical shifts of Cd(II) and Pb(II) halides.

X	$^{111}CdX_2$ ppm	$^{113}CdX_2$ ppm	$^{207}PbX_2$ ppm
Cl	201.3 (11)*	198.0 (10)	-1189 (48)
Br	-25.7 (25)	-27.3 (24)	-
I	-712.5 (48)	-709.4 (45)	-

* = The peak width at half height, in ppm, is given in the brackets.

C. Discussion

There are two nmr accesible isotopes of cadmium, ^{111}Cd and ^{113}Cd. The MAS nmr spectra of $CdBr_2$ and CdI_2 were recorded at the spectral frequencies of both nuclei. The relative sensitivity of ^{113}Cd is marginally better than that of ^{111}Cd (49), so ^{113}Cd is usually the preferred nucleus to study by nmr. This can be seen in the nmr spectra recorded; fewer scans were required and the baseline artifacts (observed in ^{111}Cd spectra) were non-existent with ^{113}Cd.

The trend in chemical shift for CdX_2 is Cl > Br > I (Cl most positive) which indicates that the shielding increases from Cl to I. The line widths are fairly wide for $CdBr_2$ and CdI_2 (24 and 45 ppm respectively), but comparable to that of amorphous SiC (19 ppm, ^{29}Si).

It seems as though it may be possible to study the polytypism of both $CdBr_2$ and CdI_2 by MAS nmr; the line widths are not unreasonably broad, and little time is required to attain good signal to noise (compared to SiC). Cadmium, a post transition metal element, is a fairly heavy nucleus and this may cause a greater shift anisotropy in the nmr spectrum. The chemical shift range of cadmium is about 1000 ppm (three times greater than carbon) and there is some concern that there may not be enough sensitivity to detect the subtle differences between two polytypic sites in $CdBr_2$ of CdI_2. However, there are records of

cadmium nmr being used as a tool in structure determination of cadmium compounds (101, 102).

One example is with $3CdSO_4.8H_2O$ (102); two cadmium sites were detected and there are differences in the order of fractions of angstroms between the distances of near neighbours and the cadmium sites. The ^{113}Cd MAS nmr chemical shifts are -40 and -53 ppm, the line widths at half height are both 2.4 ppm. This sample has no halogens, which tend to broaden the nmr lines. However, in the same study the MAS nmr spectrum of $CdCl_2.xH_2O$ was recorded and two cadmium sites were resolved. The chemical shifts are -296 and -275 ppm, the line widths at half height are 16.1 and 12.6 ppm, respectively. These peaks are broad but they are still clearly resolved, and the major structural difference is only in the Cd-O bond distances.

^{207}Pb MAS nmr on the other hand does not appear to be so fruitful in the study of PbI_2 polytypism. A signal was detected for $PbCl_2$ but not for $PbBr_2$ or PbI_2. The $PbCl_2$ nmr signal was fairly broad, and there were also many spinning side bands, which is indicative of large shielding anisotropies. The chemical shift range of ^{207}Pb is about 8000 ppm, also showing the large shielding experienced by the heavy lead nucleus. If the $PbBr_2$ and PbI_2 signals were severely broadened and had a large spinning side band patteren (which reduces the intensity of the central peak) then the signal may be absorbed into the baseline.

The signals may be absorbing outside of the region

considered. The usual ^{207}Pb shift range (50) plus 100 KHz to low and high field was also scanned. As one moves away from the ^{207}Pb resonance frequency the sensitivity decreases because the probe tuning is only true within a band of the tuned frequency.

The suggestion here is that polytypism in $CdBr_2$ and CdI_2 could be studied successfully by nmr. It seems as though it would be a waste of time to try to study PbI_2 polytypism, especially since a host of other methods are readily used instead (103).

Chapter VIII

CONCLUDING REMARKS

The study of the phenomenon of polytypism by solid state nmr is very promising. The polytypism of silicon carbide has basically been considered on three planes; bulk sample, minor components, and internuclear interactions.

The number and chemical shift of the ^{13}C and ^{29}Si MAS nmr peaks observed for the bulk sample can be used to verify the identification of silicon and carbon sites found by crystallographic determination. As yet not all of the sites have been identified by MAS nmr because only three polytypes have been studied. To complete the analysis more polytyes are required, especially the 2H and 9R polytypes which contain the fourth site type; type d.

In the same manner, other polytypic material may be studied. Polytypic inorganic salts were investigated to determine the feasibility of further work; $CdBr_2$, CdI_2, and PbI_2. It seems as though the cadmium salts are definite candidates for an MAS nmr study in polytypism. A number of organic molecules have a polytypic nature which would also be good study subjects. Protons abound in organic molecules and the CP/MAS nmr technique should be utilized which is more sensitive and faster than MAS

nmr.

At short recycle delays minor components of SiC are detected. This was originally considered to be surface oxidation from the industrial synthesis process. But the heat treatment study showed that surface oxidation could be removed with hydrofluoric acid washing. Most minor components are unaffected by HF washing. Also, apparently pure samples have these same components. One sample in particular, BGW22, has a different sort of minor components which is evidenced in the short delay ^{29}Si MAS nmr spectrum. These findings may be due to impurities within the lattice or even subtle structure defects. Another thought is that the semiconducting nature of SiC is reflected in the two types of extra peaks observed; preliminary testing shows that the crystals do conduct. An interesting project would be to study doped SiC semiconductors by rapid pulsing ^{29}Si MAS nmr to see if there is a difference in spectra between n and p type semiconductors.

The spin-lattice relaxation mechanism of the SiC nuclei is believed to be via spin diffusion. It has been shown that SiC is likely to have a number of T_1 relaxation times for nuclei of the same chemical shift. This can be used to determine sample homogeneity because a variety of T_1 times is indicative of a heterogeneous sample.

For the ^{29}Si T_1 analysis, the DESPOT technique was used for the first time on solid samples. This method has a lot of

potential, however a lot of work is required to reliably adapt it to solid state applications. One way to do this is to study the T_1 of a solid that is homogeneous (has only one T_1).

Finally, single crystal nmr was used to study the local magnetic environment of the silicon and carbon nuclei in 6H SiC. This is possibly the most exciting aspect of this thesis. It was fascinating to observe the change in chemical shift with orientation angle in the magnetic field. The change is indicative of a response in the nuclear environment to the alteration in the apparent applied field. The results were unexpected; it was puzzling to see that the pattern observed for silicon is not the same as for carbon. This was a preliminary study which certainly sets the mark for future single crystal studies in other SiC polytypes.

To conclude, solid state nmr of SiC is complementary to crystallographic structure determination. However, where crystallographic studies fall short, nmr can pick up and carry on as in the minor component and single crystal nmr studies. Both single crystal and MAS nmr are potentially powerful tools to study polytypism, on many levels.

References

1. I.J.Lowe, Phys.Rev.Letts. , 2 , 285, (1959).

2. E.R.Andrew, A.Bradbury, R.G.Eades, Nature , 182 , 1659, (1958).

3. E.Lippmaa,M.A.Alla, T.J.Pehk,G.Engelhardt, J.Am.Chem.Soc. , 100 , 1929, (1978).
E.Lippmaa, M.Magi, A.Samoson, G.Engelhardt, A.-R.Grimmer J.Am.Chem.Soc. , 102 , 4889, (1980).

4. C.A.Fyfe, "Solid State NMR For Chemists", C.F.C.Press, Guelph, Ont., (1983).

5. C.A.Fyfe, L.Bemi, R.Childs, H.C.Clark,D.Curtin, J.Davies, D.Drexler,R.L.Dudley, G.C.Gobbi, J.S.Hartman, P.Hayes, J.Klinowski,R.E.Lenkinski,C.J.L.Lock,I.C.Paul,A.Rudin W.Tchir, J.M.Thomas, R.E.Wasylishen, Phil.Trans.Royal Soc. London , A305 , 591, (1982a).
C.A.Fyfe, L.Bemi, H.C.Clark, J.A.Davies, G.C.Gobbi, J.S.Hartman, P.J.Hayes, R.E.Wasylishen, inInorganic Chemistry Toward the 21st Century , Am.Chem.Soc., Washington, D.C., 405, (1983d).

6. E.Fukushima, S.B.W.Roeder, "Experimental Pulse NMR, A Nuts and Bolts Approach", Addison-Wesley, Reading, Mass., (1981).

7. R.K.Harris, "Nuclear Magnetic Resonance Spectroscopy", Pitman, London, (1983).

8. R.J.Kirkpatrick, R.A.Kinsey, K.A.Smith, D.M.Henderson, E.Oldfield, Am.Mineral. , 70 , 106, (1985).

9. C.A.Fyfe, J.M.Thomas, J.Klinowski, Angew.Chim.Int.Ed.Eng. , 122 , 259, (1983).

10. J.B.Murdoch, J.F.Stebbins, I.S.E.Charmichael, Am.Mineral. , 70 , 332, (1985).

11. R.Dupree, D.Holland, D.S.Williams, Phys.Chem.Glasses , 26 , 50, (1985).

12. D.E.Axelson, "Solid State Nuclear Magnetic Resonance of Fossil Fuels", Multiscience Pub.Ltd., Montreal, 1985.

13. K.W.Zilm, G.G.Webb, Fuel , 65 , 721, (1986).

14. M.J.Trewhella, I.J.F.Poplett, A.Grint, Fuel , 65 , 541,1986.

15. E.O.Stejskal, J.Shaeffer, R.A.McKay, J.Mag.Res. , 54 , 471, (1984).

16. V.W.Miner, J.H.Prestegard, J.Am.Chem.Soc. , 107 ,2177 (1985).

17. N.M.Szeverenyi, G.A.Maciel, J.Mag.Res. , 60 , 460,(1984).

18. G.A.Maciel, M.F.Davis, J.Mag.Res. , 64 , 356, (1985).

19. E.D.Becker,"High Resolution NMR"2nd Ed., Academic Press, N.Y., (1980).

20. A.Abragham, "The Principles of Nuclear Magnetism",Oxford University Press, (1961).

21. J.S.Waugh, L.M.Huber, U.Haeberlen, Phys.Rev.Lett. , 20 , 180, (1968).

22. M.Mehring, "Principles of High Resolution NMR in Solids", 2nd ed., Verlag, Berlin, (1983).

23. P.G. Stecher (Ed.), " The Merck Index", Merck and Co., N.Y.,(1968).

24. A.R.West, "Solid State Chemistry and its Applications", J.Wiley and Sons, N.Y., (1984).

25. A.R.Verma and P.Krishna, "Polymorphism and Polytypism in Crystals", New York, John Wiley Inc., (1966).

26. Gmelin Handbook of Inorganic Chemistry (8^{th}Ed Si-Silicon Sup.Vol B2), Properties of Crystalline Silicon Carbide , J.Schlichting, G.Czack, E.Koch-Bienemann, P.Kuhn, F.Schroder (Volume authors), Springer-Verlag, Berlin, (1984).

27. IBID , Supplement vol. B3, System Si-C , V.Haase, G.Kirschstein, H.List, S.Ruprecht, R.Sangster, F.Schroder,W.Topper, H.Vanecek, W.Heit, J.Schlichting (volume authors), Springer-Verlag, Berlin, (1986).

28. H.Baumhauer, Z. Krist ; 50 , 33 (1912), from ref. 25.

29. Z.Inoue, H.Komatsu in "Silicon Carbide-1973", R.Marshall, I.W.Faust jr., and C.E.Ryan (Eds.), U.South Carolina Press, Columbia, 191 (1973) and T.Yuasa, T.Tomita, M.Tokanami, J.Physics Society of Japan , 23 ,136 (1967).

30. N.W.Jepps, T.F.Page in "Progress In Crystal Growth and Characterization", Vol.7,ed. P.Krishna, Pergamon Press, Oxford, (1983).

31. P.Krishna, M.T. Sebastian, Bull.Min. , 109 , 99, (1986).

32. J.M.Yeomans, G.D.Price, IBID , 109 , 3, (1986).

33. L.S.Ramsdell, American Mineralogist , 32 , 64 (1947).

34. G.Hagg, Arkiv. Fur Kemi. Mineralogi Ock Geology , 16B , 1 (1943), from ref.25.

35. G.Zhdanov, Compt. Rend. Acad. Sci. URSS , 48 , 43 (1945), from ref.25.

36. R.S.Rai, P.Korgul, G.Singh, Acta Cryst. , B40 , 132 (1984)

37. M.C.Ladd, P.A.Palmer, "Structure Determination by X-Ray Crystallography"; Plenum Press, N.Y. (1978)

38. R.S.Mitchell, Am.Min. , 38 , 60 (1953).

39. G.R.Finlay, J.S.Hartman, M.F.Richardson, B.L.Williams, Chemical Communications , 159 (1985).

40. J.S.Hartman, B.L.Williams, Poster Presentation, 26th Experimental NMR Conference, Asilomar, Cal. (1985).

41. H.F.G.Ueltz, "Keynote Paper 1", General Abrasive Co., N.Y., (1971).

42. G.H.Stout and L.H.Jensen,"X-Ray Structure Determination", MacMillan Co., N.Y., (1968). p. 190.

43. N.W.Thibault, Am.Min. , 29 , 327, (1944).

44. M.F.C.Ladd, R.A.Palmer, "Structure Determination by X-Ray Crystallography", Plenum Press, N.Y., (1985).

45. CAD-4 Operation Manual, ENRAF NONIUS, Deft, Chapt XII,(1977).

46. Reference 42. p. 37.

47. Ibid . p. 31.

48. C.A.Fyfe, G.C.Gobbi, J.S.Hartman, R.E.Lenkinski, J.H.O'Brien, E.R.Beange, M.A.R.Smith, J.Magn.Res. , 47 , 168, (1982).

49. R.G.Kidd, R.J.Goodfellow in "NMR and The Periodic Table",

R.K.Harris and B.E.Mann (Eds.), Academic Press, London, (1978). p. 261.

50. R.K.Harris, J.D.Kennedy, W.McFarlane in IBID . p. 366.

51. J.Homer, M.S.Beevers, J.Mag.Res. , 63 , 287, (1985).

52. C.S.Blackwell, J.J.Pluth, J.V.Smith, J.Phys.Chem. , 89 , 4420, (1985).

53. W.H.Zachariason, J.Am.Chem.Soc. , 54 , 3841, (1932).

54. J.O.M.Bockris, J.W.Tomlinson, J.C.White, Trans.Far.Soc. , 52 , 299, (1956).

55. C.H.L.Goodman in, "Structure of Non-Crystalline Materials", P.H.Gaskell, J.M.Parker, E.A.Davis (Eds.), 151, (1982).

56. R.Dupree, D.Holland, P.W.McMillan, R.Pettifer, J.Non-Cryst. Sol. , 68 , 399, (1984).

57. C.M.Schramm, B.H.W.S.deJong, V.E.Parxiale, J.Am.Chem.Soc. , 106 , 4396, (1984).

58. J.S.Hartman, M.F.Richardson, B.L.Sherriff, B.G.Winsborrow, J.Am.Chem.Soc. , accepted for publication.

59. A.H.Gomes de Mesquita, Acta Cryst. , 23 , 610, (1967).

60. "International Tables for X-Ray Crystallography", Vol.IV, Kynoch Press, Birmingham, England, (1968).

61. A.R.Grimmer, R.Radeglia, Chem.Phys.Lett. , 106 , 262, (1984).

62. G.Engelhardt, R.Radeglia, Chem.Phys.Lett. , 108 ,271,(1984).

63. M.J.Duijvestijn, C.Van DerLugt, J.Smidt, R.A.Wind, K.W.Zilm, D.C.Staplin, Chem.Phys.Lett. , 102 , 25, (1983).

64. Private Communication, R.Van deMorwe, Norton Co.

65. N.W.Jepps, D.J.Smith, T.F.Page, Acta.Cryst. , A35 , 916,(1979).

66. J.V.Smith, C.S.Blackwell, Nature , 303 , 223, (1983).

67. D.W.Sindorf, G.E.Maciel, J.Am.Chem.Soc. , 105 , 1487,(1983).

68. T.M.Duncan, C.Dybowski, Surf.Sci.Rep. , 1 , 157, (1981).

69. D.J.Cookson, B.E.Smith, J.Mag.Res. , 63 , 217, (1985).

70. H.Marsmann in, "NMR Basic Principles and Progress", P.Dehl, E.Fluck, R.Kosfeld (Eds.), Springer-Verlag, Berlin, Vol. 17, (1981).

71. R.K.Harris, J.D.Kennedy, W.McFarlane in "NMR and The Periodic Table", R.K.Harris, B.E.Mann (Eds.), Academic Press, London, (1978).

72. R.Dupree, M.H.Lewis, G.Leng-Ward, D.S.Williams, J.Mat.Sci. Lett. , 4 , 393, (1985).

73. G.L.Turner, R.J.Kirkpatrick,S.H.Risbud, E.Oldfield, Am.Ceram. Soc.Bull. , 66 , 656, (1987).

74. J.Klinowski, T.A.Carpenter, J.M.Thomas, J.Chem.Soc.,Chem. Comm. , 956, (1986).

75. N.D.Butler, R.Dupree, M.H.Lewis, J.Mat.Sci.Lett , 3 , 469, (1984).
J.Klinowski, J.M.Thomas, D.P.Thompson, P.Korgul, K.H.Jack, C.A.Fyfe, G.C.Gobbi, Polyhedron , 3 , 1267, (1984).

76. A.P.Legrand, H.Hommel, L.Faccini, Bull.Soc.Chim. , 6 , 1103, (1985).

77. G.I.Finch, H.Wilman, Trans.Far.Soc. , 33 , 337, (1937).

78. J.A.Costello, R.E.Tressler, J.Am.Ceram.Soc. , 69 ,674,(1986).

79. B.E.Deal, A.S.Grove, J.Appl.Phys. , 36 , 3770, (1965).

80. J.R.O'Connor, J.Smiltens (Eds.), "Silicon Carbide, A High Temperature Semiconductor", Pergamon Press, NY, (1960).

81. C.Kittel, "Introduction To Solid State Physics", J.Wiley and Sons, NY, (1967).

82. V.M.Bermudez, T.M.Parrill, R.Kaplan, Surf.Sci. , 173 , 234, (1986).

83. R.Vold, J.Waugh, M.P.Klein, D.E.Phelps, J.Chem.Phys. , 48 , 3831, (1968).

84. G.G.McDonald, J.S.Leigh, J.Magn.Reson. , 9 , 358, (1973).

85. R.Freeman, H.D.Hill, J.Chem.Phys. , 54 , 3367, (1971).

86. K.A.Christensen, D.M.Grant, E.M.Schulman, C.Walling, J.Phys. Chem. , 78 , 1971, (1974).

87. W.S.Veeman, Prog.NMR Spec. , 16 , 193, (1984).

88. U.Haeberlen, "High Resolution NMR in Solids, Selective Averaging", J.S.Waugh (ed), Academic Press, NY, (1976).

89. M.Mehring, "Principles of High Resolution NMR in Solids", 2nd ed, Springer-Verlag, Berlin, (1983). Chapter 7.

90. S.Pausak, A.Pines, J.S.Waugh, J.Chem.Phys. , 59 , 591, (1973).

91. J.C.Facelli, D.M.Grant, J.Michl, Acc.Chem.Res. , 20 , 152, (1987).
C.M.Carter, D.W.Alderman, J.C.Facelli, D.M.Grant, J.Am.Chem. , Soc. , 109 , 2639, (1987).

92. J.Kempf, H.W.Spiess, U.Haeberlen, H.Zimmerman, Chem.Phys. , 4 , 269, (1974).

93. Reference 4. Chapter 5.

94. J.Van Dongen Torman,W.S.Veeman, E.deBoer, J.Mag.Res. , 32 , 49,(1978).

95. C.M.Carter, D.W.Alderman, D.M.Grant, J.Mag.Res. , 65 , 183, (1985).

96. D.W.Alserman, M.S.Solum, D.M.Grant, J.Chem.Phys. , 84 , 3717, (1976).

97. M.Schindler, W.Kutzelnigg, J.Am.Chem.Soc. , 105 , 1360,(1983).

98. C.J.Jameson, Specialist Periodical Reports, NMR , 15 , 1, (1985).

99. W.M.Sears, M.L.Klein, J.A.Morrison, Phys.Rev.,B. , 19 , 19, (1979).

100. B.Palosz, S.Gierlotka, "Proceedings on the 11th Conference on Applied Crystallography", Vol.1, 25, (1984).

101. P.G.Mennitt, M.P.Shatlock, V.J.Bartuska, G.E.Maciel, J.Phys. Chem. , 85 , 2087, (1981).

102. T.T.Cheung, L.E.Worthington, P.DuBois Murphy, B.C.Gestein, J.Magn.Res. , 41 , 158, (1980).

103. W.M.Sears, Ph.D. Thesis, Department of Chemistry, McMaster University, Hamilton, 1978.

VOLUME= 124.9607 GA10 (STANDARD DEVIATIONS)

CELL PARAMETERS			SIGMA CELL PARAMETERS		
a= 3.0846	b= 3.0856	c=15.1500	a= 0.0008	b=0.0018	c= 0.0084
~~α=89.9856~~	~~β=~~ 89.9960	γ=60.0679	α= 0.0524	~~β=~~ 0.0305	γ= 0.0281

VOLUME= 124.6442 BGW4

CELL PARAMETERS			SIGMA CELL PARAMETERS		
3.0791	3.0835	15.1394	0.0044	0.0018	0.0125
89.8357	89.9440	60.1304	0.0573	0.1015	0.1149

VOLUME= 123.6785 BGW18

CELL PARAMETERS			SIGMA CELL PARAMETERS		
3.0656	3.0790	15.1464	0.0006	0.0022	0.0171
89.9340	89.8698	59.8935	0.0853	0.1010	0.0711

VOLUME= 125.1742 BGW20

CELL PARAMETERS			SIGMA CELL PARAMETERS		
3.0805	3.0926	15.1458	0.0028	0.0033	0.0072
89.9881	89.6978	60.1746	0.0621	0.0711	0.0967

VOLUME= 125.0252 BGW22

CELL PARAMETERS			SIGMA CELL PARAMETERS		
3.0857	3.0889	15.1325	0.0005	0.0019	0.0073
89.8972	89.9486	60.0933	0.0750	0.0373	0.0267

VOLUME= 124.8610 BGW23

(STANDARD DEVIATIONS)

CELL PARAMETERS			SIGMA CELL PARAMETERS		
a= 3.0920	b=3.1171	c=14.8906	a= 0.0186	b= 0.0283	c=0.2439
α= 87.9531	β=89.0663	γ=60.5241	α= 1.1956	β= 0.8375	γ= 0.9355

VOLUME= 125.0029 BGW27

CELL PARAMETERS			SIGMA CELL PARAMETERS		
3.0870	3.0882	15.1307	0.0029	0.0049	0.0128
89.8825	89.8636	60.0677	0.1037	0.0763	0.1159

VOLUME= 125.1847 BGW48a

CELL PARAMETERS			SIGMA CELL PARAMETERS		
3.0853	3.0901	15.1459	0.0028	0.0027	0.0127
89.7603	89.8537	60.1055	0.0786	0.0868	0.0578

VOLUME= 125.4882 BGW48f

CELL PARAMETERS			SIGMA CELL PARAMETERS		
3.0890	3.0943	15.1811	0.0040	0.0051	0.0163
90.0740	90.1632	120.1402	0.1589	0.0958	0.2306

VOLUME= 125.6807 BGW51

CELL PARAMETERS			SIGMA CELL PARAMETERS		
3.0878	3.0908	15.2020	0.0016	0.0025	0.0239
89.7615	89.7731	60.0257	0.0919	0.0756	0.0656

Appendix II: Data for the study on the percent observable silicon detected , Chapter V. Data is given for results relative to the HMDSO, hexamethyldisiloxane, and BGW12A, 3C SiC, signals.

Experiment 1: 300 scans. Recycle delay is 5 seconds for all SiC samples. Recycle delay for HMDSO was 120 seconds.

Sample	Moles of Si($*10^{-2}$)	Wt.of Spectra ($*10^{-2}$ g)	Unit Wt. of Spectra(g/m)	Rel To HMDSO (% Si)
HMDSO	.38	14.323	38.19	100
BGW12A (3C)	1.18	5.239	4.440	11.64
BGW12B (3C)	.44	1.469	3.362	8.80
BGW4 (6H)	2.05	4.720	2.302	6.03
BGW26 (6H)	3.08	11.175	3.628	9.50
GA15 (15R)	2.24	6.234	2.783	7.29

Sample	Moles of Si($*10^{-2}$)	Wt.of Spectra ($*10^{-2}$ g)	Unit Wt. of Spectra(g/m)	Rel To BGW12A (% Si)
BGW12A (3C)	1.18	23.488	19.91	11.64##
BGW12B (3C)	.44	9.729	22.26	13.01
BGW4 (6H)	2.05	16.747	8.169	4.78
BGW26 (6H)	3.08	56.878	18.47	10.80
GA15 (15R)	2.24	31.729	14.16	8.29

indicates the percent silicon used in Table 5.1.

Experiment 2: 100 Scans. Recycle delay was 30 seconds for all SiC samples. Recycle delay is 120 seconds for HMDSO.

Sample	Moles of Si($*10^{-2}$)	Wt.of Spectra ($*10^{-2}$g)	Unit Wt. of Spectra(g/m)	Rel To HMDSO (% Si)
HMDSO	.38	12.547	33.46	100
BGW12A (3C)	1.18	12.924	10.95	32.73
BGW12B (3C)	.44	3.810	8.719	26.06
BGW4 (6H)	2.05	9.799	4.780	14.29
BGW26 (6H)	3.08	19.200	6.234	18.63
GA15 (15R)	2.24	10.368	4.650	13.85

Sample	Moles of Si($*10^{-2}$)	Wt.of Spectra ($*10^{-2}$g)	Unit Wt. of Spectra(g/m)	Rel. To BGW12A (% Si)
BGW12A (3C)	1.18	18.708	15.85	32.73##
BGW12B (3C)	.44	7.099	16.25	33.56
BGW4 (6H)	2.05	14.764	7.20	14.87
BGW26 (6H)	3.08	34.852	11.32	23.37
GA15 (15R)	2.24	18.819	8.40	13.85

indicates the relative percent silicon is used in Table 5.2.

Experiment 3: 30 scans. Recycle delay was 300 seconds for SiC samples. Recycle delay was 120 seconds for HMDSO.

Sample	Moles of Si($*10^{-2}$)	Wt.of Spectra ($*10^{-2}$g)	Unit Wt. of Spectra(g/m)	Rel. To HMDSO (% Si)
HMDSO	.371	4.272	11.50	100
BGW12A(3C)	1.407	9.073	6.45	56.1
BGW26 (6H)	2.226	11.033	4.96	43.2
GA15 (15R)	1.618	7.999	4.88	42.5